CIVIL ENGINEERING STUDIES
STRUCTURAL RESEARCH SERIES NO. 257

ANALYTICAL ~~AND~~ EXPERIMENTAL STUDIES OF CURVED MEMBERS OF CLOSED THIN-WALLED SECTIONS

By
MOHAMMAD AMIN
and
ALFREDO ANG

Approved by:
William H. Munse

Final Report of a
Research Program to
CATERPILLAR TRACTOR COMPANY
PEORIA, ILLINOIS

UNIVERSITY OF ILLINOIS
URBANA, ILLINOIS
SEPTEMBER 1962

Final Report

of a

Research Program

To

CATERPILLAR TRACTOR COMPANY

Peoria, Illinois

ANALYTICAL AND EXPERIMENTAL STUDIES OF CURVED MEMBERS OF CLOSED THIN-WALLED SECTIONS

by

Mohammad Amin and Alfredo Ang

Approved by:

William H. Munse

Department of Civil Engineering

University of Illinois

Urbana, Illinois

1 September 1962

TABLE OF CONTENTS

TABLE OF CONTENTS (Cont'd)

LIST OF FIGURES

LIST OF FIGURES (Cont'd)

LIST OF FIGURES (Cont'd)

LIST OF TABLES

Chapter I

INTRODUCTION

1.1 Object and Scope

Very little data from analytical or experimental studies on curved members of closed thin-walled cross sections are available in the literature. The only information known to the authors are, an approximate equivalent straight beam analysis to determine the axial flexural stress (in the direction of the axis of the member) at any point of a symmetrical box structure, as described in Ref. (1), and the experimental results obtained by the sponsor in a full-scale test of C-frames.

The principal objectives of this study were to develop simple expressions for the components of stress at any point in a curved member of box section subjected to torsional and bending loads, to obtain measurements of strains and deflections in a test specimen with simple geometry for the purpose of evaluating the validity of the new formulas, and to provide a better understanding of the over-all behavior of such members.

The analytical studies are reported in Chapter II. An approximate formula is developed for calculating the transverse flexural stresses which result from the distortion of cross-sections. This component is usually higher in magnitude than the other components of stress. Also included are a semi-emperical formula for axial flexural stress, and a description of the method used to investigate the effect of plate bending on the stresses in the walls of the box member in regions of high torsional loads. The approximate formula for the transverse flexural stress is applied to an idealized structure in Appendix A for illustrative purposes.

The experimental investigation is reported in Chapter III, wherein a detailed description of the test specimen, instrumentation, loading, and the

test procedure is given. The specimen was tested for loads normal to and in the plane of curvature of the member. These loads were applied independently, and no simultaneous application of the two loads was considered. The test results for loads normal to the plane of curvature are of primary importance in this investigation since the dominant stress component is that resulting from distortion of the sections under such loads.

The experimental results are presented and compared with the analytical results in Chapter IV. The results indicate that the approximate formula developed for the transverse flexural stress yields results which agree very well with the corresponding experimental values. Both experimental and analytical results obtained in this investigation are tabulated in Appendix B.

Chapter V includes a brief summary of the results and conclusions.

1.2 Notation

The symbols used in this report are summarized here for convenient reference.

a = distance across the top wall, measured from the inner wall to the point where the axial flexural stress on the top wall is zero. (See Fig. A)

A = cross sectional area

b = mean dimension of the walls

D = diagonal dimension of an undeformed 11.25 x 11.25 square closed thin-walled section

D_1^*, D_2^* = diagonal dimensions of 11.25 x 11.25 square closed thin-walled section in deformed state

E = modulus of elasticity

F = the shear resisted by plate action when a torque, T, is transmitted through a section 10λ away from the support.

G = modulus of elasticity in shear

I = centroidal moment of inertia of cross section

J = St. Venant's Torsion constant

M = bending moment

m = transverse flexural moment per unit width

m_i, m_o = transverse flexural moments per unit width at the inner and outer corners, respectively.

m_η = transverse flexural moment at a point η distance from the midpoint of a wall

P = a point on the test specimen

P_h = load applied at the trunion normal to the plane of curvature

P_v = load applied at the trunion in the plane of curvature

$q = \tau t = \frac{T}{2b^2}$ = magnitude of uniform shear flow

$\bar{r}$ = radius of curvature of the axis of a curved member

r_i, r_o = radii of curvature of the inner and outer walls, respectively

R_t, R_b = resultant radial forces acting on the top and bottom walls, respectively

R^* = a couple acting on the top and bottom walls as defined in page (11)

$R = R_t + R^*$ = the net resultant radial force acting on the top and bottom walls

T = twisting moment

t = wall thickness

V = shear force

$Z = -\frac{1}{A}\int_{\text{cross-section}} \frac{y}{r+y}\, dA$

$\Delta^P_{y_i}$ $(i = 2, 3)$ = deflection at point P in direction y_i related to the fully fixed support condition

$\Delta^P_{y_{im}}$ $(i = 2, 3)$ = measured deflection at point P in direction y_i

$\delta^{P}_{y_i}$ $(i = 2, 3)$ = rigid body displacement produced at point P in directions y_i

δ = centerline deflection normal to the plane of curvature

δ_c = centerline deflection normal to plane of curvature determined by the simple theory

δ_m = centerline deflections normal to plane of curvature determined from experimental data

Φ_1, Φ_2 = corrected rotations of diagonals of an 11.25 x 11.25 square closed thin-walled section in the deformed state

ϵ_r = transverse flexural strain

ϵ_θ = axial flexural strain

ϵ_{θ_i}, ϵ_{θ_o} = axial flexural strains at the inner and outer corners of a section, respectively

σ_r = transverse flexural stress

σ_{rm} = experimental transverse flexural stress

σ_{rc} = computed transverse flexural stress

$\sigma_{r\eta}$ = computed transverse flexural stress at a point with radius r and η distance from the midpoint of a wall

σ_θ = axial flexural stress

σ_{θ_i}, σ_{θ_o} = axial flexural stresses at the inner and outer corners of a section, respectively

$\sigma_{\theta m}$ = experimental axial flexural stress

$\sigma_{\theta c}$ = computed axial flexural stress

$\bar{\sigma}_\theta$ = average axial flexural stress acting on top or bottom wall

θ^{o}_i $(i = 1, 2, 3)$ = rotation of the base of the test specimen about axis X_i

$\tau = \dfrac{T}{2tb^2}$ = shear stress

λ = grid length used in the finite difference equations

μ = Poisson's ratio

1.3 Acknowledgements

This report constitutes the final report of a research project carried out in the Department of Civil Engineering of the University of Illinois under contract with the Caterpillar Tractor Company, Peoria, Illinois. The project has been under the general direction of W. H. Munse, Professor of Civil Engineering, and under the immediate supervision of A. Ang, Associate Professor of Civil Engineering.

The authors express their sincere appreciation to the Caterpillar Tractor Company for having made this investigation possible, and particularly to Mr. H. Fall of their Engineering Division. Thanks are also expressed to the staff of the Structural Research Laboratory Shop for their cooperation during the experimental phase of this investigation.

Chapter II

ANALYTICAL INVESTIGATION

2.1 Introductory Remarks

The analysis of a curved member built up of thin plate elements and subjected to both torsional and bending loads can theoretically be considered a problem in shell analysis. By making certain assumptions about the geometry of the structure and the distribution of stresses at any cross section it is possible to develop approximate, but simple expressions for various components of stress at any point in the member. Specifically, these studies were aimed at developing formulas for rapid calculation of stresses in such members rather than a rigorous analysis of the behavior of such members.

In a member composed of thin plate elements stresses normal to the faces of the plates are usually negligible at points which are distant from the points of application of concentrated loads. Also, the shearing stresses normal to the plates can be neglected. It follows that the state of stress at any point in the structure may be reduced to a two dimensional state of stress as shown in Fig. (1). The three components of stress to be determined at any point, therefore, are the following: transverse flexural stress, σ_r, axial flexural stress, σ_θ, and the shear stress, τ.

For a member of square thin-walled cross section τ is obtained by assuming a uniform shear flow at the section in question. Approximate methods of determining the stress components σ_r and σ_θ in a prismatic curved member of square thin-walled cross section with constant radius of curvature are discussed below.

2.2 Approximate Formula for Transverse Flexural Stress

2.2.1 Assumptions. The approximate formula for transverse flexural stress, σ_r, is based on the following assumptions:

1. The member is a curved member of uniform radius of curvature and of square thin-walled cross section.

2. The member has a uniform wall thickness.

3. The material of which the member is composed is homogeneous isotropic, and linearly elastic.

4. Deformations are small.

5. The distribution of axial flexural strains is linear across the width and through the depth of the cross section, and the distribution of the axial flexural stress is as given in Sect. 2.4.

6. Shearing stresses in a wall resulting from bending in its own plane are neglected; that is, plate bending is approximated by bending of transverse strips acting as beams. The walls actually act as plate elements, but for cases where the moment and torque gradients are not excessively high this assumption gives fair results for the transverse flexural stresses in the walls. The effect of plate bending on flexural stresses in regions of high torsional loads is discussed in Sect. 4.4.

2.2.2 Derivation. A circular element of the member between two radial planes having an infinitesimal dihedral angle $d\theta$ is shown in Fig. (2). The resultant forces on the circular element can be resolved into three components: torque, T, bending moment, M, and shear, V. These components of the resultant force are shown in plan view in Fig. (3). The following sign convention is used (see Fig. 3): Couples are represented by vectors according to the left hand screw rule; the cross section of the circular element facing the positive direction of θ is called the positive face or the positive section; all vectors

are positive if they are oriented in the positive directions of the reference axes in the positive face, and in the negative directions of the reference axes in the negative face. With such a convention, positive bending moment gives tension in the bottom wall.

Because of assumption (1), torque, bending moment and shear are functions of θ alone and, if denoted by T, M, and V, respectively on the negative face, will have values T + dT, M + dM, and V + dV on the positive face. Equilibrium of moment vectors in the direction of the tangent gives the equilibrium of moments about the θ-axis, thus

$$- T + M \frac{d\theta}{2} + (M + dM) \frac{d\theta}{2} + T + dT = 0.$$

Simplifying and neglecting terms of higher order,

$$M + \frac{dT}{d\theta} = 0 \qquad (1)$$

Similarly equilibrium of moments about the r-axis yields,

$$- T \frac{d\theta}{2} - M + V\bar{r} \frac{d\theta}{2} + (V + dV) \bar{r} \frac{d\theta}{2} + M$$

$$+ dM - (T + dT) \frac{d\theta}{2} = 0.$$

After simplifying and neglecting terms of higher order, this becomes

$$\frac{dM}{d\theta} - T + V \bar{r} = 0 \qquad (2)$$

where $\bar{r}$ is the mean radius of the circular element.

Equations (1) and (2) result from the application of the laws of statics to the circular element and are, therefore, independent of material properties. Equation (2) gives a relationship between M, T, and V and is

analogous to the M - V relationship in a straight beam. In fact, when $\theta \to 0$, $\bar{r}\, d\theta \to dx$, and T is equal to zero, Eq. (2) is reduced to the shear-moment relationship for a straight beam. Any assumption regarding the nature of the distribution of stresses at cross sections of the member must yield a resultant force whose components satisfy Eqs. (1) and (2).

A schematic representation of the assumed distribution of the axial flexural stresses, σ_θ, and the shear flow, q, acting on the circular element of Fig. (2) is shown in Fig. (4). Axial flexural stresses are assumed to vary linearly across the width and through the depth of the circular element. In the following development the net forces acting in the radial directions at the top and bottom walls of the circular element will first be computed; then, the circular element will be treated as a square frame subjected to these forces which tend to distort the cross section, thus inducing transverse flexural stresses, σ_r.

The free-body diagrams for the top, bottom, inner and outer walls are shown in Figs. (5a), (5b), (5c), and (5d), respectively, where the following notation is used:

σ_{θ_i} and σ_{θ_o} denote the axial flexural stresses acting at the inside and outside corners, respectively. Tensile stresses are considered positive.

$\bar{\sigma}_\theta$ = the average axial flexural stress acting on the top and bottom walls

q = the magnitude of the uniform shear flow = $\tau\, t = \frac{T}{2b^2}$, where, t is the wall thickness and b is the mean dimension of the walls.

Projecting the forces acting on the top wall onto the r-axis, we obtain

$$R_t = bt\, \bar{\sigma}_\theta \frac{d\theta}{2} + bt\, (\bar{\sigma}_\theta + d\bar{\sigma}_\theta) \frac{d\theta}{2} + b\, dq$$

which, after neglecting the term of second order, takes the form

$$R_t = bt\,\bar{\sigma}_\theta\,d\theta + bdq \tag{3}$$

where, R_t is the resultant radial force acting on the top wall; directed in the positive direction of r-axis.

A similar consideration with respect to the forces acting on the bottom wall yields a radial force R_b on the bottom wall equal to R_t in magnitude but in the opposite direction. Figure (6) is a side view, projected on the r-z plane, of the circular element of Fig. (2), where in addition to the resultant forces R_t and R_b acting on the top and bottom walls, the radial component of the stresses in the two side walls are shown. These stresses are the r-components of the stresses shown in Figs. (5c) and (5d). The maximum values of these stress components are

$$2(\sigma_{\theta_i} \cdot \frac{d\theta}{2}) = \sigma_{\theta_i}\,d\theta,$$

$$2(\sigma_{\theta_o} \cdot \frac{d\theta}{2}) = \sigma_{\theta_o}\,d\theta.$$

The moment about the θ-axis produced by these stresses is

$$\frac{tb^2}{6}(\sigma_{\theta_i} - \sigma_{\theta_o}) = \frac{tb^2}{3}\,\bar{\sigma}_\theta\,d\theta.$$

A couple R* acting in the top and bottom walls that will produce the same moment is

$$R^* = \frac{tb}{3}\,\bar{\sigma}_\theta\,d\theta.$$

Hence, replacing the stresses on the side walls by R*, the net resultant forces in the radial direction acting on the top and bottom walls are

$$R = R^* + R_t = \frac{4}{3} tb\, \bar{\sigma}_\theta\, d\theta + b\,dq \tag{4}$$

where,

$$\bar{\sigma}_\theta = \frac{Mb}{2I} = \frac{3}{4} \frac{M}{tb^2}\ , \tag{5}$$

and in view of Eq. (1)

$$dq = \frac{dT}{2b^2} = -\frac{M}{2b^2}\, d\theta. \tag{6}$$

Using Eqs. (5) and (6) in Eq. (4)

$$R = \frac{M}{b}\, d\theta - \frac{M}{2b}\, d\theta \tag{7}$$

$$= \frac{M}{2b}\, d\theta$$

Note that the first term on the right-hand side of Eq. (7) is the contribution of the bending moment, and the second term is the contribution of the torque, to the net radial force R. It is clear that the effect of bending moment is more pronounced than the effect of the torque.

In order to simplify the analysis, the components of the stresses shown in Fig. (4) that produce distortion of the cross section are represented by a couple R acting at the top and bottom walls in the radial direction as shown in Fig. (7a). It must be emphasized that the state of stress in Fig. (4) is a self-equilibrating stress condition, but the distribution of the stress and the geometry of the section give rise to distortion of the cross section, as represented by Fig. (7a). In Fig. (7a) the frame will be assumed to have prismatical members throughout. Such an assumption greatly simplifies the analysis; otherwise a frame of varying stiffness has to be considered. In Fig. (7b) are shown the free-body diagrams for the inner and outer members.

Equilibrium of moments acting on the top wall requires that

$$m_i \, r_i \, d\theta = m_o \, r_o \, d\theta,$$

or

$$m_i \, r_i = m_o \, r_o$$

where m_i and m_o are derived as follows:

The equilibrium for the inner wall requires that,

$$b\left(\frac{M}{4b}\right) d\theta = 2 \, m_i \, r_i \, d\theta,$$

or

$$m_i = \frac{M}{8r_i} \tag{8}$$

A similar consideration for the outer wall yields

$$b\left(\frac{M}{4b}\right) d\theta = m_o \, r_o \, d\theta,$$

or

$$m_o = \frac{M}{8r_o} \, . \tag{9}$$

In Eqs. (8) and (9) m_i and m_o denote the moments per unit width acting at the corners of the top member with inner and outer members respectively; r_i and r_o are the corresponding radii of curvature. Equations (8) and (9) are the relationships required for the determination of the transverse flexural stresses in the curved member.

Let m denote the value of the transverse flexural moment at any point of the cross section. The distribution of m across the width and through the depth of the cross section is shown in Fig. (8). The moment m will cause transverse flexural stresses through the thickness of each wall which can be

found by the application of the conventional flexural formula, $\frac{My}{I}$, applied to the individual walls. The value of the transverse flexural stress at an extreme fiber, therefore, is

$$\sigma_r = \frac{m(\frac{t}{2})}{(\frac{1}{12})t^3} = \frac{6m}{t^2} \tag{10}$$

At a given section, the high stresses occur at the points where the moments, m, are maximum, which are at the corners of the section, and are:

$$\sigma_{r_i} = \frac{3}{4} \frac{M}{r_i t^2}, \tag{11}$$

$$\sigma_{r_o} = \frac{3}{4} \frac{M}{r_o t^2}. \tag{12}$$

Since $r_i < r_o$, it follows that the absolute maximum values of the transverse flexural stresses at any section, occur at the inner corners, and are given by Eq. (11).

2.2.3 Sign Convention. In the previous section it has been demonstrated that σ_r at any section is a function of the force R acting at the top and bottom walls of the circular element, which in turn is a function of the axial flexural stress and the shear flow; hence, bending moment and torque. Equation (7) clearly indicates that the contribution of the bending moment to R is more pronounced than that of the torque. In view of these observations the following procedure for sign convention is suggested.

A positive moment (tension bottom wall) will cause R on the top wall to be directed in the direction of increasing r. The sign of the transverse flexural stress at any point of the cross section can be determined then from the distortion of the frame shown in Fig. (7a).

2.3 Varying Radius of Curvature

Equations (8) and (9) in Sect. 2.2.2 were derived under the assumption that the member is a curved member with uniform radius of curvature. In practice, two variations from this assumption may occur.

First, the center line of the member may be a curve of continuously varying curvatures. At any section, the curvature of such a member can best be approximated by the curvature of the osculating circle applicable at the section. Then the procedure of Sect. 2.2.2 for the determination of the transverse flexural stresses becomes applicable and Eqs. (8) and (9) can be used to determine the transverse flexural moments m_i and m_o with the understanding that r_i and r_o, now, are the radii of curvature of the inner and outer walls drawn from the center of curvature of the curved axis at the section in question.

Second, the member may be a compound curve composed of several circular arcs. Equations (8) and (9) are of course applicable within individual circular segments. However, at the point of tangency of the two circular arcs these formulas are no longer strictly applicable. It is suggested that Eqs. (8) and (9) be used to determine m_i and m_o at such sections with the r_i and r_o being taken as the average of the values corresponding to the adjacent circular segments.

A special case of the latter situation arises when a circular arc is followed by a straight portion. The radius of curvature, in this case, is infinite immediately to one side and it is finite immediately to the other side of the point of tangency. Furthermore, because of the geometry of the axis the axial flexural stresses acting on the straight portion do not have radial components, whereas those acting on the curved portion do have radial components.

In such a case it is suggested that Eqs. (8) and (9) be applied to determine m_i and m_o using the values of r_i and r_o applicable to the circular portion and the values thus computed be divided by 2.

An illustrative example showing the uses of the suggested techniques is given in Appendix A.

2.4 Approximate Procedure for Axial Flexural Stress

2.4.1 General. It is recalled that when a prismatic straight member of non-circular cross section is subjected to a constant torque the cross sections warp, and if all the sections are free to warp no axial stresses accompany the twist. This is not the situation, however, when warping is prevented or restricted in some way due to support conditions, or non-uniform twist. Under these conditions normal stresses will be induced which vary from section to section.

The normal stresses that result from a prevention of warping in some section or because of non-uniform twist are intensified in the case of a curved member because the longitudinal fibers of the member are not of the same length. Indeed, the experimental results presented in Chap. IV of this report clearly indicate that the distribution of the axial flexural stresses in the test specimen differ considerably from those obtained under the "plane section" assumption, which would hold if there were no axial normal stresses induced due to torsion. There seems to be no rigorous solution available for the axial normal stresses induced due to torsion in a curved member of closed thin walled section and a study of this problem is beyond the scope of the investigation reported herein. However, a semi-empirical procedure, which gives stresses that agree closely with the maximum measured stresses, is presented.

2.4.2 Semi-empirical Formula for the Axial Flexural Stress. The axial normal stresses induced by the torque, whatever their distribution, must satisfy the following condition of equilibrium: the resultant axial force and bending moment produced by these stresses must equal zero at every cross section. When this stress system is superimposed on the stresses which are produced by the bending moment alone, the resulting stress distribution at any section will be of the type shown in Fig. (4). The resulting formula gives a stress distribution that agrees with the experimental results presented in Chap. IV of this report.

In Fig. (4) let "a" denote the distance across the top wall, measured from the inner wall to the point where the axial flexural stress on the top wall is zero. Equilibrium of moments about the r-axis requires that

$$\left[\frac{1}{2}\,\sigma_{\theta_o}\,t\,\left(\frac{a}{b-a}\right)\,a - \frac{1}{2}\,\sigma_{\theta_o}\,t\,(b-a)\right] b$$

$$+\left[\frac{1}{2}\,\sigma_{\theta_o}\,t\,\left(\frac{a}{b-a}-1\right)\frac{b}{2}\right]\frac{2}{3}\,b = M$$

which, after simplification yields

$$\sigma_{\theta_o} = \frac{3}{2}\,\frac{M}{tb^2}\cdot\frac{b-a}{2a-b} \qquad (13)$$

The value of "a" in Eq. (13) was so determined that the maximum stresses computed from this formula closely approximate the corresponding measured values as will be discussed in Sect. 4.2.2.

2.4.3. Formula for Axial Flexural Stress Based on "Plane Section" Assumption. It has been pointed out that the axial flexural stresses derived from the "plane section" assumption for a curved member under torsional and bending loads are not in agreement with the experimental results. As a means

of providing a convenient reference, the formula to determine the axial flexural stresses in a curved member having the geometry described in Sect. 2.2.1, under the assumption that plane sections remain plane after loading, is derived in this section.

Under the "plane section" assumption the variation of strains, and hence stresses, is linear through the depth of the member. However, the variation of strains across the width (on the top and bottom walls) is such that

$$\epsilon_{\theta_o} r_o \, d\theta = \epsilon_\theta \, r \, d\theta$$

or

$$\epsilon_{\theta_o} r_o = \epsilon_\theta \, r$$

where

ϵ_{θ_o} = the axial flexural strain at the outside corner,

ϵ_θ = the axial flexural strain at the point with radius r, on the top or bottom wall.

It follows that

$$\sigma_\theta \, r = \sigma_{\theta_o} r_o \tag{14}$$

Equating the applied bending moment to the resisting moment at a given section:

$$b \int_{r_i}^{r_o} t \, \sigma_\theta \, dr + \frac{2}{3} b \left[\frac{1}{2} \left(t\sigma_{\theta_o}\right) \left(\frac{b}{2}\right)\right]$$

$$+ \frac{2}{3} b \left[\frac{1}{2} \left(t\sigma_{\theta_i}\right) \left(\frac{b}{2}\right)\right] = M$$

Substituting from Eq. (14) and simplifying

$$\sigma_{\theta_o} = \frac{M}{tb\left[r_o \log_e \frac{r_o}{r_i} + \left(\frac{b}{6}\right)\left(1 + \frac{r_o}{r_i}\right)\right]} \tag{15}$$

After determining σ_{θ_o} from Eq. (15), and knowing that the axial flexural stresses for the top and bottom walls satisfy Eq. (14), and that these stresses vary linearly through the depth, the value of the axial flexural stress at any point of the cross section can be determined.

2.5 Equation for Deflection of an End-Loaded C-Frame

With the simple theory described in Ref. (2), an equation for the total displacement normal to the plane of curvature at any point within the curved portion of the idealized end-loaded C-frame, Fig. (9a), was derived and is given below.

$$\delta_c = \frac{P_h}{4EI}\left\{c\bar{r}^2\left[2\cos\alpha - (\pi - 2\alpha)\sin\alpha\right] + \bar{r}^3(\pi - 2\alpha)\cos\alpha\right.$$

$$\left. + 2\bar{r}\,d^2(1 + \cos\alpha) + 4\bar{r}^2 d\cos\alpha + \frac{4}{3}d^3\right\}$$

$$+ \frac{P_h}{4GJ}\left\{2c\bar{r}^2\cos\alpha - c\bar{r}^2(\pi - 2\alpha)\sin\alpha + \bar{r}^3\left[(\pi - 2\alpha - 4)\cos\alpha\right.\right.$$

$$\left.\left. + 4\sin\alpha + 2(\pi - 2\alpha - 2)\right] + 4\bar{r}\,d(c + \bar{r})(1 - \sin\alpha)\right\} \tag{16}$$

where,

P_h = load applied normal to the plane of curvature; considered positive when directed away from the reader in Fig. (9a).

c, d, are the dimensions shown in Fig. (9a).

$\bar{r}$ = radius of curvature of the axis

EI = flexural rigidity

GJ = torsional rigidity

α = angle in radians, which locates the point where δ is desired (see Fig. 9a). $0 \leq \alpha \leq \frac{\pi}{2}$

δ_c = deflection normal to plane of curvature; positive when it is in the direction of the applied load.

2.6 Determination of Axial Flexural Stresses for Bending in the Plane of Curvature

The problem of determining the axial flexural stresses, σ_θ, in a curved member, where the bending moment at each section is in a plane normal to the plane of curvature, was discussed in Sect. 2.2. For bending in the plane of curvature, the Winkler-Bach formula is used to determine the axial flexural stresses. A derivation of this formula is given in Ref. (3). The formula is summarized here for convenient reference.

$$\sigma_\theta = \frac{M}{A\bar{r}}\left[1 + \frac{1}{Z} \cdot \frac{y}{\bar{r} + y}\right] \tag{17}$$

where,

M = bending moment; positive when it decreases the radius of curvature

y = distance from the centroidal axis of a transverse section; positive when measured toward the convex side of the beam.

$$Z = -\frac{1}{A}\int_{\text{cross-section}} \frac{y}{\bar{r} + y}\, dA$$

A = cross sectional area

2.7 Plate Bending

2.7.1 General. In members such as box-sections that are built up of plate elements, the individual walls have a tendency to bend in their own planes when the members are subjected to torsion. In most cases the effect of this plate bending can be considered as secondary and neglected. However, under certain conditions of support and high torsional loads the effect of plate bending may be of significance.

The approximate analytical studies carried out to determine the effect of plate bending on axial and the transverse flexural stresses in a box section are discussed in this section.

2.7.2 Method of Analysis. Analytical studies to determine the effect of plate bending on stresses in a square box section at the region of high torsion were carried out by considering one wall of the section as a square plate as shown in Fig. (10). In all cases considered the side AD was fixed against deflection and rotation. The effect of a torsional load was produced by considering the deflection surface of the plate to be anti-symmetrical about the center line of the plate and by assigning a unit downward deflection of $F \frac{\lambda^2}{N}$ to the corner B where,

λ = one-tenth the width of the wall, used as grid length in the finite difference equations

$$N = \frac{Et^3}{12\,(1-\mu^2)}$$

E = modulus of elasticity

t = wall thickness

μ = Poisson's ratio

F = the shear resisted by plate action when a torque, T, is transmitted through a section 10λ away from the support. Considering the plate in Fig. (10) as the top wall of the box section, the side walls along AB and DC are assumed to deflect

as end loaded cantilever beams of length 10λ. F is then computed by assuming a uniform shear flow at the section 10λ from the support and by satisfying the condition of equal deflections between top and side walls at points B and C.

Finite difference equations were used to determine the deflection and bending moments in the square plate under various boundary conditions for the sides AB and BC.

2.7.3 Cases Considered. For all problems considered Poisson's ratio, μ, was considered to be zero. The following cases were investigated.

(1) The edge AB was free to rotate, and was forced to assume the elastic line of an end loaded cantilever beam with the end deflection equal to $+ \frac{F\lambda^2}{N}$. Side BC was also free to rotate, but it had a linearly varying deflection curve from $+ F \frac{\lambda^2}{N}$ at B to $- \frac{F\lambda^2}{N}$ at C.

(2) This case was similar to case (1) except that the deflection curve along AB was assumed to be that of a uniformly loaded cantilever beam.

In order to study the interaction between the horizontal and vertical walls of the section, a third case was studied.

(3) The side AB was assumed to rest on a flexible beam without torsional resistance and with the end deflection equal to $+ F \frac{\lambda^2}{N}$ at Point B. The flexural rigidity of the beam was taken equal to one-half the flexural rigidity of the vertical wall. The side BC was assumed free to rotate and to deflect.

After taking into consideration the condition of anti-symmetry of the deflection surface, cases (1) and (2) each required solving 36 simultaneous equations and case (3) required solving 49 simultaneous equations to determine the deflection at each node point.

The results of this analytical investigation are given in Chap. IV.

Chapter III

EXPERIMENTAL INVESTIGATION

3.1 Introductory Remarks

Test results for members of closed thin-walled sections subjected to torsion and bending are not readily available in the literature. This is particularly true for curved members.

The only experimental data that are known to the investigators are those obtained by the sponsor in the full-scale tests of C-frames. These members, however, were of a very complex geometrical configuration such that the test results cannot be fully used for experimental verification of the analytical studies reported in Chap. II.

3.2 Object and Scope of Tests

The object of the tests reported herein was to obtain measurements of strains and deflections in a curved member of square thin-walled cross section having simple geometry. The strain measurements were of primary importance in these tests and were used for the purpose of evaluating the validity of the proposed analytical procedures for determining the transverse and axial flexural stresses. In combination with the data of the previous C-frames, the strain data from these tests can also serve as a guide in extending the approximate analytical methods to more complex structures, such as those of varying radii of curvatures.

Deflections were obtained to provide a means of comparison with the predictions of the simple theory. Although deflections are not of great interest in statically determinate structures, they may be used to determine the distribution of loads to various members in indeterminate structures; also, the design of a member may sometimes be governed by deflection rather than stress or strength considerations.

A detailed description of the test specimen, instrumentation, loading, and the procedures used for data reduction is given in the following sections. The results of these tests are presented and compared with the analytical studies in Chap. IV.

3.3 Test Specimen

The details of the full-scale test specimen are presented in Figs. (11) through (13). All materials were of low-alloy high-strength structural steel meeting the requirements of Specification IE 170, Caterpillar Tractor Company. In order to provide a section of uniform thickness, the specimen was built up of 3/4 in. thick plates assembled by welding as shown in Fig. (11b). The fabrication of the specimen was done by the Caterpillar Tractor Company.

The specimen consisted of a circular curved portion of 32 in. inner and 44 in. outer radii over a quadrant followed, on one side, by a long (114.5 in.) straight moment arm and, on the other side, by a short (11.8 in.) straight portion which was welded to a 1 1/4 in. thick base plate. The long moment arm of the test specimen was closed by another 1 1/4 in. thick plate to which a trunion was welded. Loads were applied only at the trunion. The specimen was bolted through its base plate to a supporting frame (see Sect. 3.4). This connection was designed to simulate as nearly as possible the conditions of a fixed support.

3.4 Supporting Frame

The supporting frame was rectangular in plan as shown in Fig. (18). It was tied down to the laboratory floor by six 2 1/2 in. diameter tie rods, and consisted of a box member built of 2 - 15 in. Channel Sections and 2 - 21 in. x 1 in. plates on which the test specimen was bolted; two 13 ft long members each having 2 - 15 in. channels connected together by 1/2 in. stay plates; and

one 7 ft long member having 2 - 15 in. channels. The 13 ft members rested, on one end, on the 7 ft member and, on the other end, on the box member to which they both were welded to provide more rigidity for the box section. In addition to the members mentioned above, the supporting frame also had two vertical WF members. A 10 WF member was connected to the 7 ft member through a plate and was used to support the horizontal loading equipment. Another WF member, shorter than the former, rested directly on the floor and was centered under the trunion. The latter was used to support the vertical loading equipment.

3.5 Loading Apparatus

The specimen was tested for loads applied perpendicular to the plane of curvature (that is, horizontally), and in the plane of curvature (that is, in the vertical direction). These loads were applied individually, and no simultaneous application of the two loads was considered. In both cases 20-ton capacity hydraulic rams were used for load application.

The arrangement of loading equipment for horizontal loads is presented in Figs. (14) and (19). The hydraulic ram was attached to an adjustable assembly that was kept in contact with the 10 WF vertical member. The other end of the hydraulic ram was connected to a load cell and then the load was applied to the specimen through a ball connection between the load cell and the trunion. In assembling the equipment and during testing, special care was exercised to maintain the line of action of the force in a horizontal direction and concentric with the centerline of the member.

The arrangement of equipment for vertical loading is presented in Figs. (14) and (20). The hydraulic ram, in this case, rested on the top of a WF column. The connection between the ram and the load cell was similar to that for the horizontal loading. The load was transferred from the load cell to

a ball connection and then to the trunion through a curved fitting. By this arrangement, the line of action of the force remained vertical and concentric with the centerline of the member during testing.

3.6 Instrumentation

3.6.1 Load Measurements. The applied loads for both horizontal and vertical loadings were measured using load cells which were designed for a working load of 35 kips. The load cells (electric resistance strain gage load cells) were calibrated in a 120,000 lb. hydraulic universal testing machine. Prior to calibration, they were loaded in excess of their expected working load several times so that all zero shift in the gages which might result from local inelastic action would be eliminated. The load cells had a sensitivity of 134 lb. per dial division on the strain indicator.

3.6.2 Strain Measurements. The locations on the specimen in which strains were measured are shown in Fig. (11a). A total of 144 Type AX-5 SR-4 electric strain gages having a nominal gage length of 7/16 in. and gage factor of 1.97 $\pm$ .01 were used to obtain strain measurements in two mutually perpendicular directions at 72 points of the test specimen. The two strains of interest at each location were parallel and normal to the axis of the member.

The lead wires from the gages were run along the sides of the specimen and connected to a switch board which was in turn connected to a portable strain indicator as shown in Fig. (12). The strain measurements were read from the portable strain indicator.

3.6.3 Deflection Measurements. In addition to vertical and horizontal movements of the corners of the base plate of the test specimen, the movements of the four corners of the member at Sections D, E, and F shown in Fig. (11a), were measured. In the plane of each section the directions of interest for

each corner were the radial direction, and the direction normal to the radius in the plane of the member. All deflections were measured with 0.001 in. dial indicators.

To substantially eliminate the effect of out of plane deformation of the corners on the measured deflections, the dials were mounted on a specially fabricated frame made of 2 x 2 x 1/4 angles, and assembled as shown in Figs. (15), (16), and (17). The frame was anchored to the floor independently of the loading frame, and was held in position so as to act as a fixed reference frame on which the dials were mounted at the levels of the points whose deflections were desired, and parallel to the direction of movements which they were intended to measure.

Two 1/4 in. diameter, 3/8 in. deep holes were drilled and tapped 3/8 in. from the edge of the specimen at each corner whose deflections were to be measured. Piano wire, 0.002 in. in diameter, was used to connect the dials to the corresponding points of the test specimen. It was imperative that the wires remain under sufficient tension during testing. This was accomplished by presetting the dials prior to testing. At each load increment the wires were checked for tightness before recording the corresponding reading. Figure (21) shows the arrangement used to connect the dials to the test specimen by means of piano wire.

3.7 Testing Procedure

The specimen was tested for loads applied perpendicular to the plane of curvature (horizontally), and in the plane of curvature (vertically). These loads were applied individually, and no simultaneous application of the two loads was considered. The horizontal loading was of primary importance for this investigation. Because this type of loading produces bending and torsion in the

curved portion of the specimen, whereas, vertical loading causes bending only, and under this latter type the specimen is expected to behave as a curved beam.

Prior to recording data for any one of the loading conditions described above, the specimen was loaded to the maximum test load several times in order to eliminate the effects of residual stresses, and zero-shift in gages which might result from local inelastic action. During these preliminary loadings, the strains at several locations of the specimen which were expected to be stressed most, were recorded for each increment of load.

There were two tests for horizontal loading; hereafter, called Tests 1 and 2 for brevity. In Test 1 the horizontal load was increased from zero to 16 kips in increments of 4 kips and decreased from 16 kips to zero in the same increments. Readings for all strain gages and all dial indicators were recorded for all load levels. In Test 2 the horizontal load was increased from zero to 16 kips in increments of 4 kips, and decreased from 16 kips to zero in increments of 8 kips. Since this test was planned primarily to provide data on deflections, no strain gage readings were taken, and the dial indicator readings were recorded only for the base and Sections D, E, and F.

There was only one test for vertical loading, hereafter called Test 3. Since a preliminary study had indicated that the allowable load in the vertical plane is governed by the capacity of the base plate of the specimen and that this load must not exceed 9 kips, the vertical load in Test 3 was increased from 0 to 8 kips in increments of 4 kips and decreased to zero with the same increments. Readings for all strain gages were taken for all load increments. Dial indicator readings, however, were not recorded in this test because of excessively large base movements.

3.8 Data Reduction

3.8.1 Determination of Stresses. For each gage location, the recorded strain readings at the same load level during loading and unloading cycles were averaged. From these average readings the values of the transverse flexural strain, ϵ_r, and the axial flexural strain, ϵ_θ, were determined. Recalling that the state of stress at any point is two dimensional, Hooke's relationships were used to determine the transverse and axial flexural stresses from the strains. Hooke's law for a two dimensional state of stress reads:

$$\sigma_r = \frac{E}{1 - \mu^2} (\epsilon_r + \mu \epsilon_\theta),$$

$$\sigma_\theta = \frac{E}{1 - \mu^2} (\epsilon_\theta + \mu \epsilon_r). \tag{18}$$

In applying Eqs. (18) to determine the experimental values of stresses from the measured strains, the following values of E and μ were used: E = 30,000 ksi; μ = 0.30.

3.8.2 Effect of Base Rotations on Deflections. The support of the test specimen moved during testing, as it had been predicted. It translated in the direction of the axes X_1, X_2, and X_3, shown centered on the base plate in Fig. (22a), and also it rotated about the three axes. The translation of the base was not significant, and its effects on the measured deflections could be neglected. The rotations of the base about the three axes, however, affected the magnitudes of the measured deflections significantly. In order to correct the measured deflections of the various points on the test specimen for the rotation of the support the following procedure was employed:

In Fig. (22a) let θ_1^0, θ_2^0, and θ_3^0 denote the rotations about the axes X_1, X_2, and X_3, respectively, which are produced at the center of the base plate

due to the movement of the support; the positive directions of these rotations are as indicated in Fig. (22b). For each load level, the rotations θ_1^0, θ_2^0, and θ_3^0 were calculated from the measured deflections of the base plate, Fig. (22a). Determination of θ_1^0 for a specific load level will be explained in detail, as an example. Dividing the difference in the elevations of the points A_1, A_2 and A_3, A_4 by the distances between these points two angles of rotation, θ_1^{OE} and θ_1^{OW}, about the axis X_1 were obtained. The average of angles θ_1^{OE} and θ_1^{OW} was taken to be the angle of rotation of the support about axis X_1, namely, θ_1^0, for the load level in question. The values of the θ's thus computed are given in Table (B.4).

After computing the values of the θ's for each load level, the rigid body displacements produced at any point, P, on the test specimen in directions y_2 and y_3, Fig. (22c), due to these base rotations were computed from Eqs. (19) derived using matrix algebra as described in Ref. (4):

$$\delta^P_{y_2} = - X_3(\theta_1^0 \sin \varphi + \theta_2^0 \cos \varphi) + \theta_3^0(X_1 \sin \varphi + X_2 \cos \varphi),$$

$$\delta^P_{y_3} = X_2\, \theta_1^0 - X_1\, \theta_2^0 \,. \qquad (19)$$

where,

$\delta^P_{y_2}$, $\delta^P_{y_3}$ = rigid body displacements produced at point P in directions y_2 and y_3, respectively.

φ = position angle shown in Fig. (22c).

X_1, X_2, and X_3 = cartesian coordinates of the point P referred to the set of X-axes at point O, i.e., center of the base plate.

The above formulation provides a means of making a correction due to base movements. The deflection at point P in direction y_i related to the fully fixed support condition is therefore:

$$\Delta^{P}_{y_i} = \Delta^{P}_{y_{im}} - \delta^{P}_{y_i}, \quad i = 2, 3 \tag{20}$$

where

$\Delta^{P}_{y_i}$ = deflection at point P in direction y_i related to the fully fixed support condition

$\Delta^{P}_{y_{im}}$ = the measured deflection at point P in direction y_i

Equations (19) and (20) were used to determine, with respect to the fully fixed support condition, the deflections at the corners of the test specimen at sections D, E, and F.

3.8.3 Determination of Centerline Deflections. In order to determine the horizontal displacement of the centerline of the test specimen at Sections D, E, and F, for different loads, an 11.25 in. x 11.25 in. square was considered. The measured corner deflections of the test specimen corresponding to each load level, which had been corrected to the fully fixed support conditions, were assumed to exist at the corners of this square. The center of the deformed section was assumed to coincide with the intersection of the diagonals of the square. The equations of the diagonals of the deformed square with respect to an arbitrary set of axes were written, and the coordinates of their point of intersection was determined. The deflection of the center at the section in question was determined from the knowledge of the coordinates of the center in the deformed and undeformed states. This analytical approach was found to be more reliable in determining the center line deflections than a graphical construction.

In order to obtain a better understanding of the deformations which take place in the member, the changes in the lengths of the diagonals of the member at Sections D, E, and F were also computed.

3.8.4 Determination of Centerline Rotations. By the angle of twist at any section is meant the angle through which the square section rotates as a rigid body about an axis passing through the center of the section and perpendicular to the plane of the section. This angle could not be determined directly from the measured displacements of the corners of the specimen; instead, the change in directions of the diagonals relative to their original directions was determined. These changes in the directions of the diagonals were averaged, and the average change was taken as a measure of the rotation of the section in question.

The square, after its corners were displaced, assumed a distorted configuration. This distortion may cause a further change in the direction of the diagonals. To correct for the distortional rotations of the diagonals the following procedure was used:

In a perfect square the angles between a diagonal and the adjacent sides are 45°. It follows that if the square were rotated about its center without distortion the angles between a diagonal and the adjacent sides would still be 45°. The angles between diagonals and the adjacent sides, in the 11.25 in. x 11.25 in. square whose corners were moved similar to those of the test specimen, however, were not 45°. To account for this distortional effect, the following procedure was used.

An 11.25 in. x 11.25 in. square ABCD, Fig. (23) was considered and its corners were displaced to assume the dotted configuration A'B'C'D' corresponding to one section of the test specimen at a particular value of the test load. Concentrating on one diagonal only, for the purpose of illustration, the angle between lines DB and D'B' was determined from their slopes. This angle was called the apparent rotation of diagonal DB. The angles C'B'D', A'B'D', A'D'B', and C'D'B' were also determined. These were found to be

different from 45°, which value they would have had if there was no distortion. Then, it was determined through what angle, α, the line O'B' must rotate about point O' to make the angle O'B"C' = 45°. Similarly, angles β, γ, and ξ were determined which would make the angles O'B"A, O'D"C', and O'D"A' all 45° angles. The angles α, β, γ, and ξ were averaged algebraically and this average value was applied as the distortional correction to the apparent angle of rotation determined for diagonal DB. The angle of rotation for the diagonal AC was determined in a similar manner. The angles thus obtained were averaged and considered as a measure of the rotation of the section. This type of computations was carried out only for one load level, $P_h = 12^k$, each in Tests 1 and 2.

Chapter IV

PRESENTATION AND DISCUSSION OF RESULTS

4.1 Introductory Remarks

The results of the experimental investigation are presented and compared in this chapter with the results of analytical investigation. Most of the results are shown in Figs. (25) through (45). All the experimental and analytical results are also presented in Tables (B.1) through (B.9) of Appendix B.

A three-dimensional schematic representation of the test specimen is shown in Fig. (24). The four walls of the specimen are called top, bottom, inner, and outer walls, respectively. At any section the radius varies from point to point on the top and bottom walls, whereas it is constant for points on the inner and outer walls. Letters B through G are used to identify the six sections along the test specimen at which strains were measured. Sections B and F are at the points of tangency; sections C, D, and E are within the curved segment, and section G is along the straight arm of the test specimen, 16 in. from the point of tangency. At each section the strain gages were placed on 12 points numbered 1 through 12, to measure the strains in the transverse and axial directions, Fig. (11a).

4.2 Results for Loads Applied Normal to Plane of Curvature, P_h

The behavior of the test specimen under loads normal to the plane of curvature, applied at the trunion, was of primary importance in this investigation. Under this type of loading, the sections in the curved portion of the test specimen were subjected to both torsional and bending loads. The values of the measured and computed stresses, and deflections for this type of load are presented and compared in the following sections.

4.2.1 Comparison of Experimental and Computed Transverse Flexural Stresses. Experimentally determined values of the transverse flexural stresses at the gage points of the test specimen at various sections are plotted in Figs. (25) through (29) for several values of P_h. Also shown in these figures are the corresponding values of the transverse flexural stresses determined by the approximate analytical procedure described in Sect. 2.2.2. The strain gage in the transverse direction at point 6 of section E was found to be loosely bonded after the completion of tests. The experimental points corresponding to this gage are indicated in Fig. (28); however, they were disregarded when plotting the experimental curves. The computed stresses were determined using the following dimensions: r_i = 32 in., r_o = 43.25 in., and b = 11.25 in.

The agreement between the experimental and computed curves in Figs. (25) through (29) at sections C, D, and E indicates a good correlation between the behavior of the curved box member under torsional and bending loads and the assumptions underlying the approximate method of analysis described in Sects. 2.2.1 and 2.2.2. The stresses at the midpoints of the sides, that is, points 2, 5, 8, and 11, Fig. (29), are of negligible magnitudes as predicted by the method of analysis.

The computed stresses were invariably greater than the measured values, and this overestimation of the stresses is probably due to the fact that the walls of the box section, which actually behave as plates, are assumed to act as beams in the analytical procedure.

At the points of tangency, (sections B and F), the curvature of the axis becomes discontinuous. This discontinuity in curvature, in addition to the plate bending action, may affect the stress behavior in the neighboring sections, and account for the deviation observed between the experimental and

computed curves of section E. It should be noted that the computed stresses at sections B and F, the points of tangency, were obtained by dividing the theoretical stresses by 2 as it was suggested in Sect. 2.3 and give results which are in fair agreement with the measured stresses. Hence the factor of 1/2 as described in Sect. 2.3 is recommended for tangent sections.

At section G, located in the straight portion, the measured transverse flexural stresses are relatively small, but definitely different from zero. By extrapolating the experimental curves it is seen that the transverse flexural stresses reduce to zero at a distance about $1\frac{1}{2}$ b to 2 b from the point of tangency.

The variation of the experimental transverse flexural stresses along the perimeter of each section is shown in Fig. (30) for $P_h = 12^k$. The ordinates drawn by heavy lines in this figure represent the measured values of the stresses. It is observed that at any given section the peak transverse flexural stresses occur at the corners with the absolute maximum values occurring at the corners of the inner wall, as predicted by the method of analysis. The variations of the stresses, drawn on the basis of measured values, appear to be approximately linear across the width and through the depth of the cross sections, which is also in agreement with the analysis.

To obtain a measure of the amount by which the predicted stresses overestimate the measured stresses, Table (B.1) is prepared. In this table the absolute values of the ratio $\frac{\sigma_{rm}}{M/rt^2}$ are given for points located 4 inches from the midpoint on all four walls of the box at sections C, D, and E for $P_h = 4$, 8, 12, and 16 kips. The stress, σ_{rm}, denotes the measured value of the transverse flexural stress; r is the radius of the point in question; M is the bending moment at the section, and t is the wall thickness. The experimental average value of this ratio for all the points considered is

$$\left[\frac{\sigma_{rm}}{M/rt^2}\right]_{ave.} = 0.418 \qquad (21)$$

It can be shown that the theoretical value of this ratio for the points considered is 0.533. Let η denote the distance measured from the midpoint to any point on the top wall. As explained in Sect. 2.2.2, the quantity (m.r) varies linearly from $+m_i r_i$ to $-m_o r_o$ on the top wall, Fig. (8). Therefore, the transverse flexural moment per unit width at a point η from the center of the top wall is given by

$$m_\eta = \frac{2\eta}{b} m_i \frac{r_i}{r_\eta}$$

Substituting from Eq. (8)

$$m_\eta = \frac{2\eta}{b} \frac{M}{8r_\eta}$$

Similarly for a point located at η from the center of the wall, on inner and outer walls we have

$$m_\eta = \frac{2\eta}{b} \frac{M}{8r_i} ,$$

$$m_\eta = \frac{2\eta}{b} \frac{M}{8r_o} .$$

It follows that the following relationship is true for the points on all walls

$$m_\eta = \frac{2\eta}{b} \frac{M}{8r} \qquad (22)$$

where r = radius at the point in question. The peak value of the transverse flexural stress at the point, without regard to sign, threfore is

$$\sigma_{r\eta} = \left[\frac{2\eta}{b} \frac{M}{8r}\right] \left(\frac{6}{t^2}\right).$$

when $\eta = 4$ in.

$$\left[\frac{\sigma_r}{M/rt^2}\right] = \frac{(12)\ (4)}{8b} = \frac{(12)\ (4)}{(8)\ (11.25)} = 0.533 \qquad (23)$$

From Table (B.1) it is also seen that the maximum and minimum values of the above ratio for the experimental results are: 0.500 and 0.346, respectively.

All of the experimentally determined values of the transverse flexural stresses referred to above are given in Table (B.2) for all values of test loads. Also given in this table are the computed values of the transverse flexural stresses for $P_h = 16^k$.

4.2.2 Comparison of Experimental and Computed Axial Flexural Stresses. Experimentally determined values of the axial flexural stresses at various sections are plotted in Figs. (31) through (34) for several values of P_h. Also shown in these figures are the corresponding values of the computed axial flexural stresses. The axial flexural stresses were computed using two procedures.

(1) The semi-empirical formula, Eq. (13), was used to determine stresses at sections C, D, and E. After several trials, the value of "a" in this formula was selected to be 8.625, which gives computed stresses that compare closely with the maximum measured stresses. It must be remarked that the semi-empirical formula is applicable only at the sections within the curved portion of the test specimen and for the particular member used in this investigation.

(2) Equation (15), which is derived on the basis of the "plane-section" assumption, was used to determine the axial flexural stresses at all sections.

In computing the axial flexural stresses the following values of inner and outer radii were used: $r_i = 32$ in., $r_o = 43.25$ in.

Measured values of the axial flexural stresses along the perimeter of each section are shown in Fig. (35) for $P_h = 12^k$. From Fig. (35) it is clear that the stress behavior exhibited at sections within the curved portion, sections C, D, and E, is different from the stress behavior at sections B and F, the points of tangency, and section G located in the straight portion of the test specimen. The stress distribution at section G, which was subjected only to bending moment, conforms with the stress distribution predicted by the plane section assumption. Within the curved portion, because of prevention or restriction of warping at various sections, combined with the variation in twisting moment, and unequal lengths of longitudinal fibers, normal axial stresses were induced and are superimposed on the stresses predicted by the plane-section formula. The stress behavior at the points of tangency is a transition from the behavior observed in the curved portion to that observed at section G.

Referring to Figs. (31) through (34) one may see that the stresses computed from the "plane-section" assumption underestimate considerably the corresponding measured stresses in the curved portion. The measured stresses are at some points twice as high as the computed stresses, and at points on the outer wall the measured stresses have signs that are opposite to the stresses computed from the "plane-section" assumption. At sections C, D, and E, where the semi-empirical formula is applicable, the stresses computed from this formula provide better correlation with the measured stresses; however, these values also underestimate slightly the maximum measured axial flexural stresses.

The results presented in this section emphatically indicate a need for a method of analysis to determine the axial flexural stresses in curved members of closed thin walled sections under combined bending and torsional loads. A more rigorous study of this problem is beyond the scope of the present

investigation. The semi-empirical formula was used to obtain a better correlation with the measured stresses in the test specimen. Additional study of this problem is certainly desirable.

Experimentally determined values of the axial flexural stresses are given in Table (B.3) for all values of test loads. Also given in this table are the computed values of the axial flexural stresses for $P_h = 16^k$.

4.2.3 Deflection Results. The experimentally determined values of angle-of-rotation at the base of the test specimen are given in Table (B.4). These values were used in Eqs. (19) to determine the effects of base movement on the measured corner deflections at sections D, E, and F of the test specimen. After reducing the measured corner deflections to the fully fixed support condition, the procedure described in Sect. 3.8.3 was used to obtain the centerline deflections at sections D, E, and F. These values are given in Table (B.5). Also given in this table are the values of the centerline deflections computed from the simple theory given by Eq. (16). The computed changes in the diagonal lengths of an 11.25 x 11.25 square hollow section subjected to the measured corner deflections of the test specimen after these deflections were reduced to the fully fixed support condition, are summarized in Table (B.7).

It is seen from Table (B.7) that the diagonal D_1 shortens, whereas D_2 lengthens under torsional and bending loads. This type of deformation is to be expected at each of the sections under the loadings imposed at the trunion. As it was pointed out in Sect. 2.2.2, the distribution of the stresses and the geometry of the sections are such that, in effect, radial forces are produced in the top and bottom walls which act in opposite directions. Under this type of loading, D_1 is expected to shorten, whereas D_2 is expected to lengthen.

Computed and experimentally determined centerline deflections are presented in Table (B.5), which show that the values predicted by the simple

theory are of the same order of magnitude as the experimentally determined values; the higher values agree closely with the corresponding experimental values. It must be emphasized, however, that there is no means of assessing the total errors involved in the measured values of the corner deflections, from which the centerline deflections were deduced. Therefore, it is not possible to arrive at any definite conclusion regarding the validity of the simple theory, other than to indicate that it will give values that will agree with measured values to within an order of magnitude.

The centerline rotations determined from the corrected corner deflections of sections D, E, and F for $P_h = 12^k$ were determined using the procedure described in Sect. 3.8.4 and are given in Table (B.6).

4.3 Results for Loads in the Plane of Curvature, P_v

Under this type of loading, the sections of the test specimen were subjected only to the bending in the plane of curvature. The results are summarized in the following sections.

4.3.1 Comparison of Experimental and Computed Axial Flexural Stresses. Experimentally determined values of the axial flexural stresses at various sections are plotted in Figs. (36) through (38). Also shown in these figures are the corresponding values of the stresses computed from the Winkler-Bach formula, Eq. (17). The following values of R and Z were used in this formula: R = 37.63 in., Z = 0.143. The variations of the experimental stresses along the perimeter of each section are shown in Fig. (39) for $P_v = 8^k$.

From Fig. (39) it is seen that the stresses are not constant across the inner and outer walls, as predicted by the Winkler-Bach formula. The measured stresses at the midpoints of the walls are smaller than those at the corners. In a box member composed of thin plate elements, because of the

stiffness at the corners, this behavior is to be expected. However, in general the measured and computed stresses are in fair agreement.

Experimentally determined values of the axial flexural stresses are given in Table (B.8) for all values of the test loads. Also given in this table are the computed values of these stresses for $P_v = 8^k$.

4.3.2 Experimental Transverse Flexural Stresses. Experimentally determined values of transverse flexural stresses at various sections are plotted in Figs. (40) and (41) and are also tabulated in Table (B.9). The variations of these stresses along the perimeter of each section are shown in Fig. (42). There is no simple procedure available for computing these stresses, which are primarily a result of bending in the plane of the individual walls.

From Fig. (42) it is seen that the transverse flexural stresses are negligible at the corners of the box, and their peak values occur at the midpoints of the walls. Such a stress behavior is to be expected from the plate action of each wall.

4.4 Effect of Plate Bending on Stresses

Curves of variation of bending moments in the x and y directions for cases 1, 2, and 3 (see Sect. 2.7.3) are shown in Figs. (43), (44) and (45), respectively. From these figures it is seen that the magnitudes of bending moments in the y-direction (transverse) are negligible. On the other hand, the bending moments in the x-direction could add a sizeable value to the axial flexural stresses. For example, the maximum stresses due to plate bending in the straight portion near the support of the test specimen in Fig. (11a) for a load of 16 kip applied at the trunion, are: 2.7 ksi, 3.7 ksi, and 2.7 ksi for cases 1, 2, and 3, respectively, which are therefore in the order of 30% of the values predicted by the "plane-section" assumption.

Chapter V

SUMMARY AND CONCLUSIONS

The major part of this research study was concerned with the behavior of curved members of closed thin-walled sections under combined torsional and bending loads. Analytical and experimental studies were involved; the experimental work being primarily concerned with verifying the analytical developments.

The objectives of the analytical studies were to develop formulas for estimating the stress condition at any point in a curved member of box section. The formulas were intended for design purposes and are thus made as simple as possible. These formulas and the assumptions underlying their development were verified by testing a full-scale member under simulated loading conditions.

Both the analytical and experimental results show that the dominant component of the stress in such members is the transverse flexural stress, σ_r, which is caused by the distortion of the cross section. In this respect the computed stresses agree very well with the measured values, and are always on the safe side. The higher values of such a stress occur at the corners of the section with the maximum values occurring at the two inner corners.

The axial flexural stresses, σ_θ, were computed from a formula based on the "plane-section" assumption for points within the curved portion of the test specimen. By direct comparison of the computed stresses with the corresponding experimental values, it was concluded that for points within the curved portion, the stresses computed on the basis of the "plane section" assumption do not agree with the experimental values. In a curved member of non-circular cross section, because of prevention or restriction of warping at various sections, combined with variable twisting moment and unequal lengths of

the longitudinal fibers, additional stresses are induced which are superimposed on the stresses predicted by the "plane-section" formula. A semi-empirical formula was presented which provides a better correlation with the test results. It is also pointed out that the stresses computed from this formula underestimate slightly the maximum measured values. A more rigorous study of this problem was beyond the scope of the present investigation; however, additional study of this problem is desirable.

The effect of plate bending on stresses near the support of the test specimen (region of high torsional load) was investigated. It was shown that the transverse flexural stresses are not affected significantly by plate bending; however, the effect of plate bending is to increase the computed axial flexural stresses by about 30%.

Translational displacements of the center line of the member, as predicted by a simple linear theory, agree reasonably well (at least to within an order of magnitude) with the measured values after corrections were made for base movements.

The specimen was also tested for loads in the plane of curvature. These tests were of secondary importance in the present investigation. It was shown that the measured axial flexural stresses verify the stresses predicted by the Winkler-Bach formula. However, the walls of the member behave as plate elements and the measured transverse flexural stresses at midpoints of the walls were of the same order of magnitude as the computed axial flexural stresses.

The transverse flexural stresses are usually negligible in structural members of open cross-sections, such as I-beams or channels. Such a stress, however, turns out to be the predominant component in members of closed square thin-walled sections. The design of structural members of this type of

cross-sections, therefore, requires a workable formula for predicting this stress component. The major contribution of this research study is the development of a formula for such purposes, and a critical evaluation of other existing formulas for estimating the other components of a stress tensor in members of the type considered. It was concluded also that the conventional formula for calculating the axial flexural stress is not applicable for curved members.

REFERENCES

1. Cutts, C. E., "Horizontally Curved Box Beams," Trans. ASCE, Vol. 118, pp. 517-528, 1953.

2. Pippard, A. S. J., Studies in Elastic Structures, Edward Arnold and Co., London, 1952, Chapt. 9.

3. Seely, F. B., and Smith, J. O., Advanced Mechanics of Materials, John Wiley and Sons, Inc., 2nd Edition, 1957, Chapt. 6.

4. Shore, S., "The Elements of Matrix Structural Analysis," Proc. 2nd Conf. on Electronic Computation, pp. 145-164, Sept. 8-9, 1960.

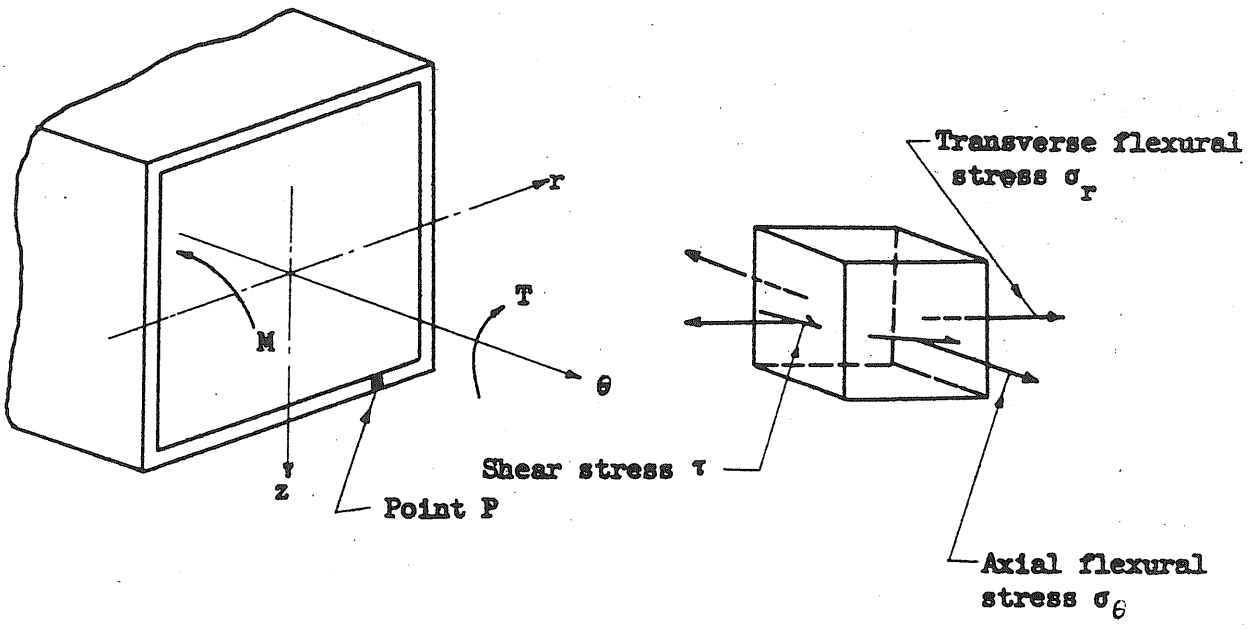

FIG. 1 STATE OF STRESS AT A POINT

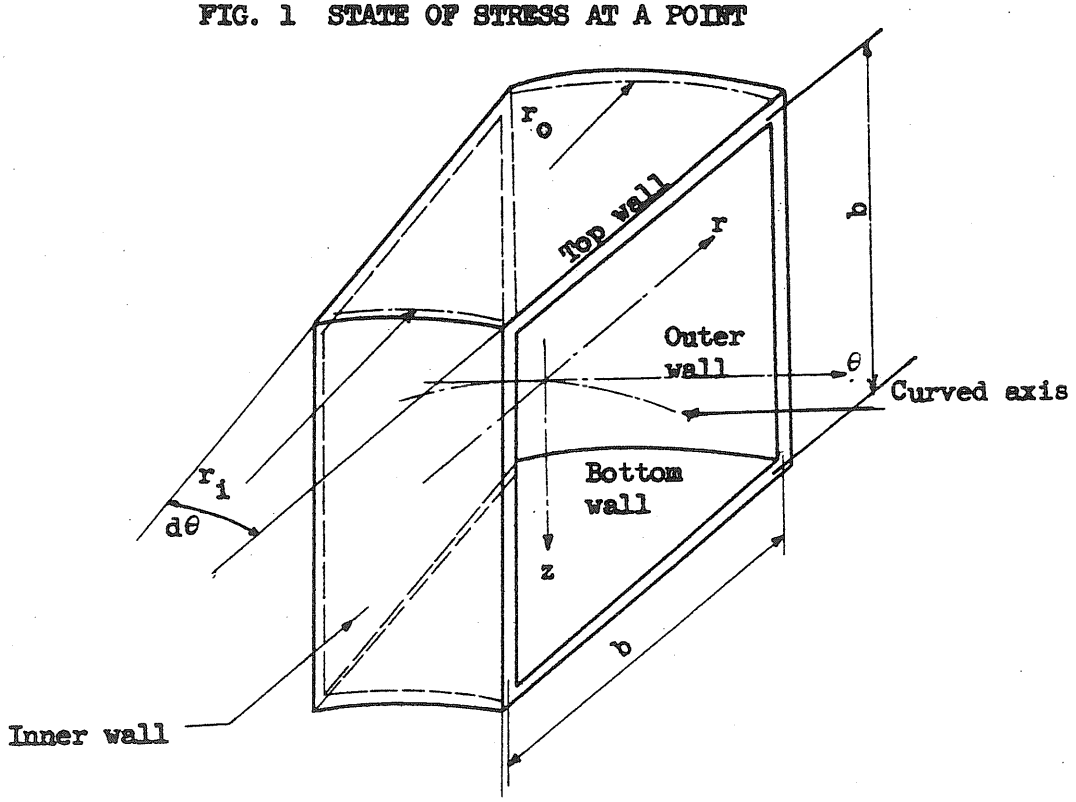

FIG. 2 CIRCULAR ELEMENT

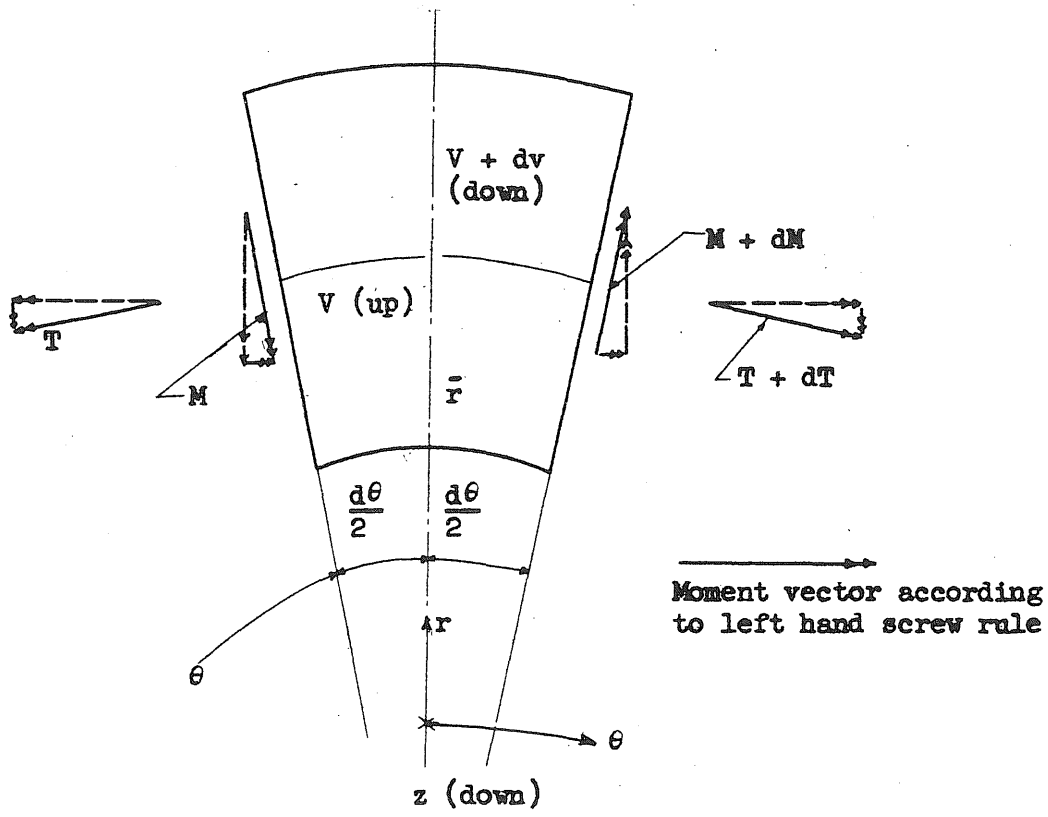

FIG. 3 FREE-BODY DIAGRAM OF CIRCULAR ELEMENT IN PLAN

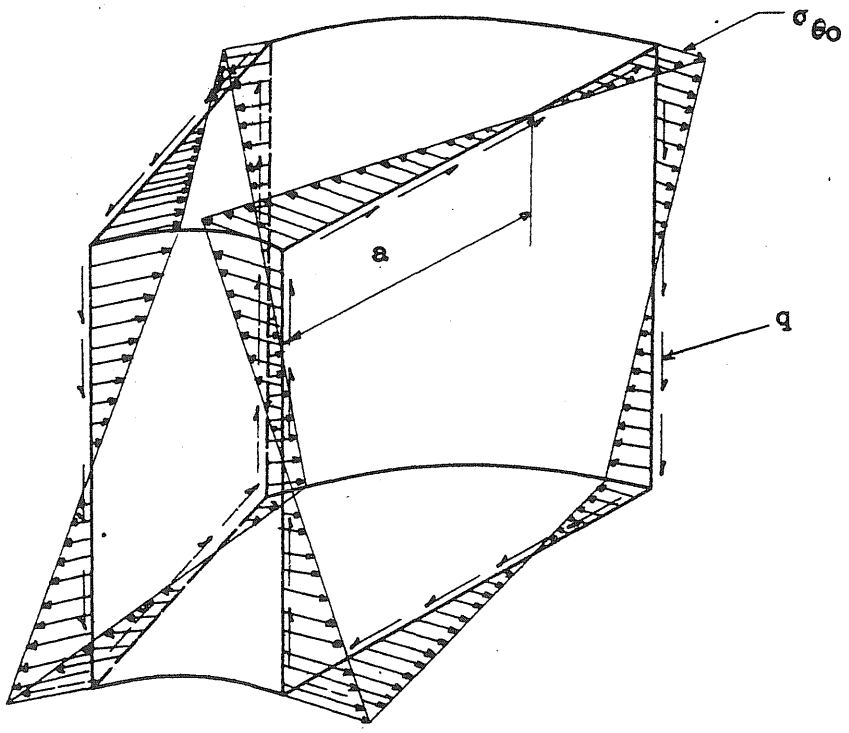

FIG. 4 AXIAL FLEXURAL STRESSES AND SHEAR FLOW ACTING ON THE CIRCULAR ELEMENT

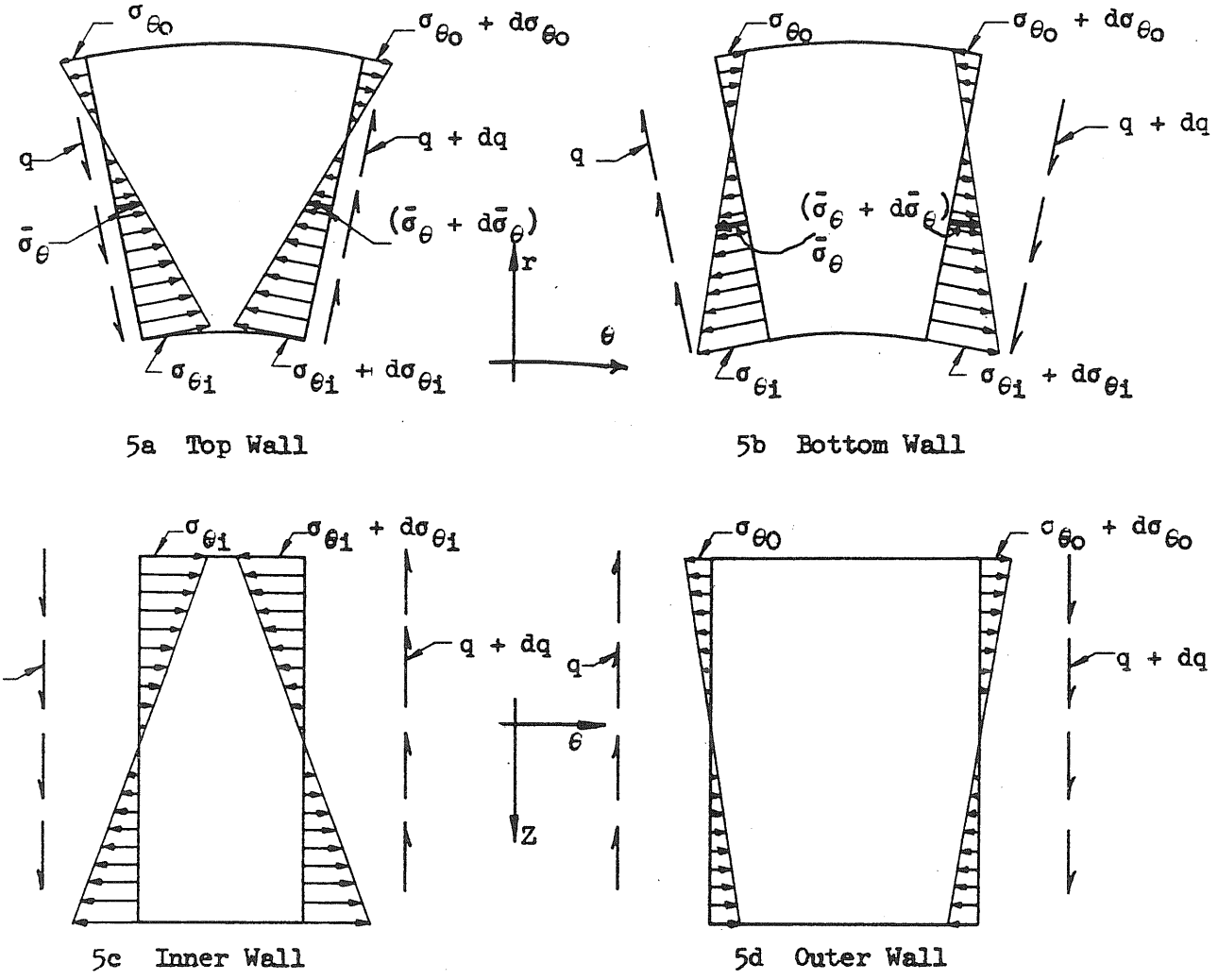

FIG. 5 FREE-BODY DIAGRAMS FOR WALLS OF CIRCULAR ELEMENT

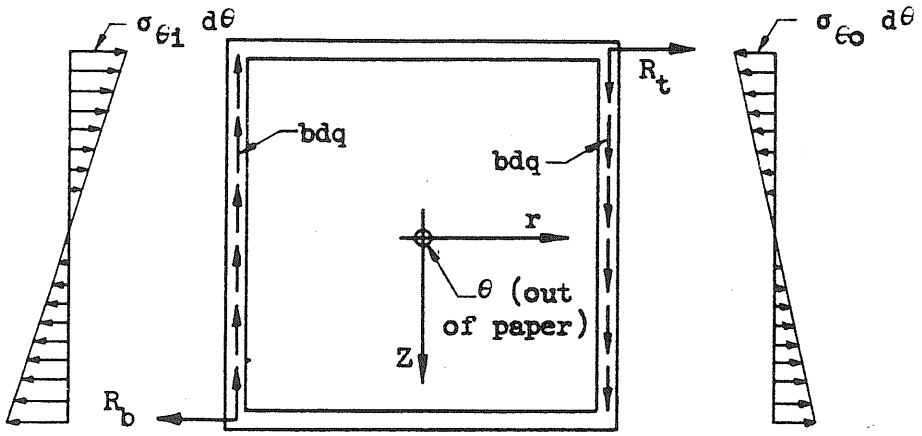

FIG. 6 SIDE VIEW OF CIRCULAR ELEMENT

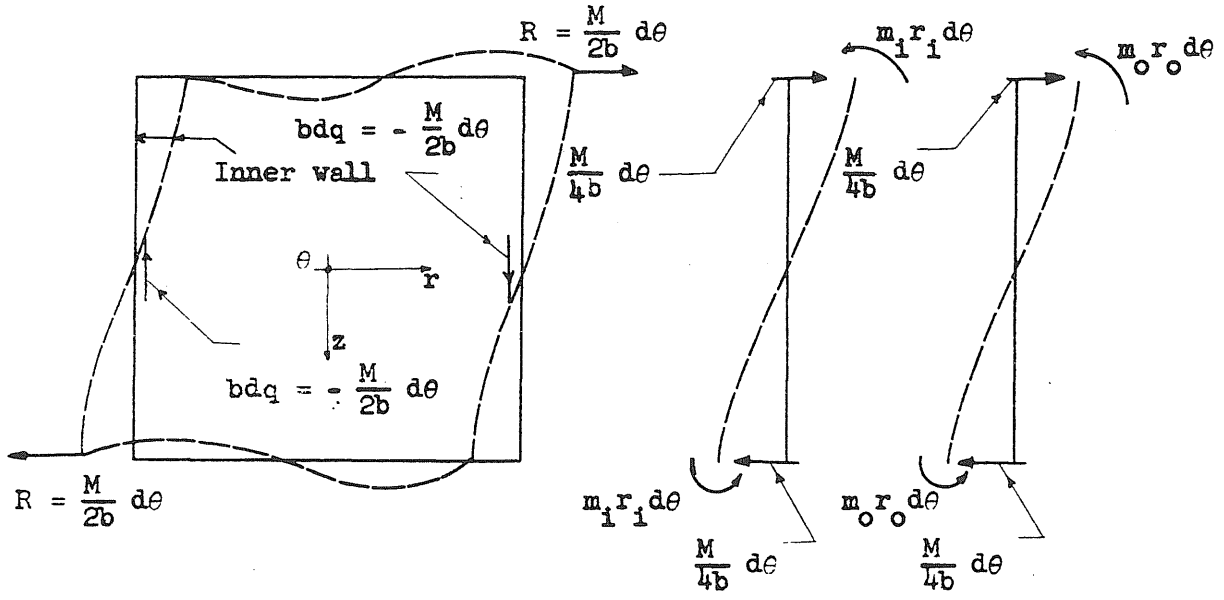

7a REPLACEMENT FRAME

7b FREE-BODY DIAGRAMS FOR INNER AND OUTER MEMBERS

FIG. 7

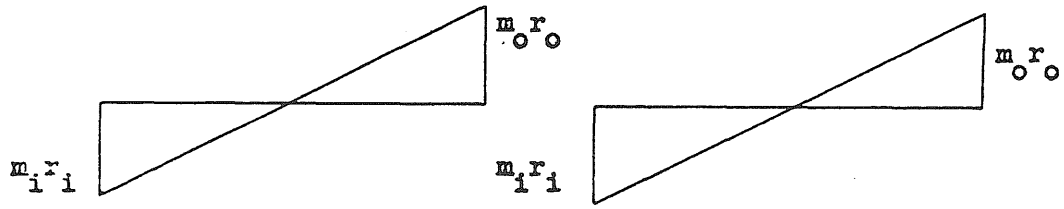

8a TOP WALL

8b BOTTOM WALL

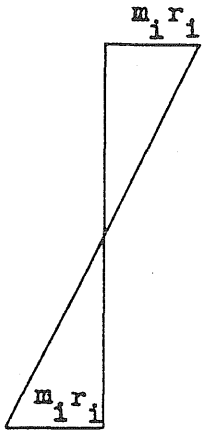

8c INNER WALL

8d OUTER WALL

FIG. 8 DISTRIBUTION OF TRANSVERSE FLEXURAL MOMENT IN VARIOUS WALLS

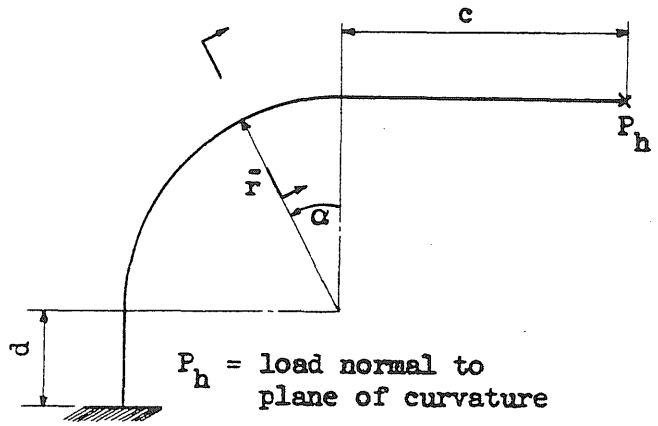

9a IDEALIZED C-FRAME

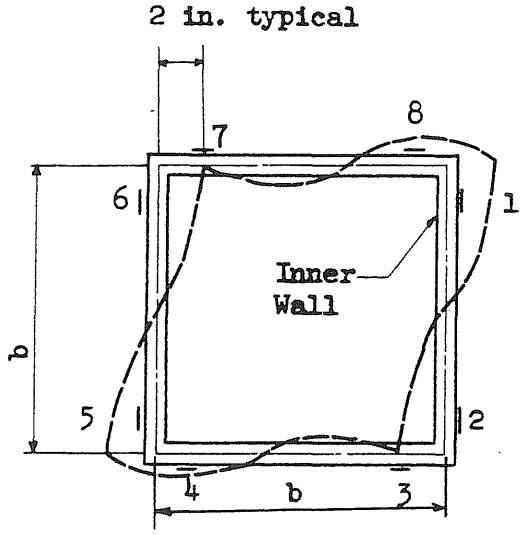

9b TYPICAL SECTION

FIG. 9

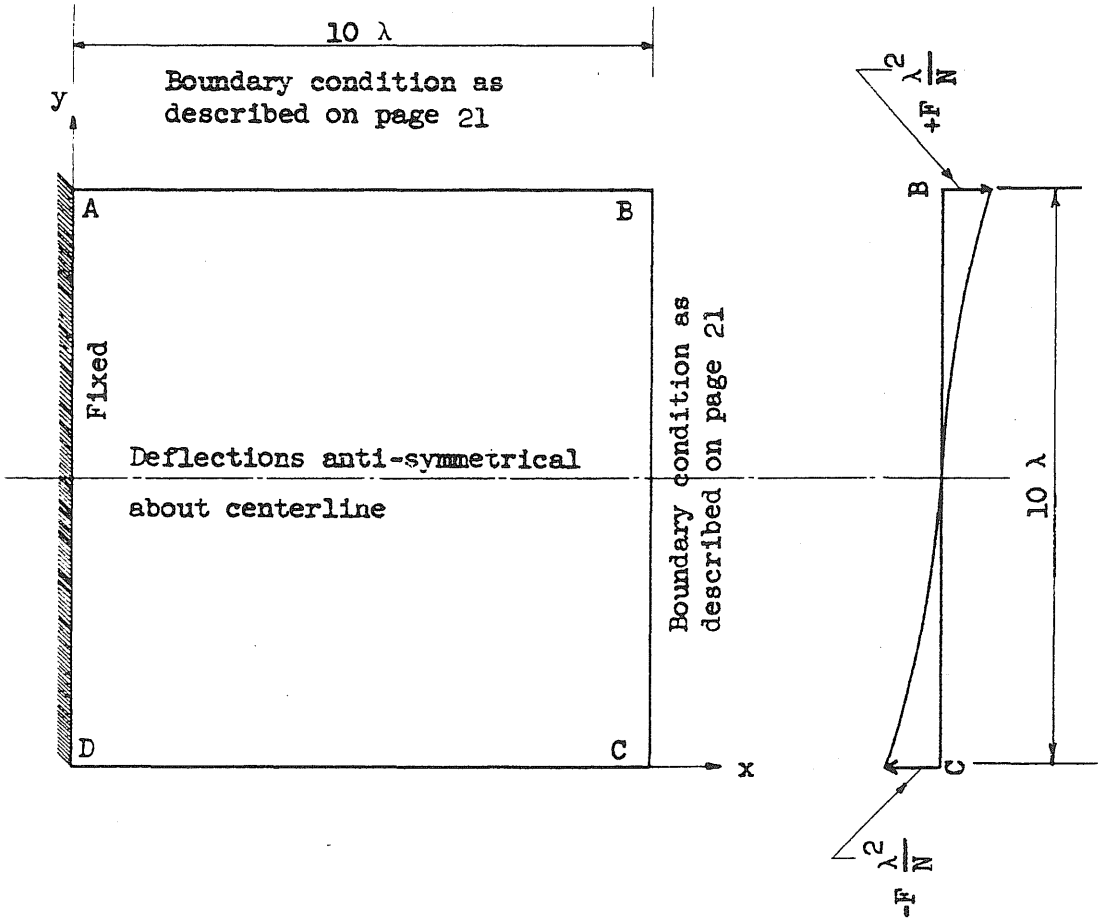

FIG. 10 SQUARE PLATE USED TO INVESTIGATE EFFECT OF PLATE BENDING

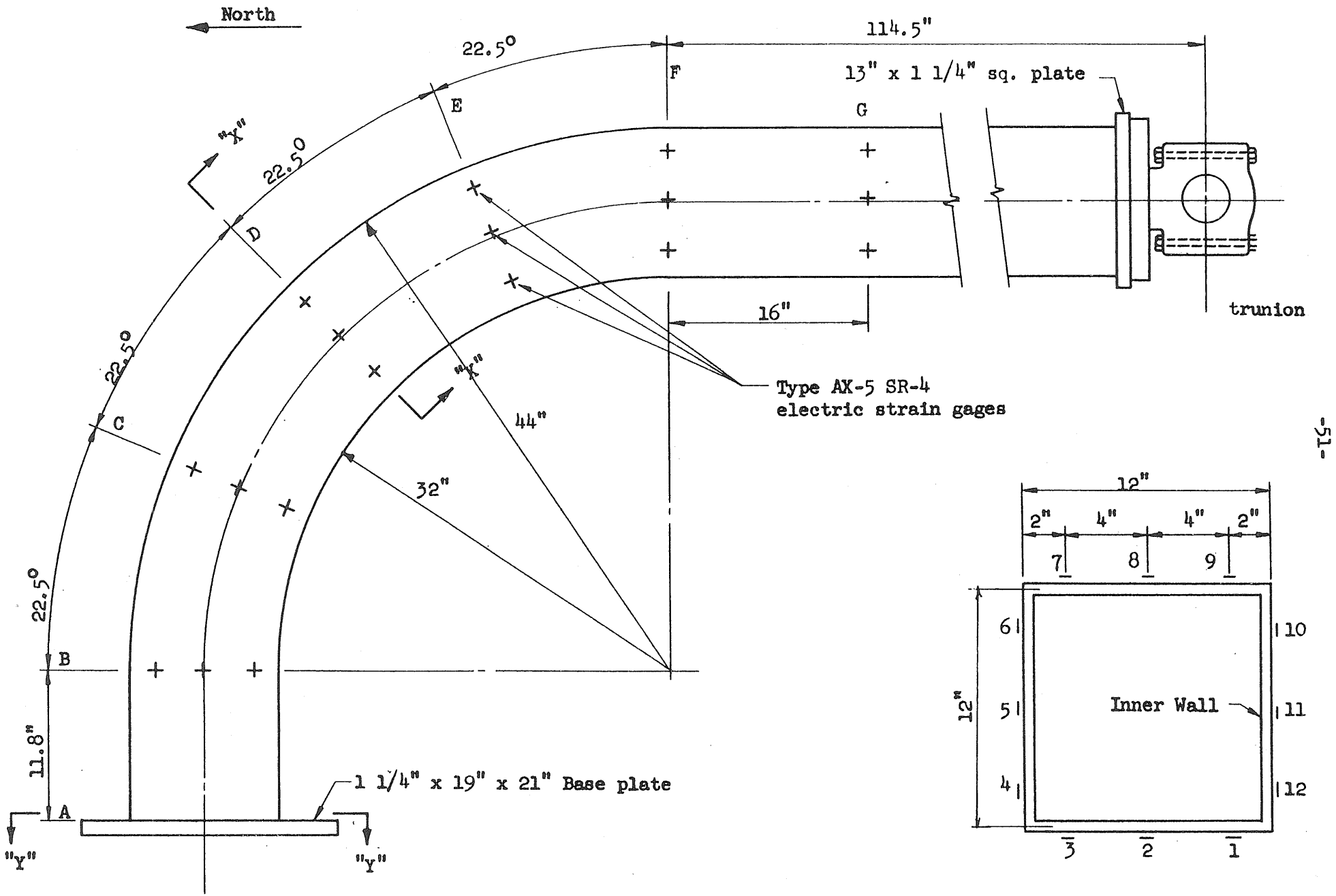

FIG. 11a TEST SPECIMEN SHOWING POSITIONS OF GAGE POINTS

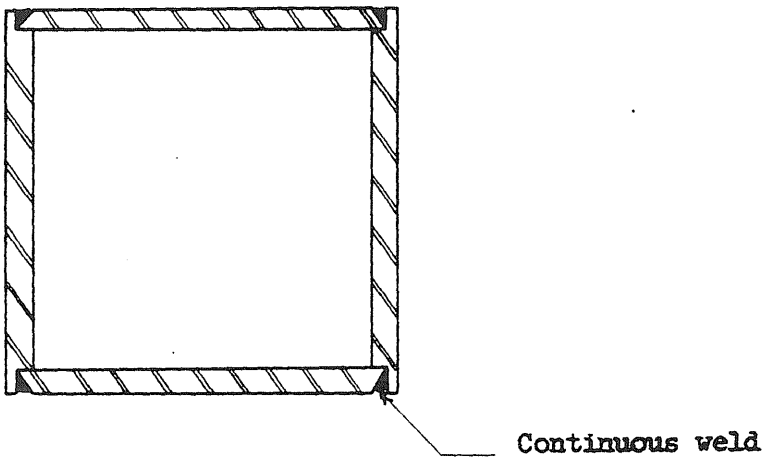

Section "X-X"

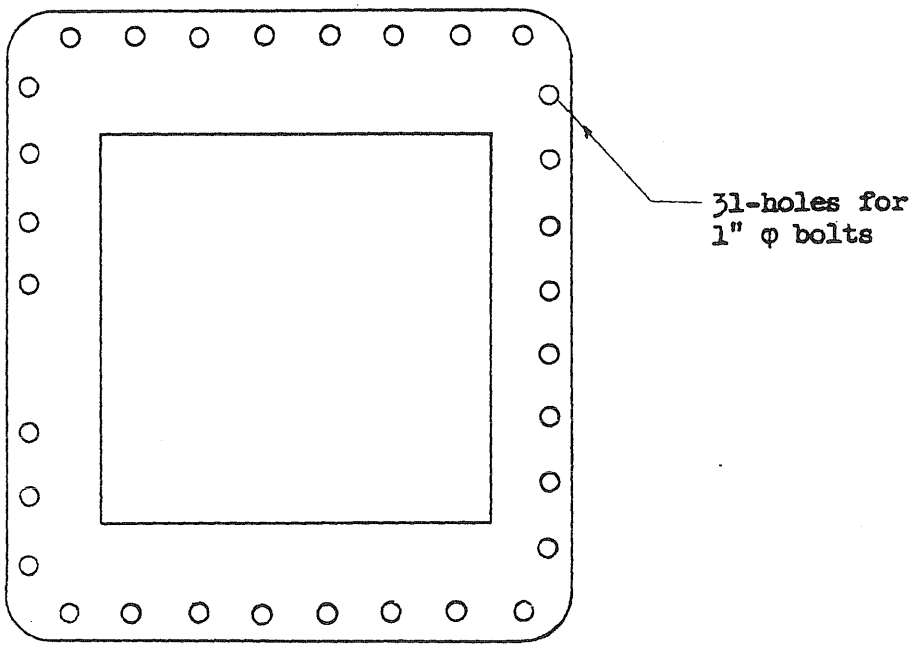

Section "Y-Y"

FIG. 11b DETAILS OF TEST SPECIMEN

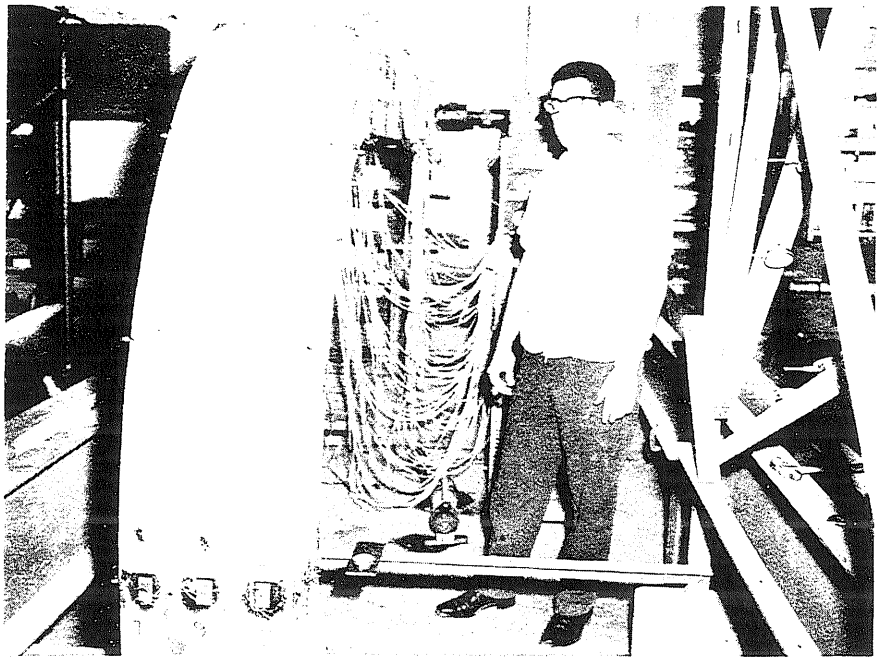

FIG. 12 THE TEST SPECIMEN

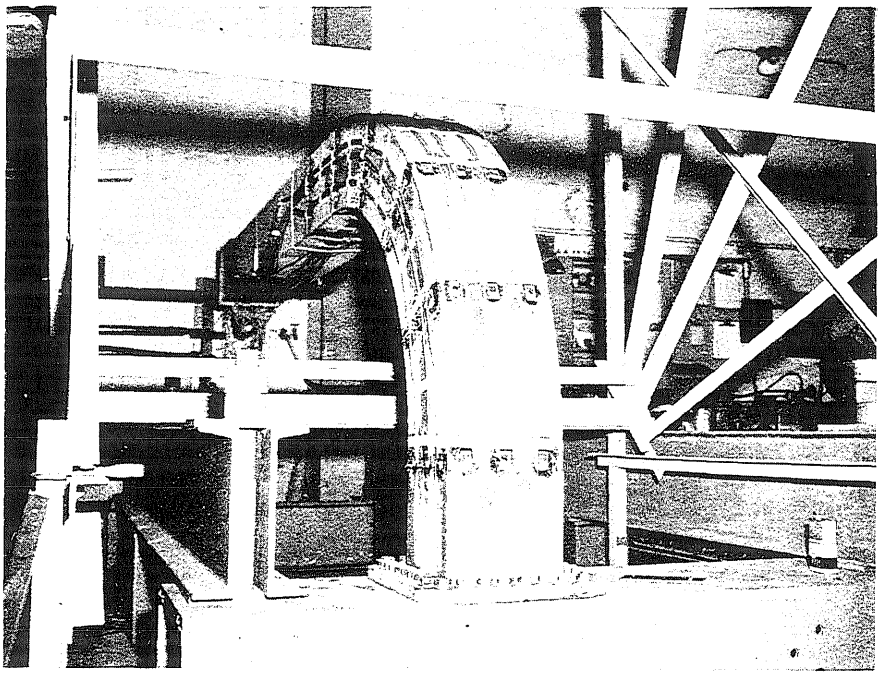

FIG. 13 CONNECTION BETWEEN THE TEST SPECIMEN AND SUPPORTING FRAME

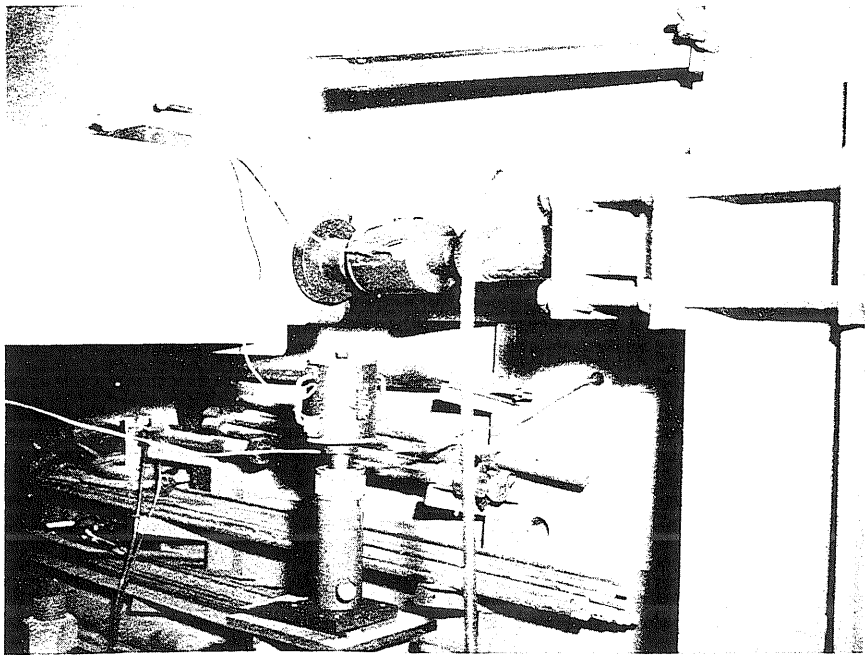

FIG. 14 LOADING EQUIPMENT

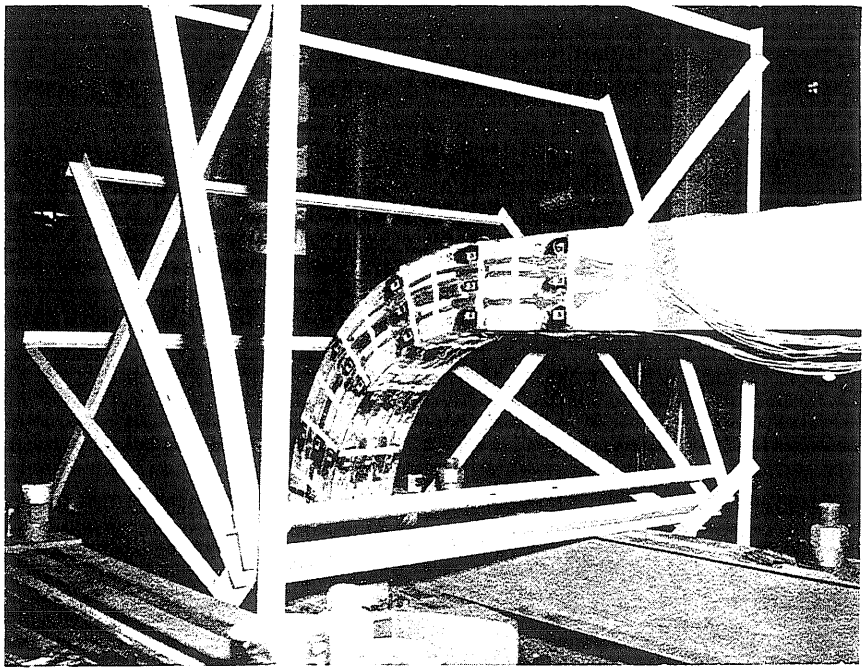

FIG. 15 ANGLE FRAME FOR DIAL INDICATORS

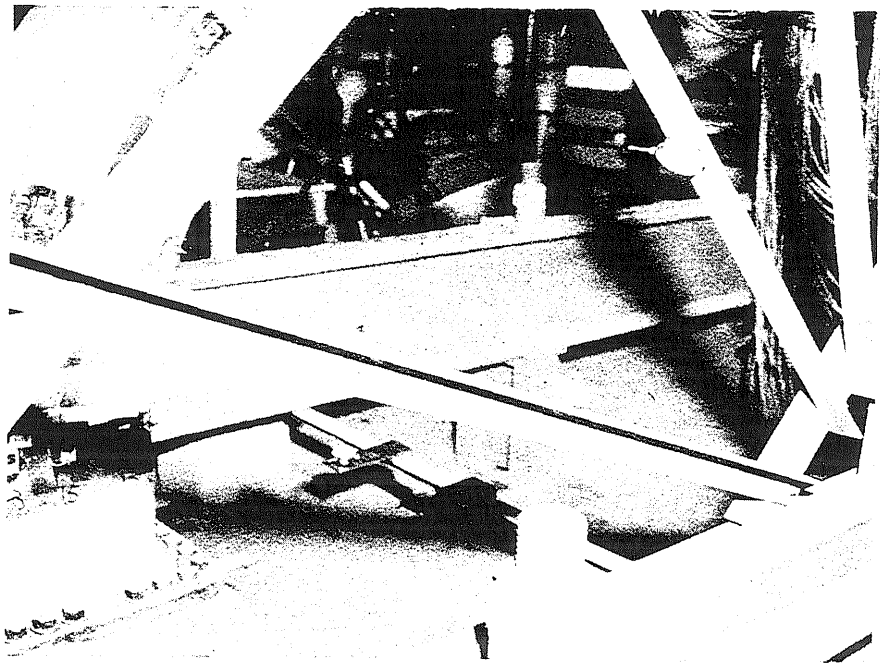

FIG. 16 DIAL INDICATORS AT A TYPICAL POINT OF TEST SPECIMEN

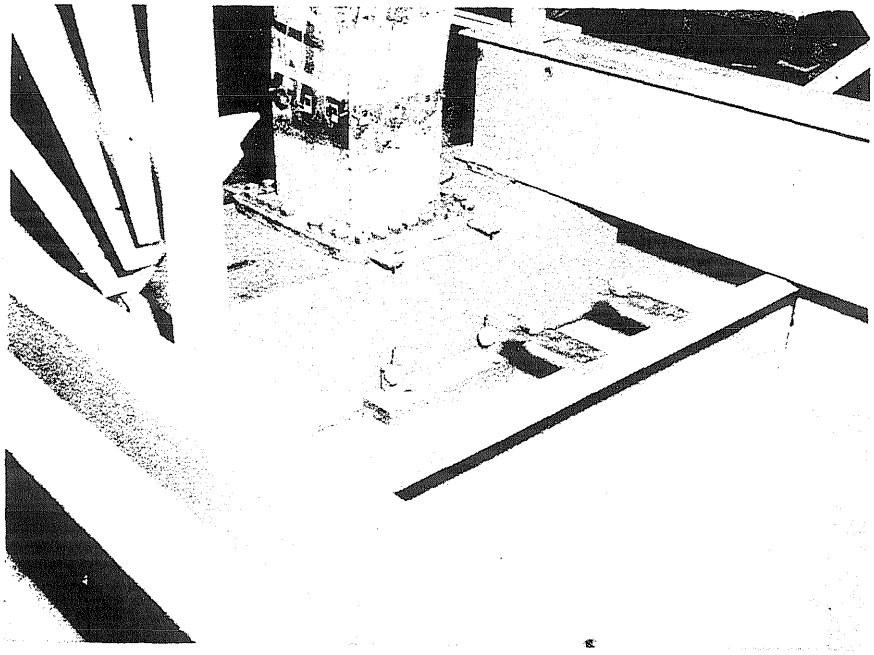

FIG. 17 DIAL INDICATORS AT THE BASE OF TEST SPECIMEN

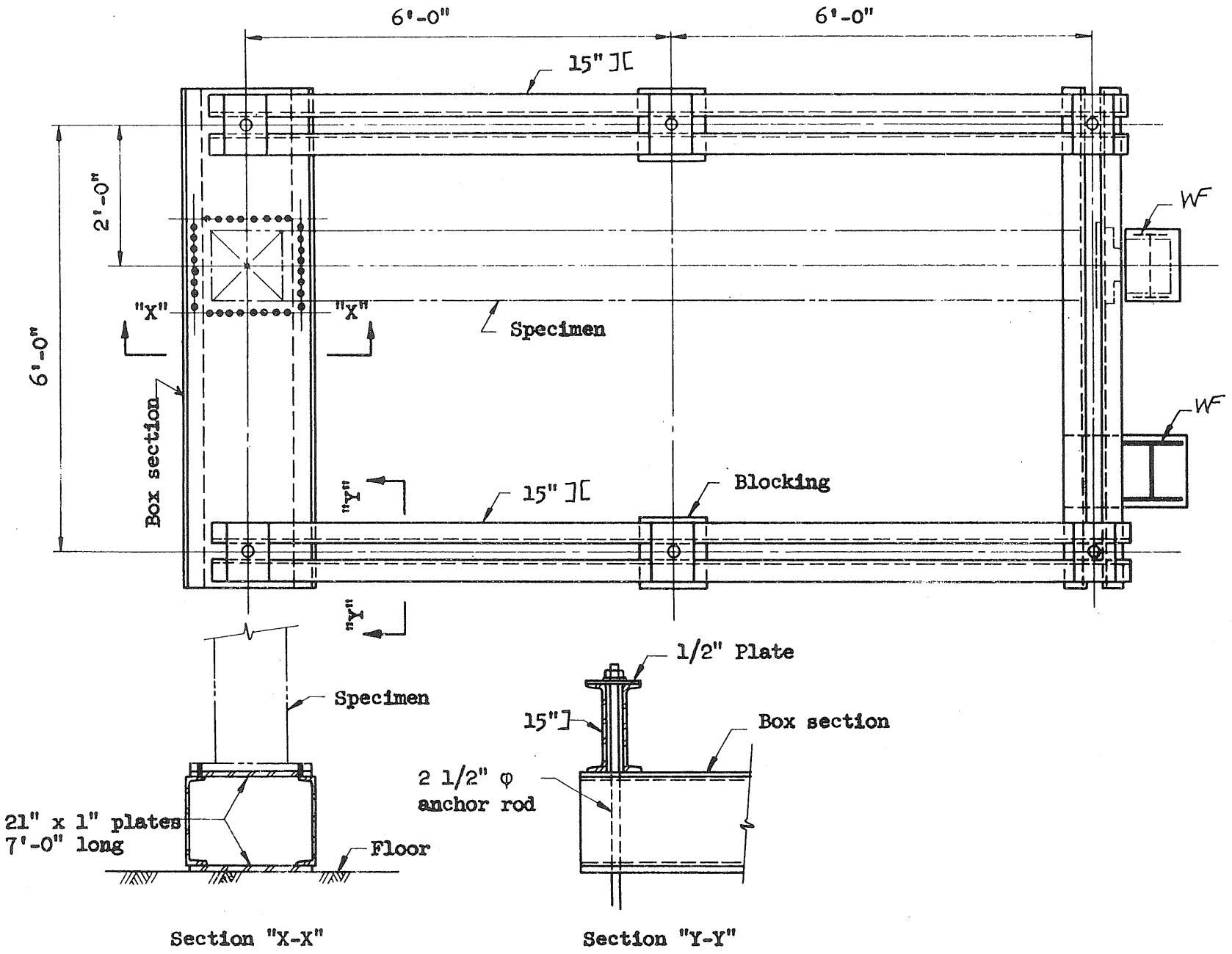

FIG. 18 PLAN OF SUPPORTING FRAME

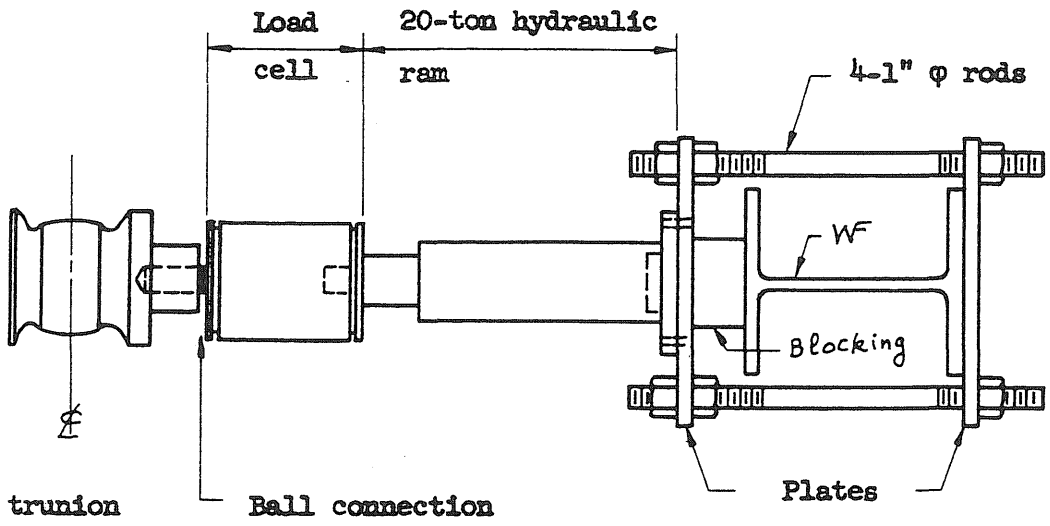

FIG. 19 ARRANGEMENT OF LOADING EQUIPMENT FOR HORIZONTAL LOAD, P_h

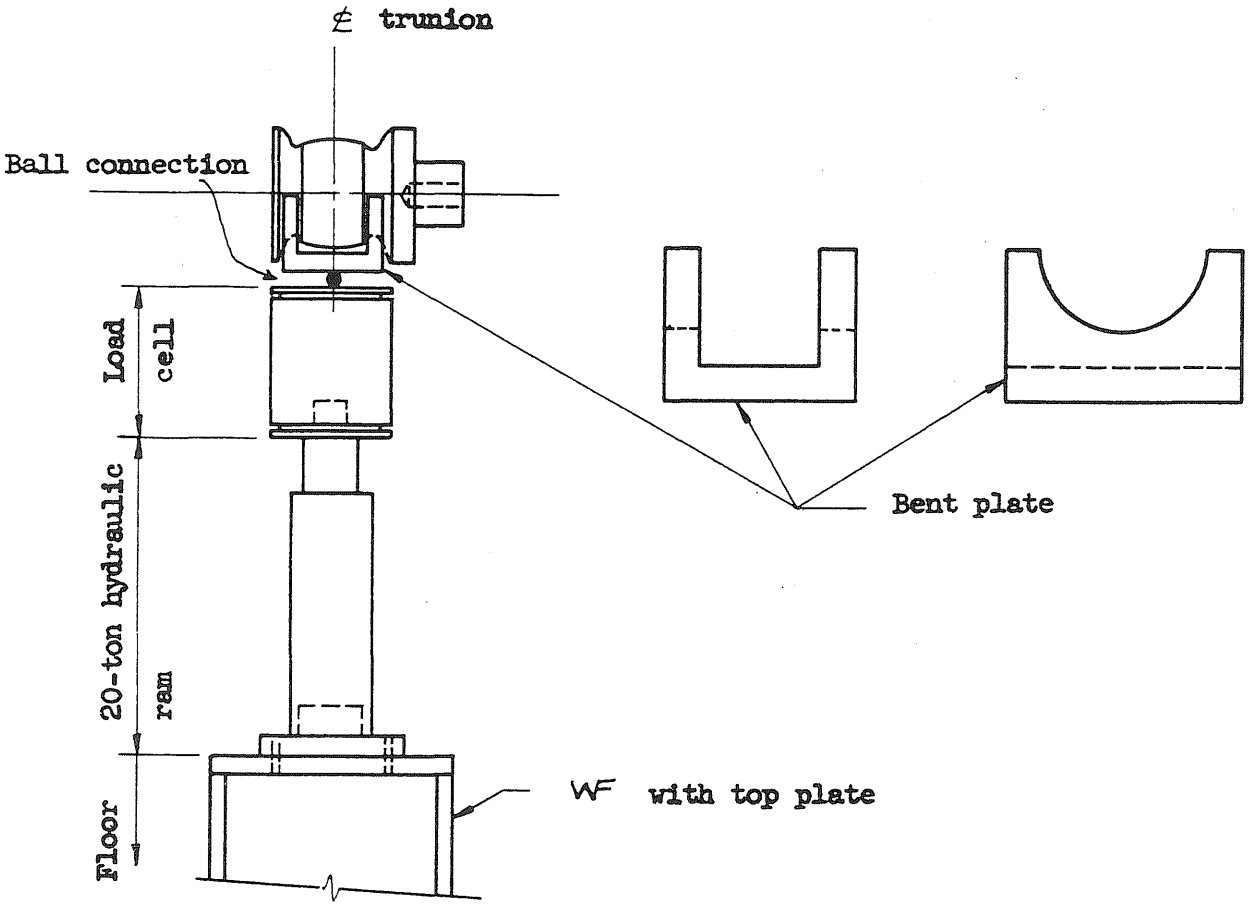

FIG. 20 ARRANGEMENT OF LOADING EQUIPMENT FOR VERTICAL LOAD, P_v

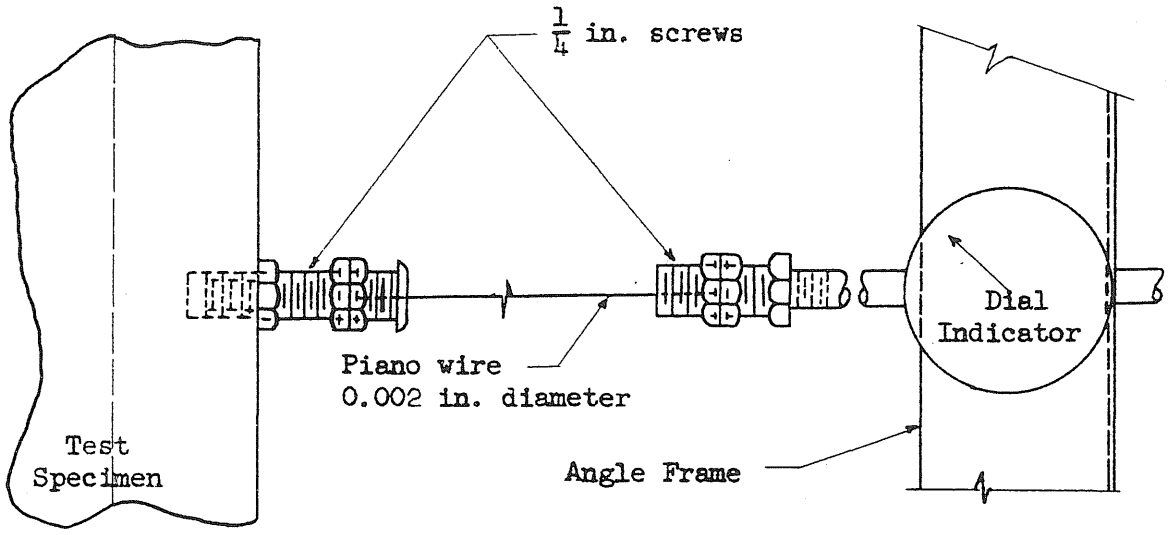

FIG. 21 TYPICAL CONNECTION BETWEEN DIAL INDICATOR AND TEST SPECIMEN

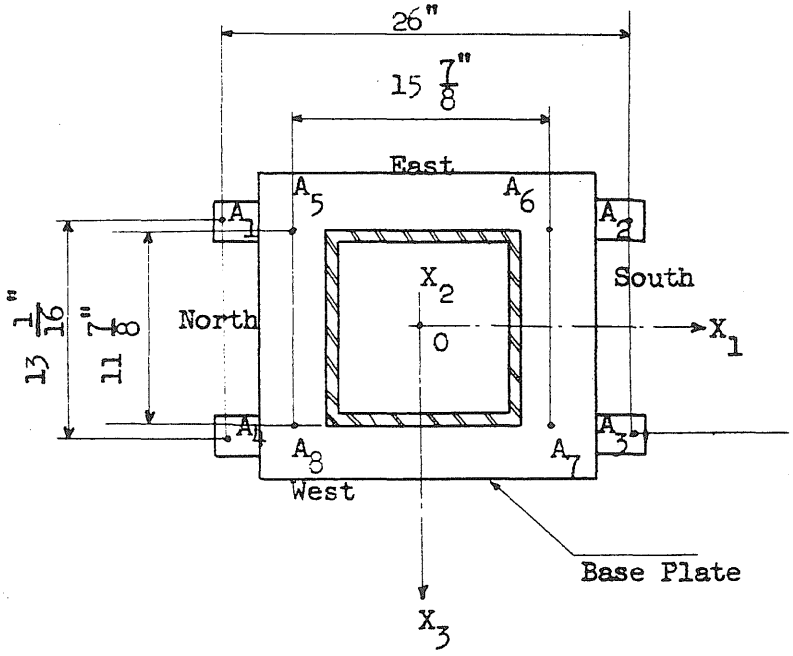

22.a LOCATIONS OF POINTS ON BASE PLATE WHOSE MOVEMENTS WERE MEASURED

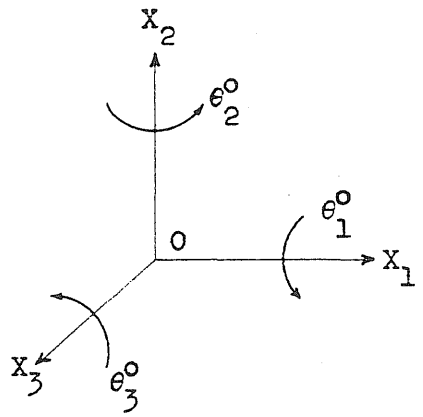

22.b POSITIVE DIRECTIONS OF BASE ROTATIONS

FIG. 22

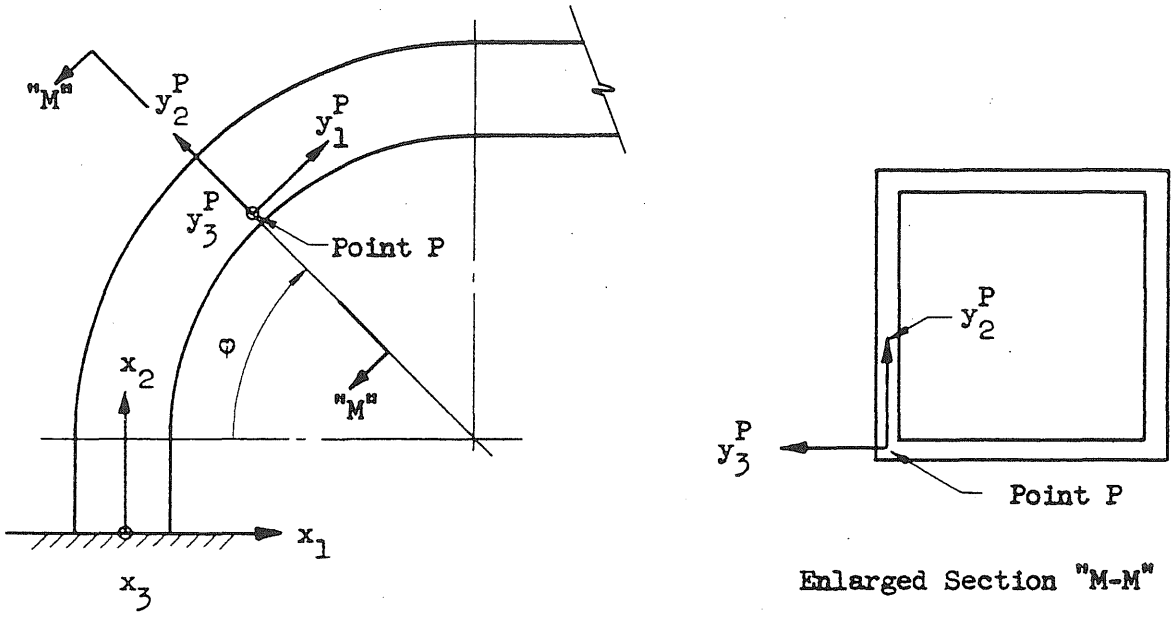

FIG. 22c DIRECTIONS OF MOVEMENTS MEASURED AT EACH CORNER

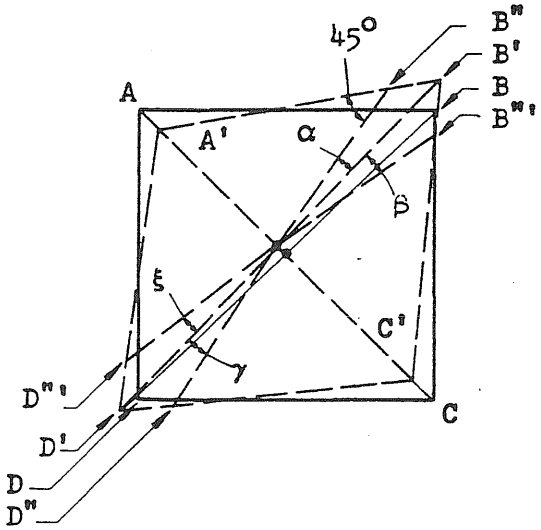

FIG. 23 DISTORTIONAL CORRECTIONS APPLIED TO A DIAGONAL

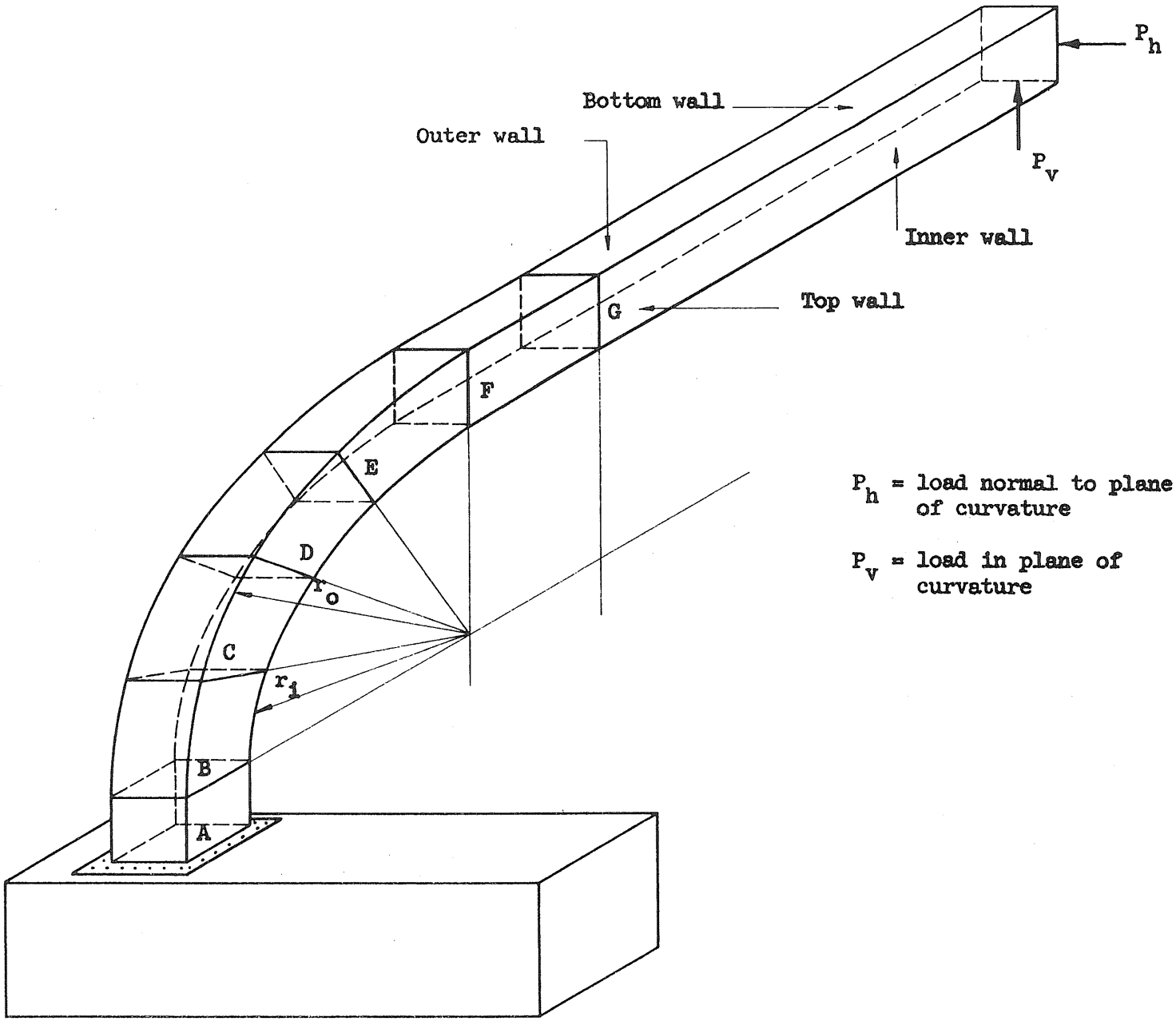

FIG. 24 SCHEMATIC REPRESENTATION OF TEST SPECIMEN

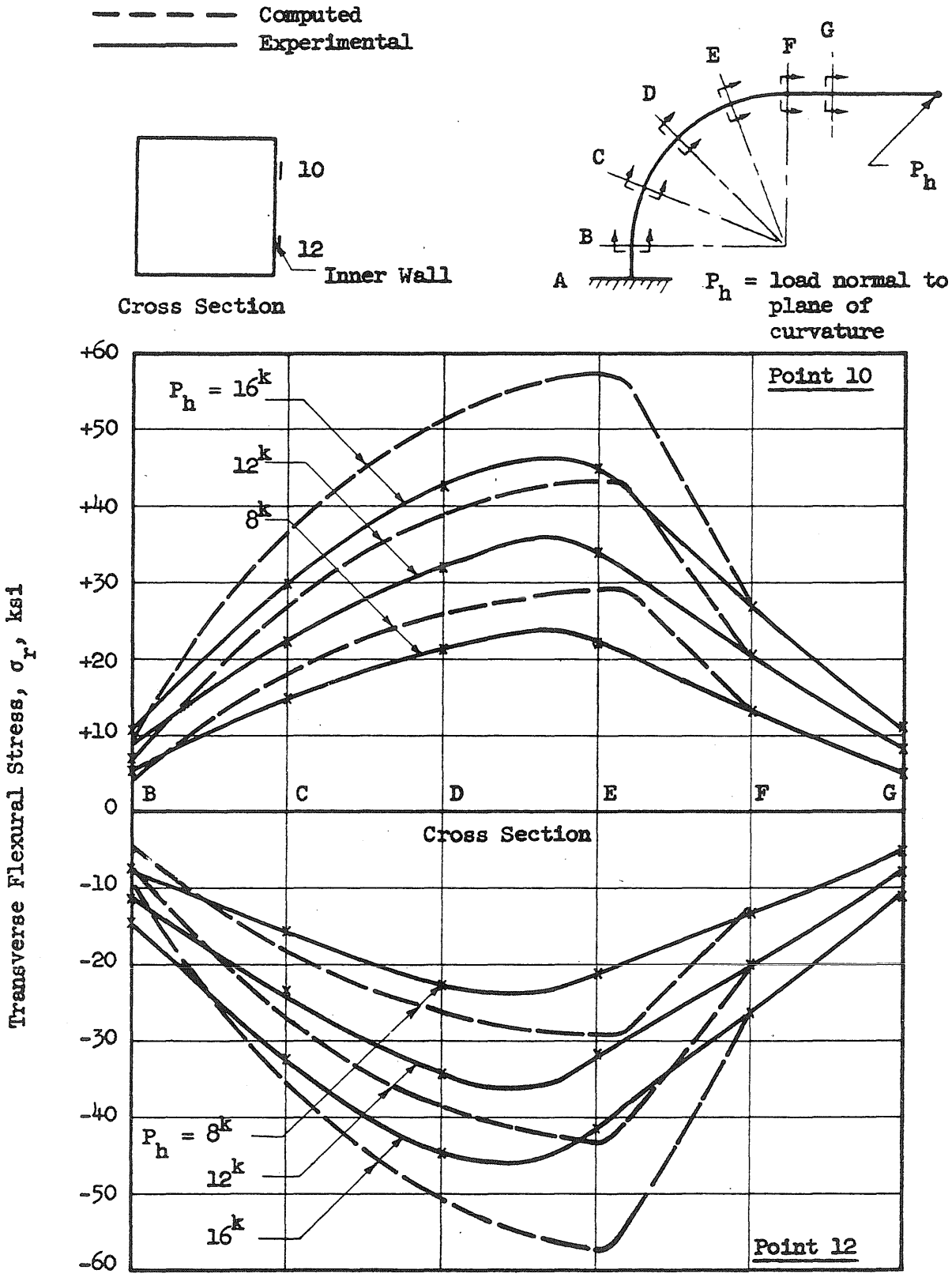

FIG. 25 COMPARISON OF COMPUTED AND EXPERIMENTAL TRANSVERSE FLEXURAL STRESSES FOR POINTS 10 AND 12

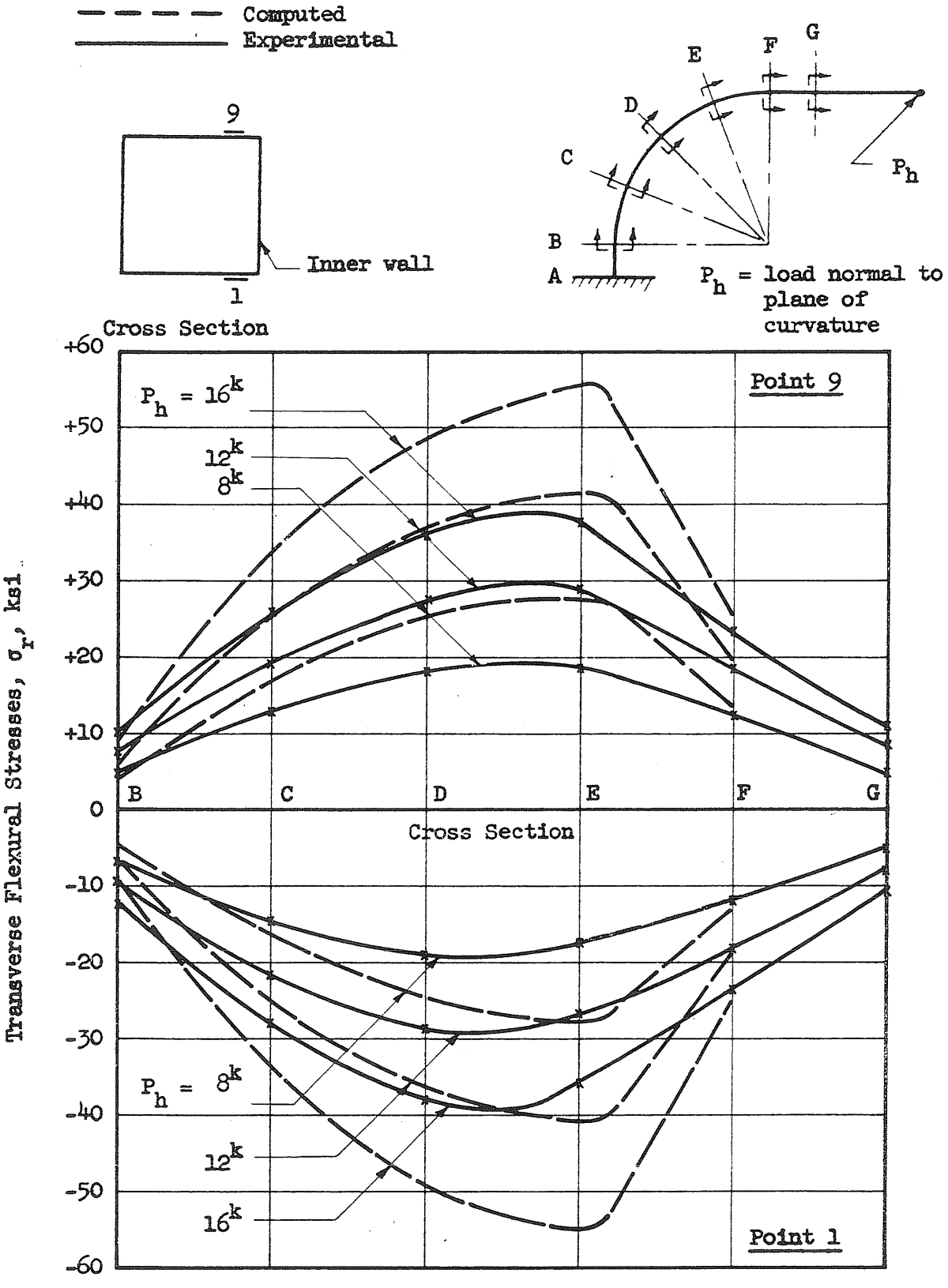

FIG. 26 COMPARISON OF COMPUTED AND EXPERIMENTAL TRANSVERSE FLEXURAL STRESSES FOR POINTS 1 AND 9

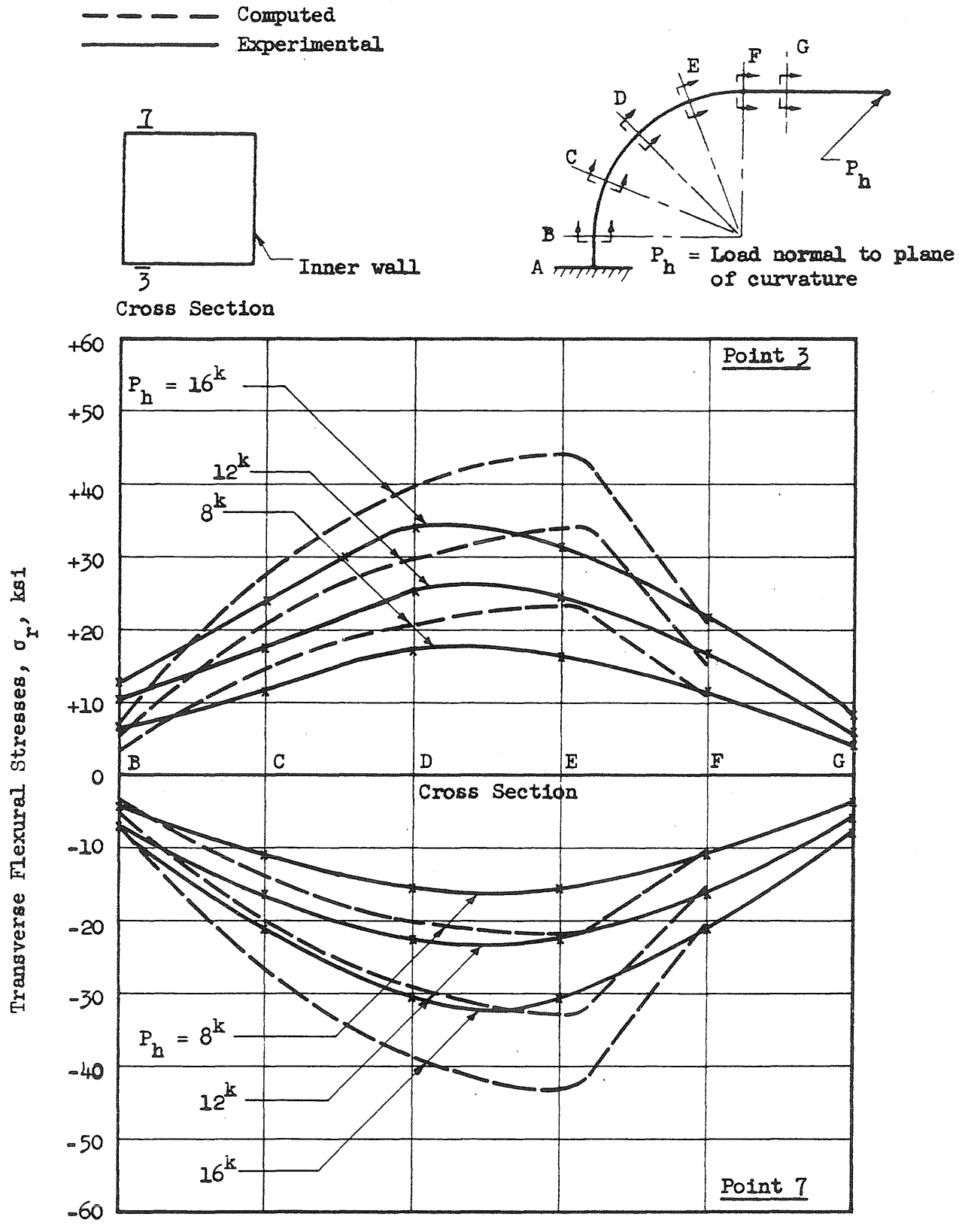

FIG. 27 COMPARISON OF COMPUTED AND EXPERIMENTAL TRANSVERSE FLEXURAL STRESSES FOR POINTS 3 AND 7

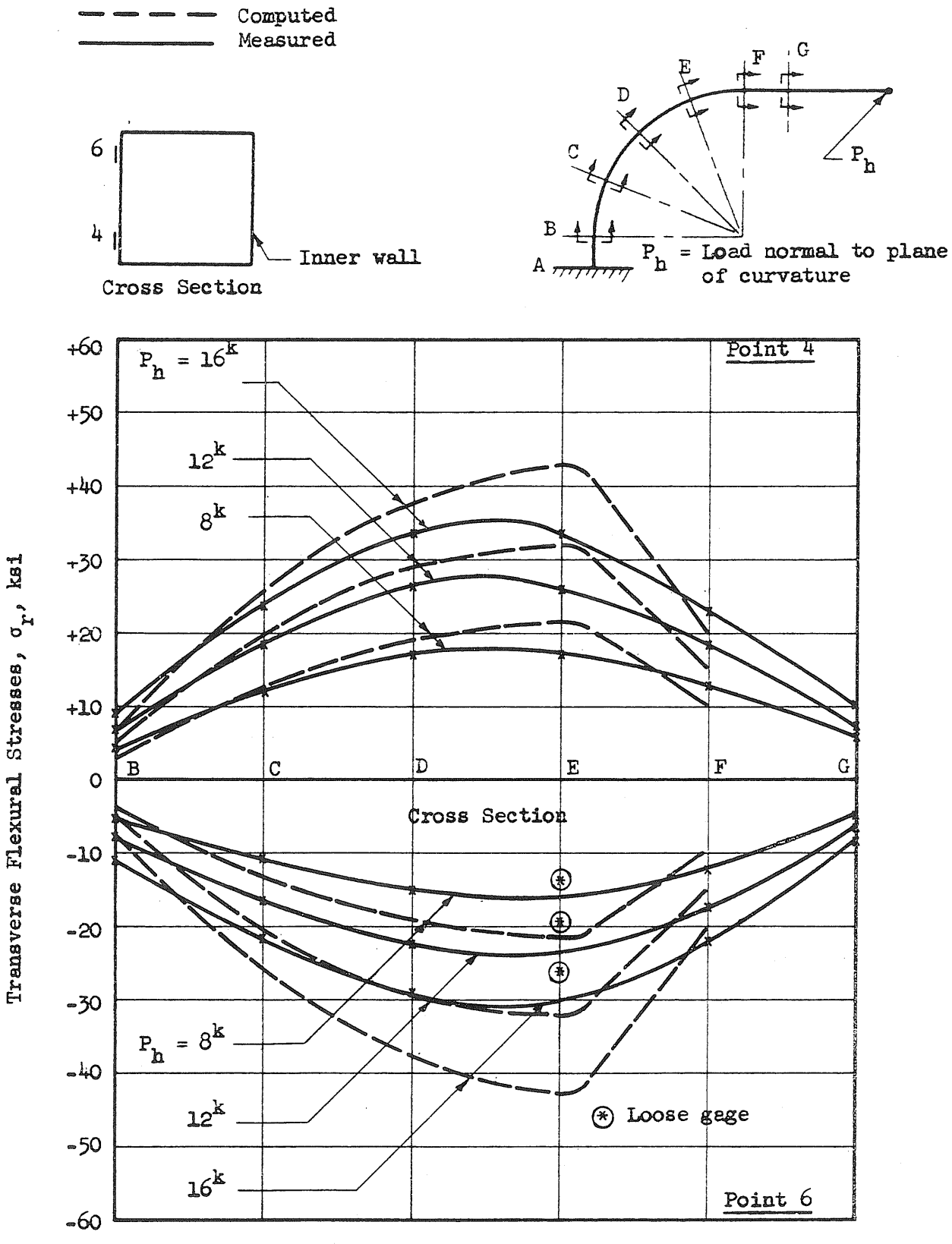

FIG. 28 COMPARISON OF COMPUTED AND EXPERIMENTAL TRANSVERSE FLEXURAL STRESSES FOR POINTS 4 AND 6

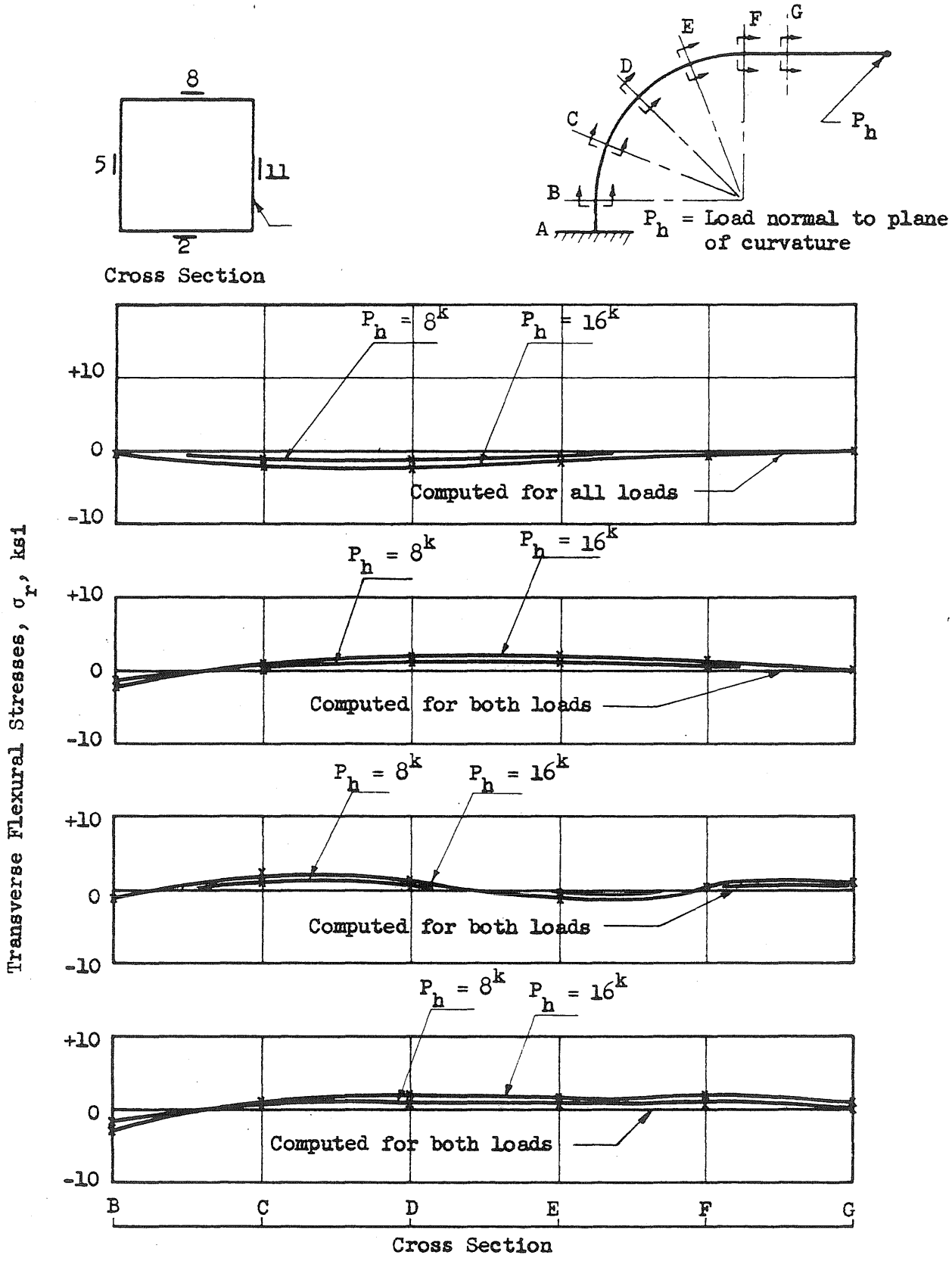

FIG. 29 COMPARISON OF COMPUTED AND EXPERIMENTAL TRANSVERSE FLEXURAL STRESSES FOR POINTS 2, 5, 8, AND 11

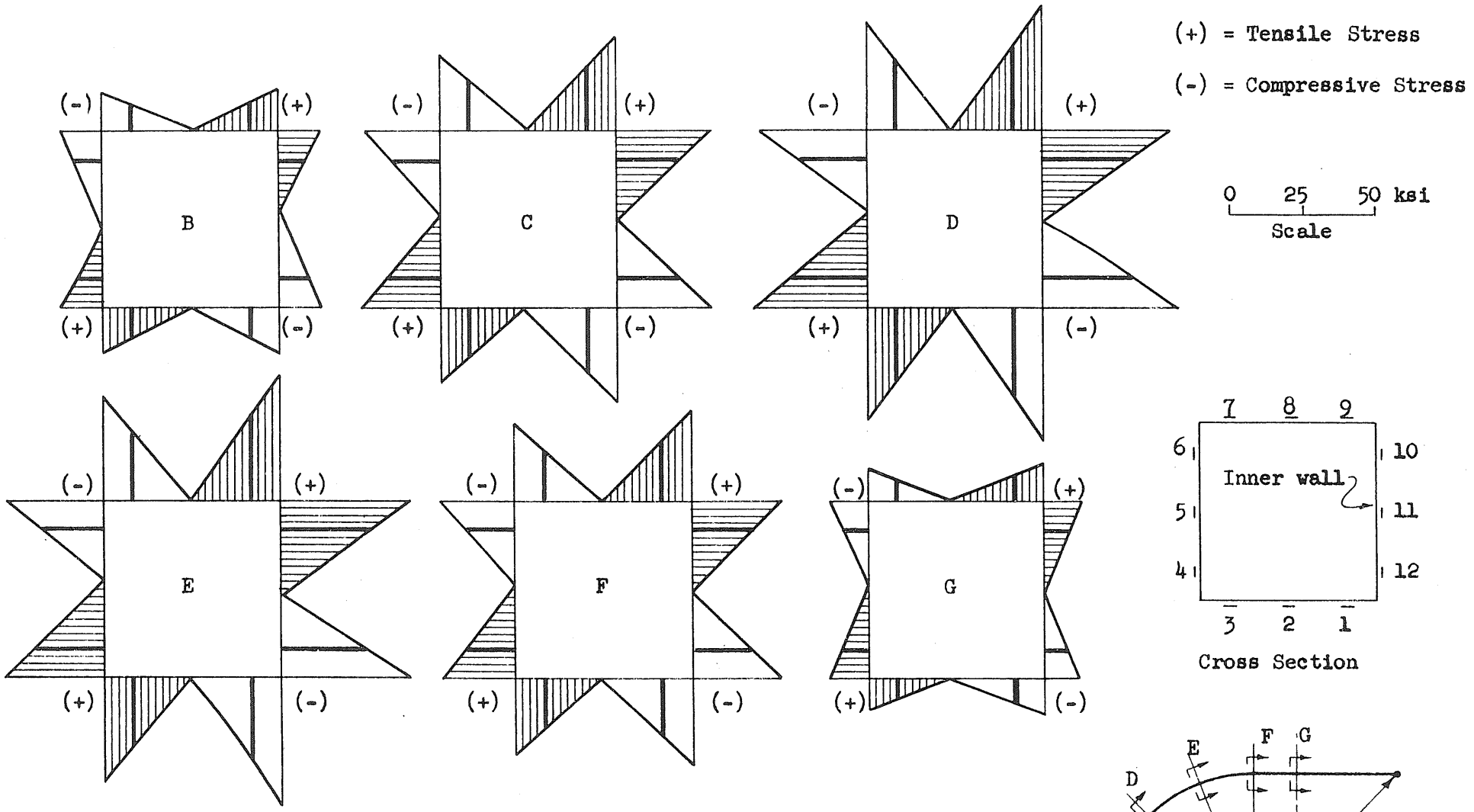

FIG. 30 EXPERIMENTAL VALUES OF TRANSVERSE FLEXURAL STRESSES AT VARIOUS SECTIONS OF TEST SPECIMEN FOR $P_h = 12^k$

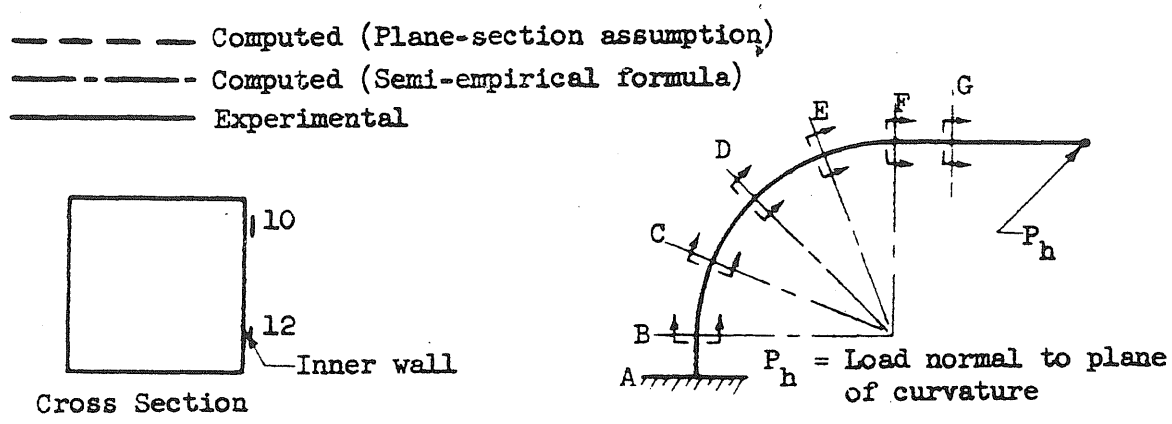

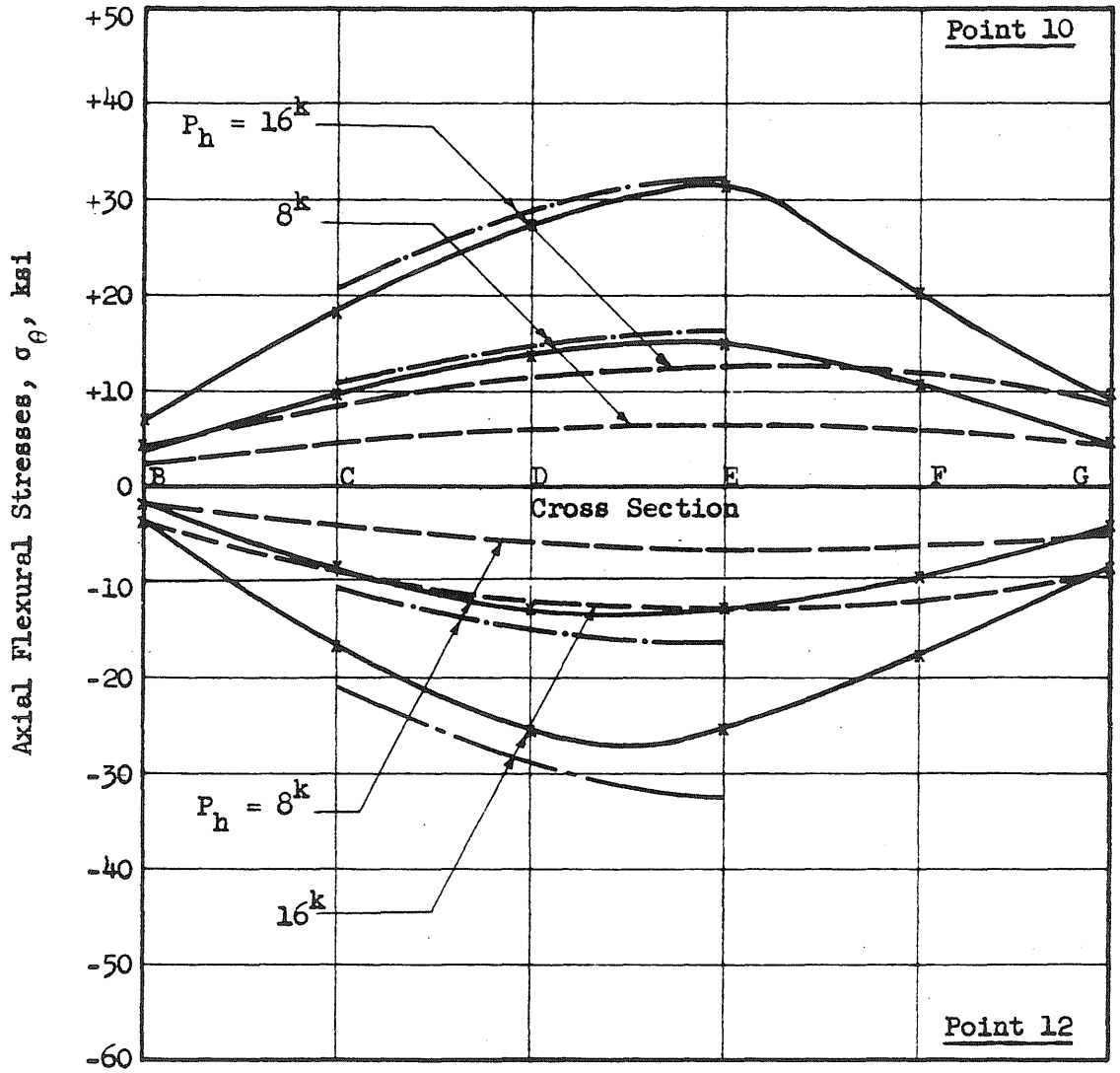

FIG. 31 COMPARISON OF COMPUTED AND EXPERIMENTAL AXIAL FLEXURAL STRESSES FOR POINTS 10 AND 12

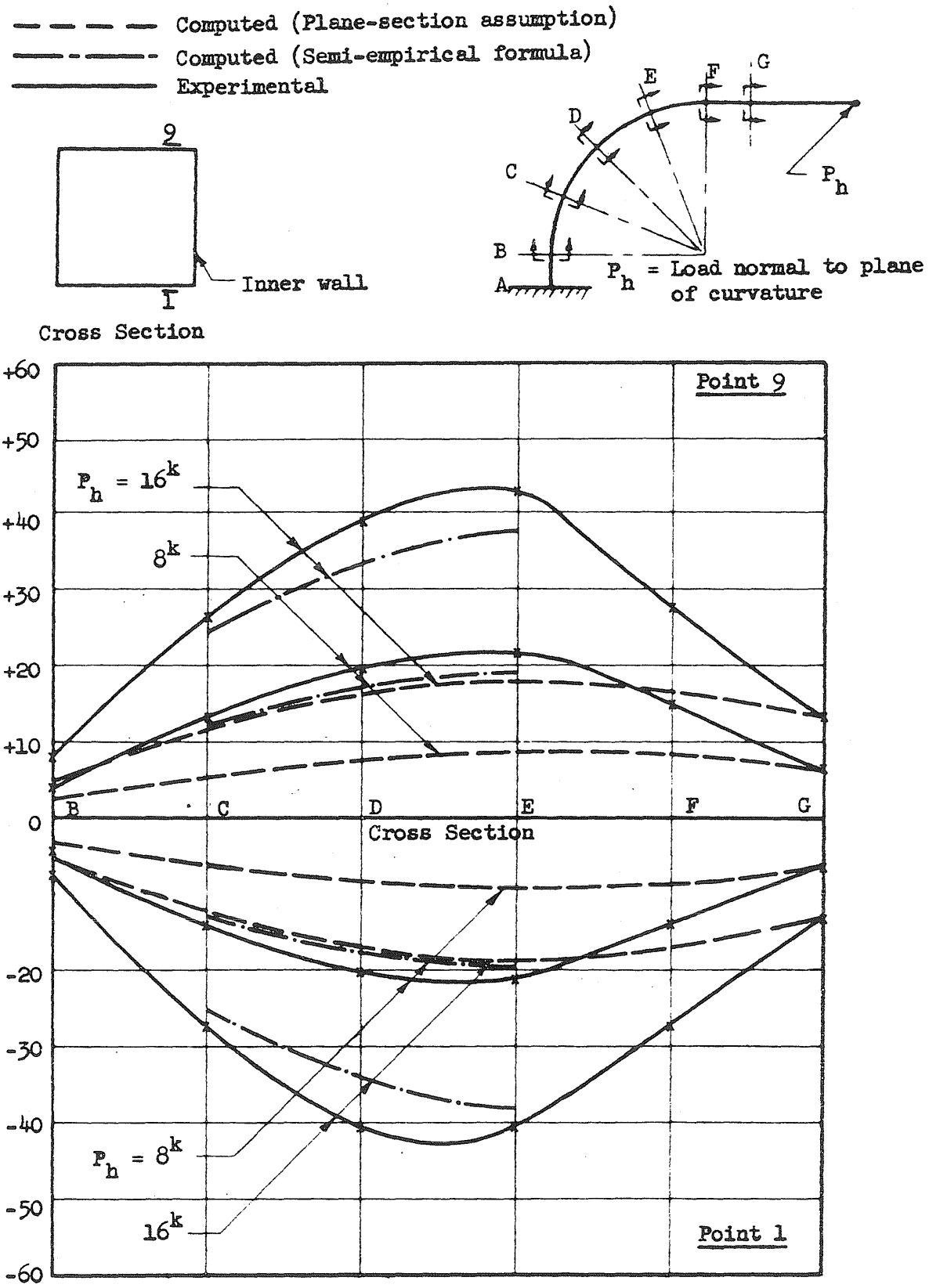

FIG. 32 COMPARISON OF COMPUTED AND EXPERIMENTAL AXIAL FLEXURAL STRESSES FOR POINTS 1 AND 9

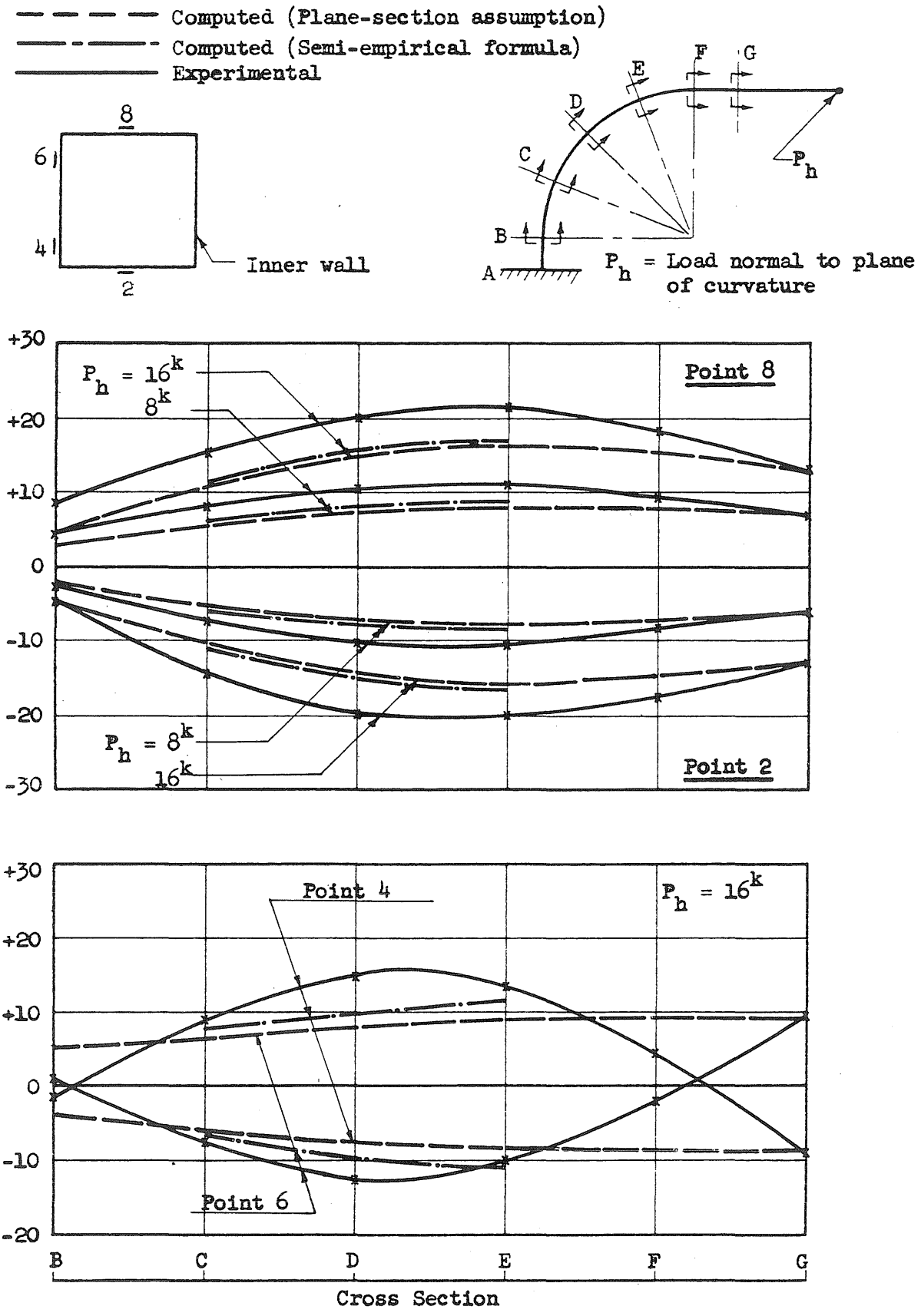

FIG. 33 COMPARISON OF COMPUTED AND EXPERIMENTAL AXIAL FLEXURAL STRESSES FOR POINTS 2, 4, 6, AND 8

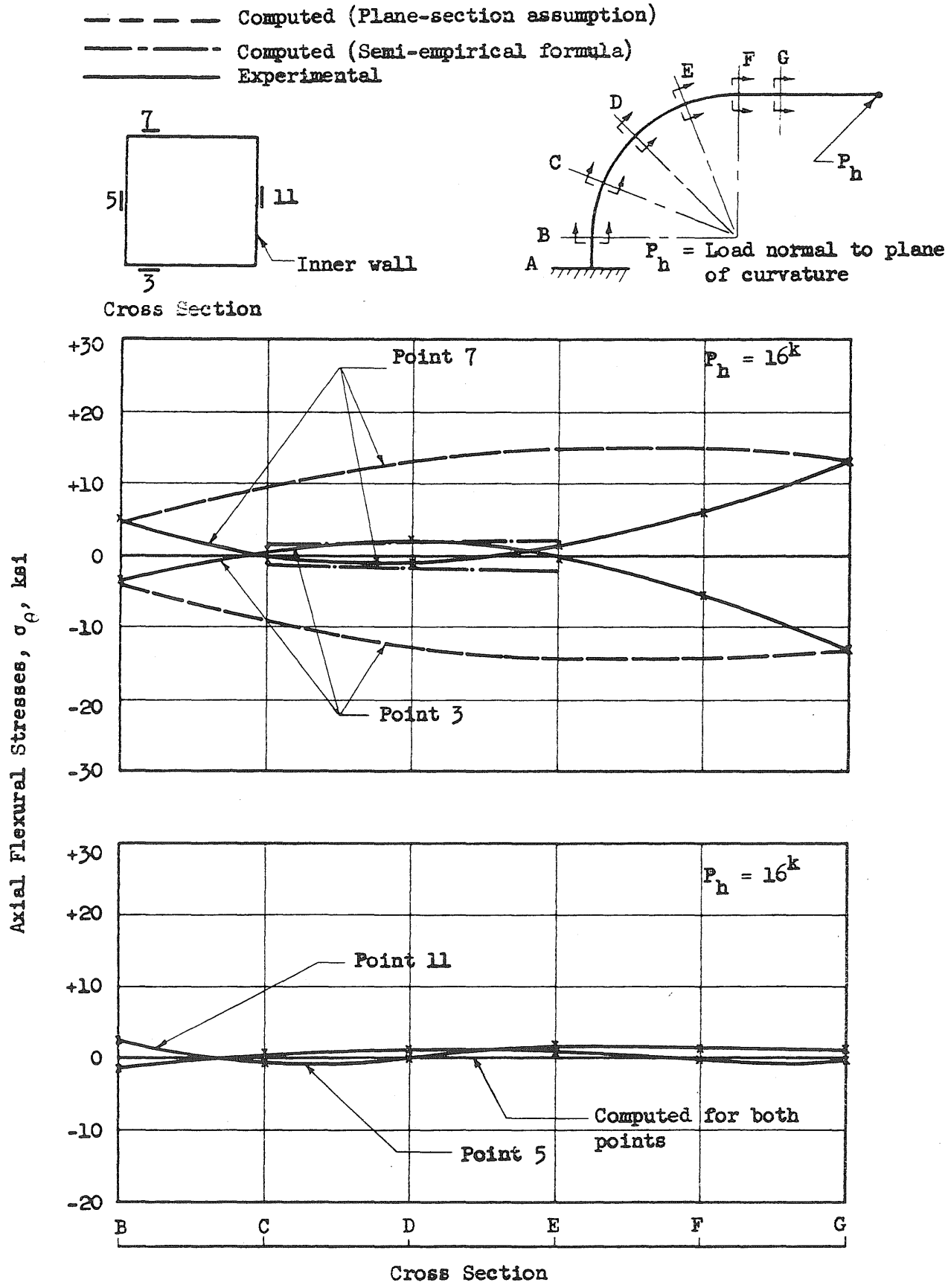

FIG. 34 COMPARISON OF COMPUTED AND EXPERIMENTAL AXIAL FLEXURAL STRESSES FOR POINTS 3, 5, 7, AND 11

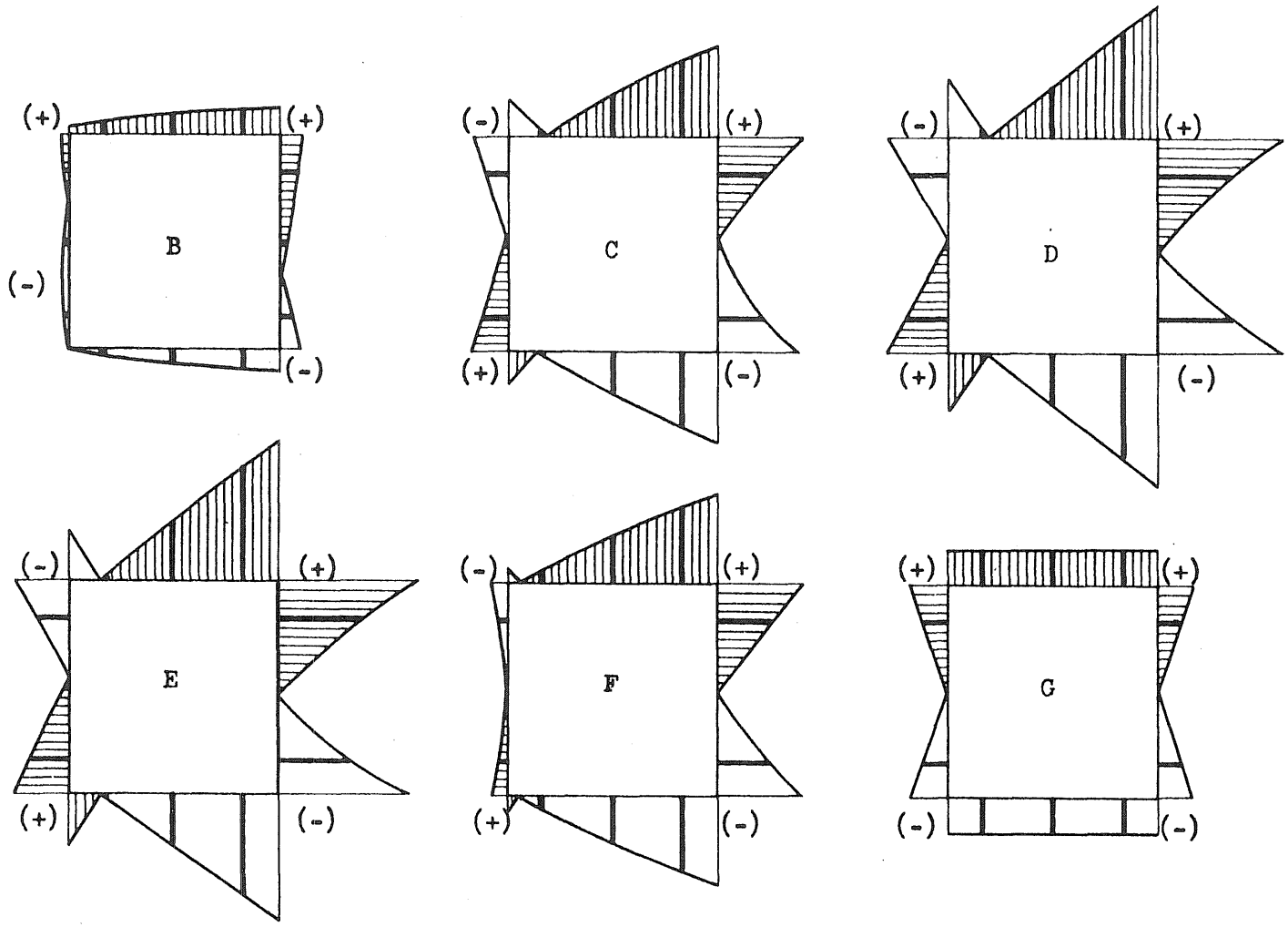

FIG. 35 EXPERIMENTAL VALUES OF AXIAL FLEXURAL STRESSES AT VARIOUS SECTIONS OF TEST SPECIMEN FOR $P_h = 12^k$

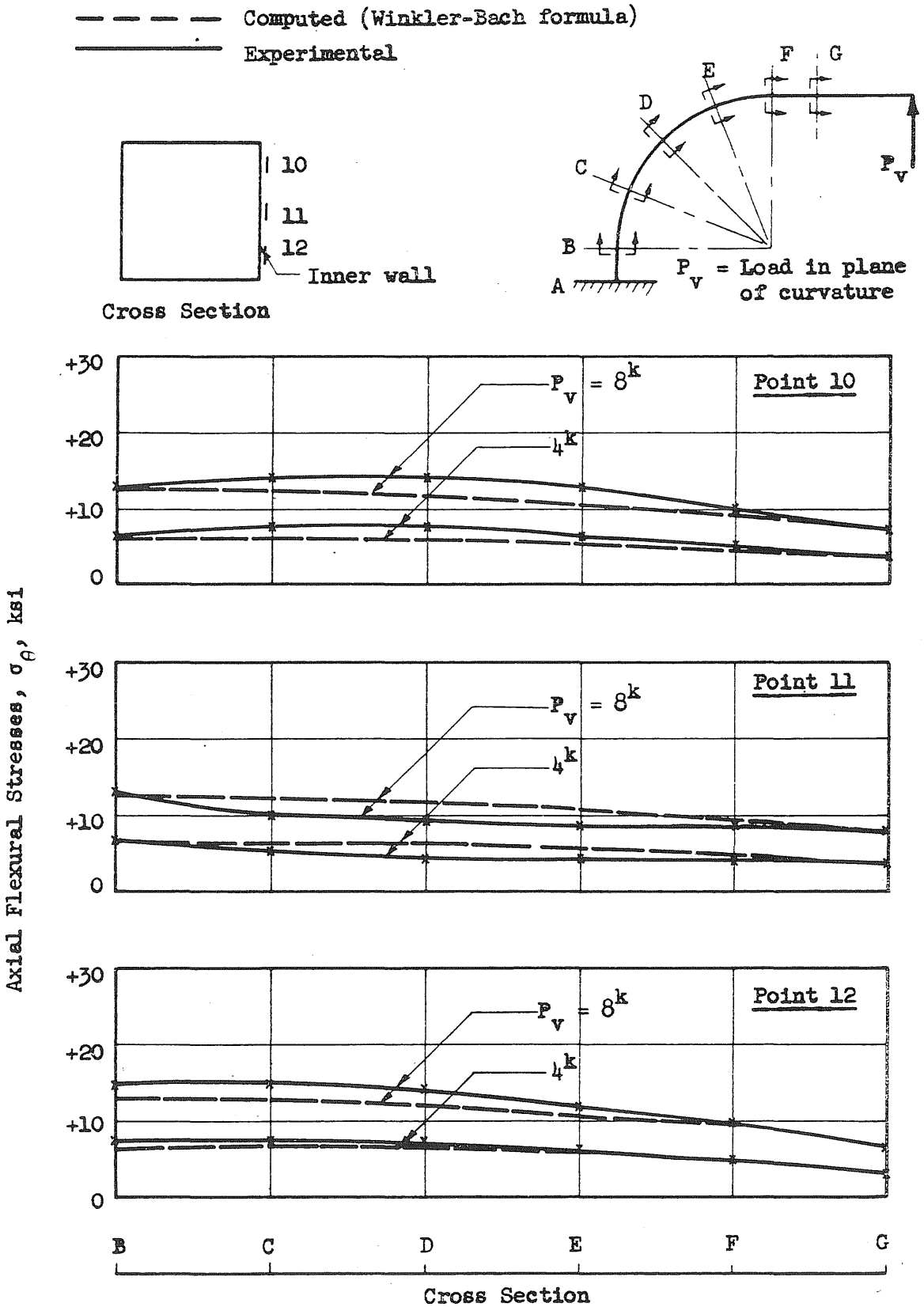

FIG. 36 COMPARISON OF COMPUTED AND EXPERIMENTAL AXIAL FLEXURAL STRESSES FOR POINTS 10, 11, AND 12

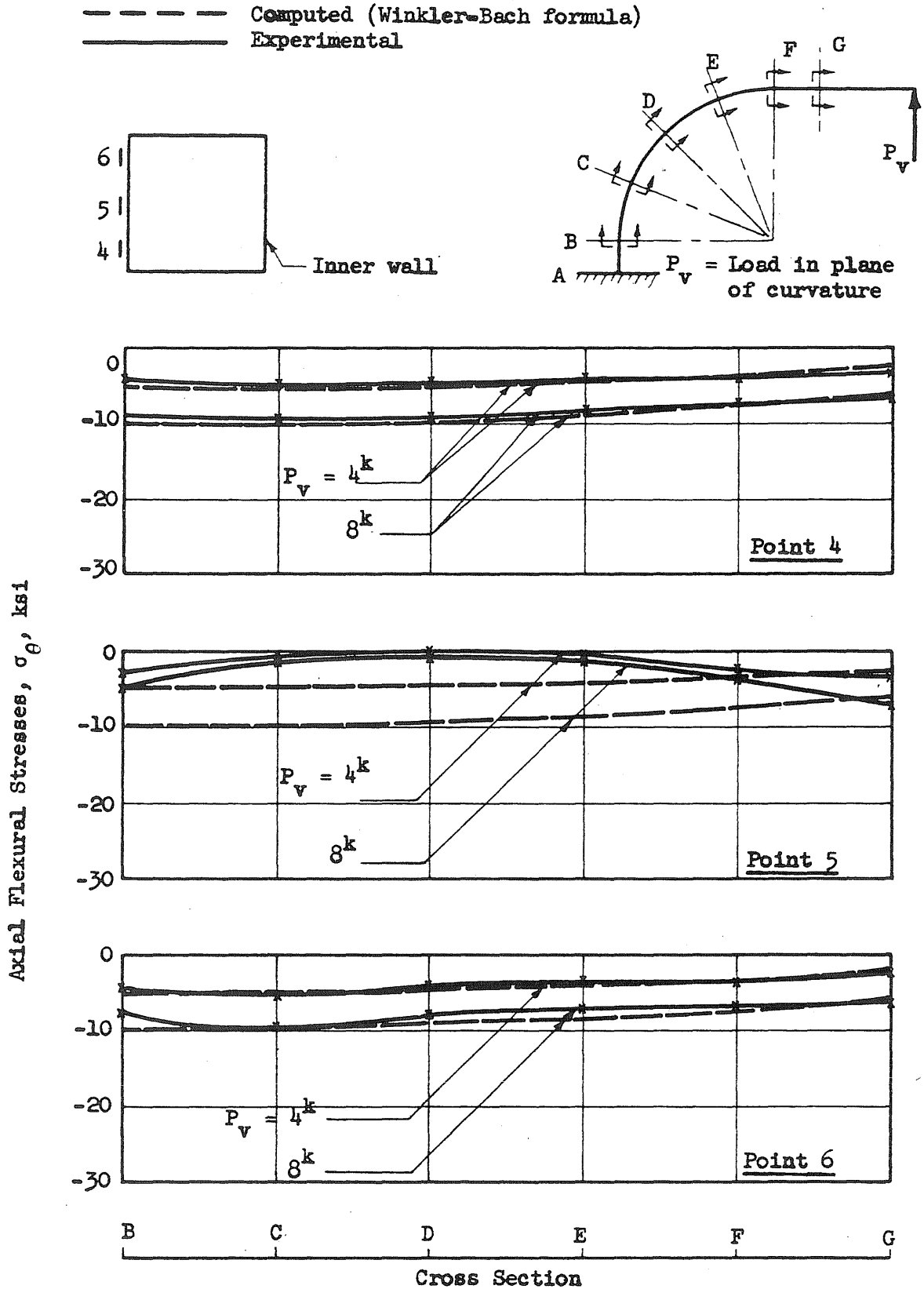

FIG. 37 COMPARISON OF COMPUTED AND EXPERIMENTAL AXIAL FLEXURAL STRESSES FOR POINTS 4, 5, AND 6

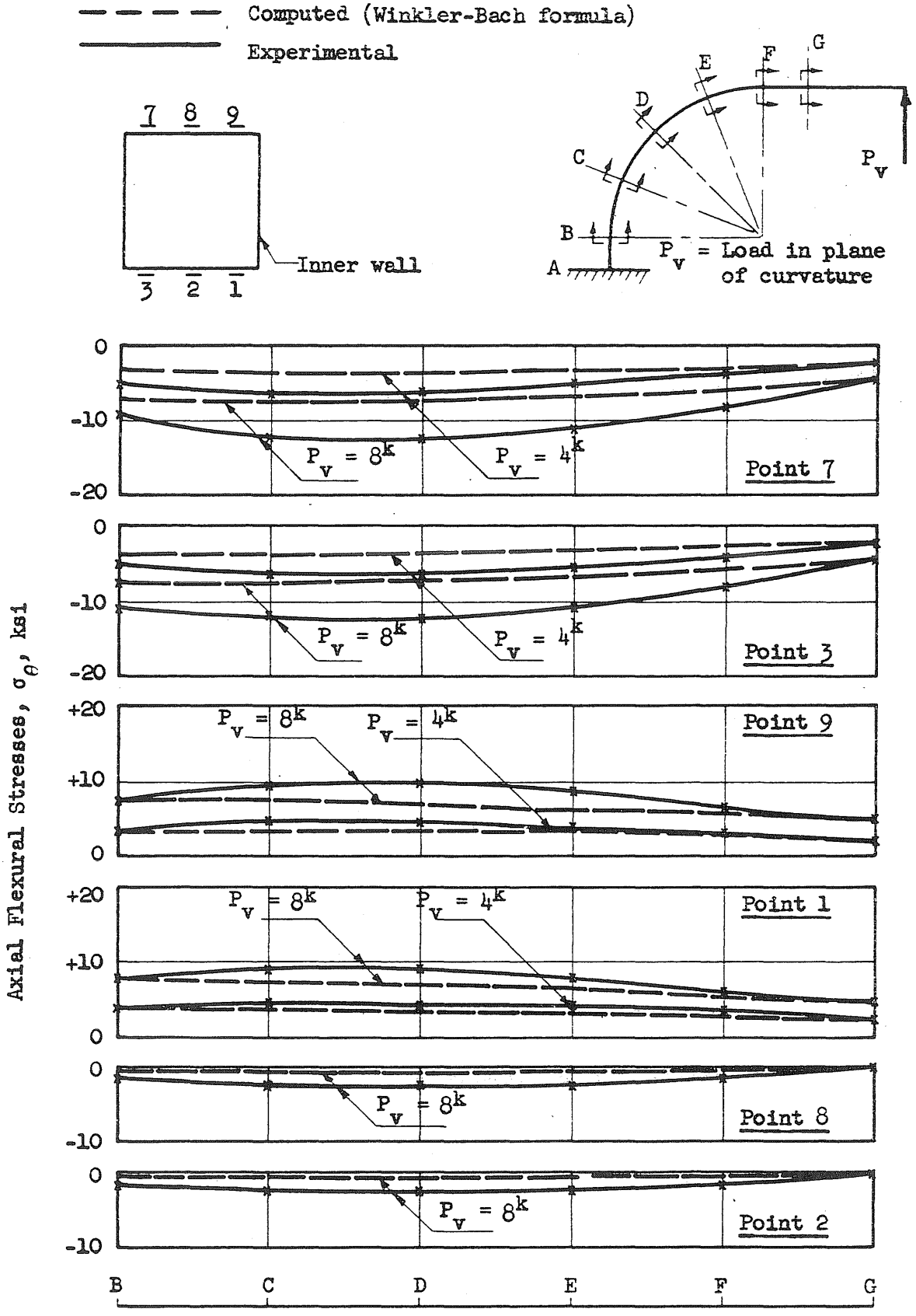

FIG. 38 COMPARISON OF COMPUTED AND EXPERIMENTAL AXIAL FLEXURAL STRESSES FOR POINTS 1, 2, 3, 7, 8, AND 9

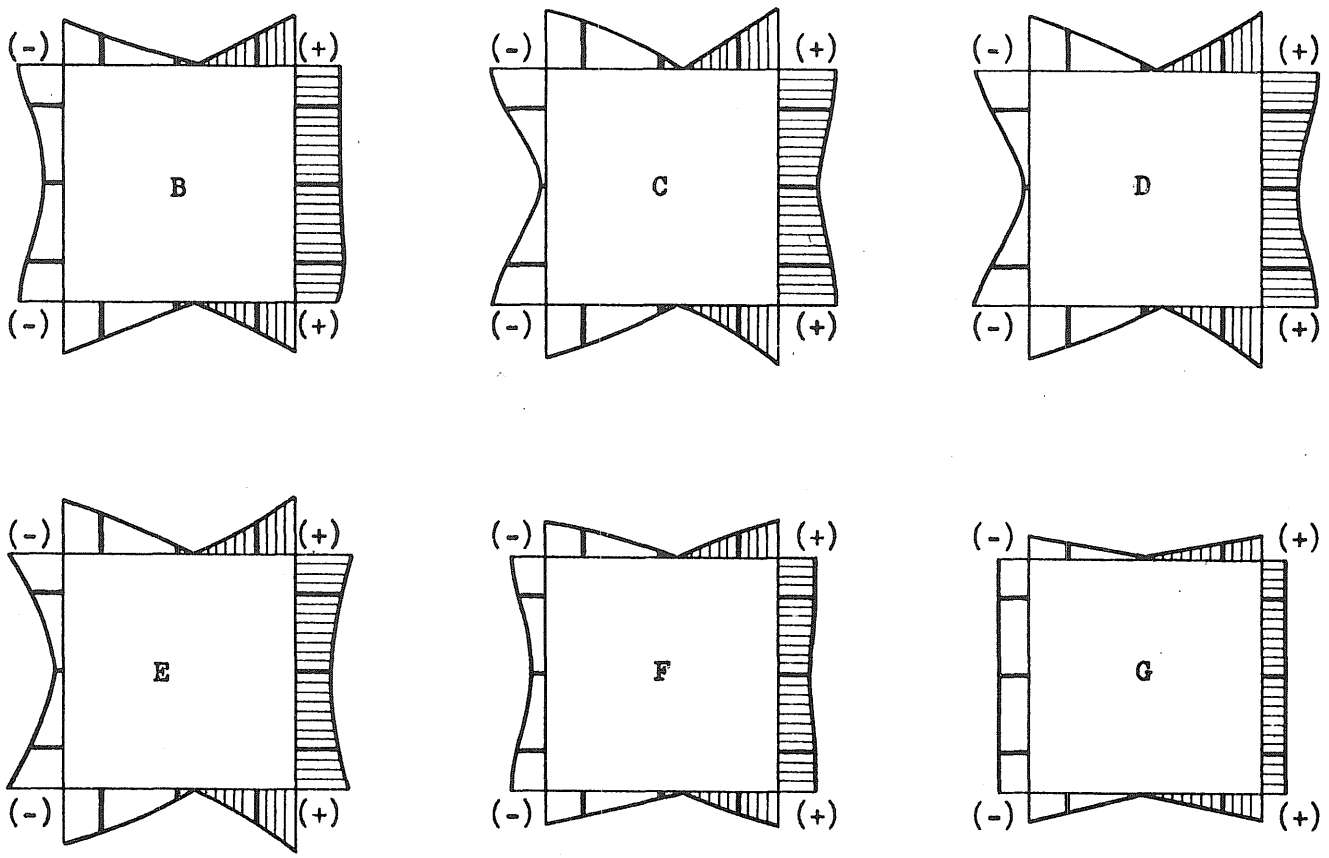

FIG. 39 EXPERIMENTAL VALUES OF AXIAL FLEXURAL STRESSES AT VARIOUS SECTIONS OF TEST SPECIMEN FOR $P_v = 8^k$

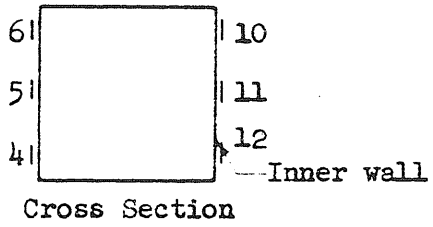

Cross Section

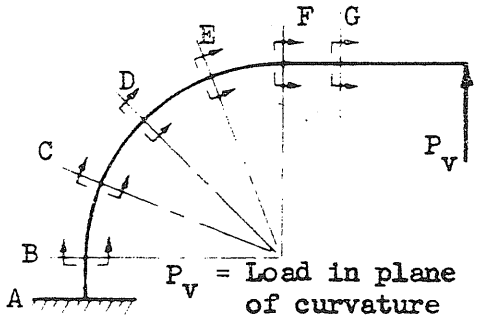

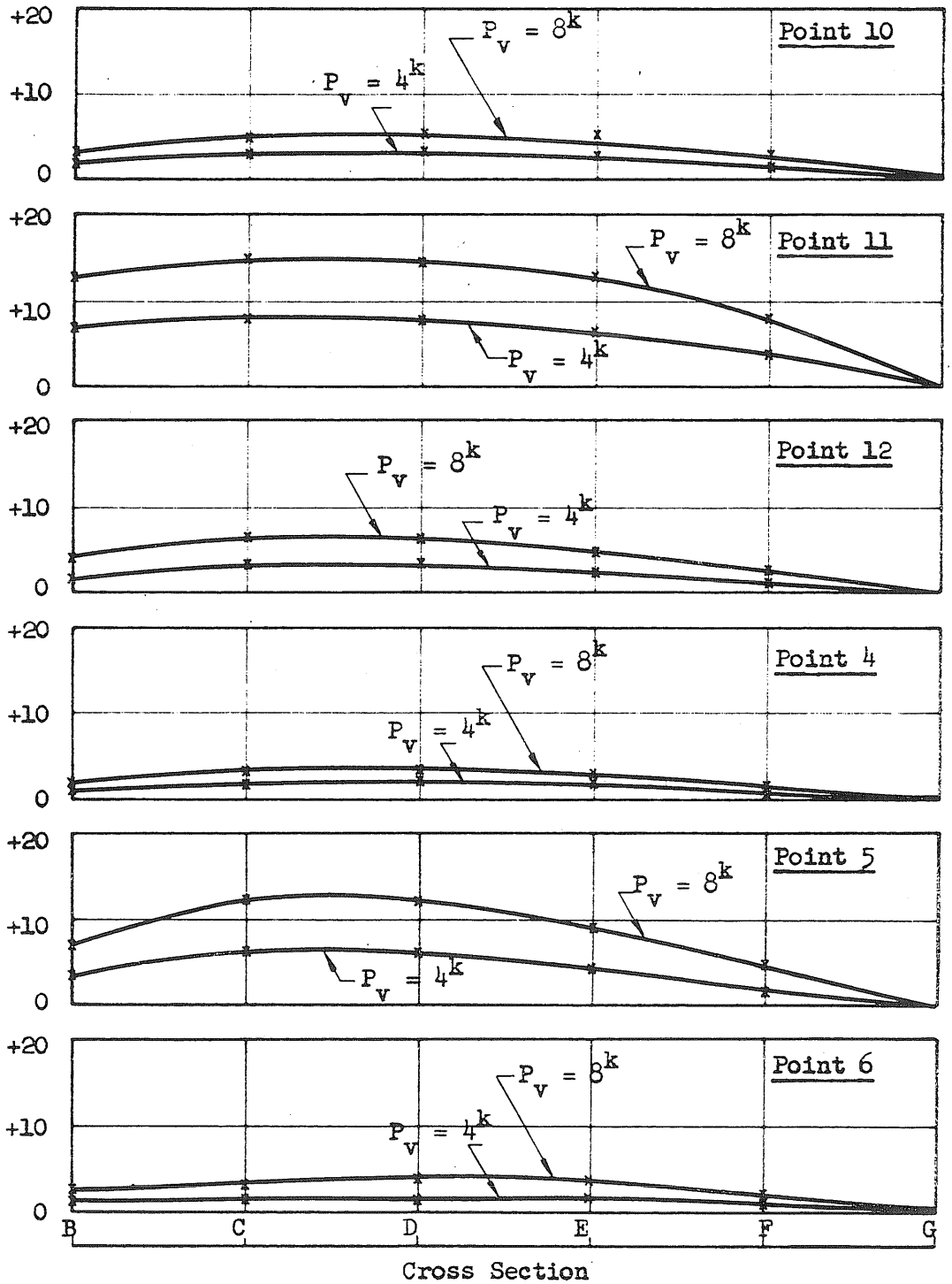

FIG. 40 EXPERIMENTAL VALUES OF TRANSVERSE FLEXURAL STRESSES AT POINTS 4, 5, 6, 10, 11, AND 12

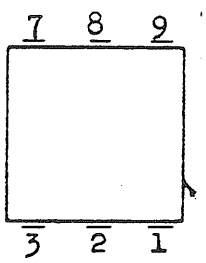

Inner wall

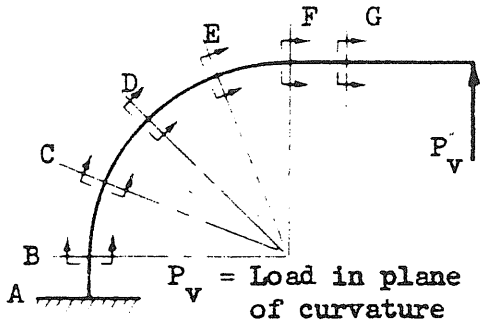

P_v = Load in plane of curvature

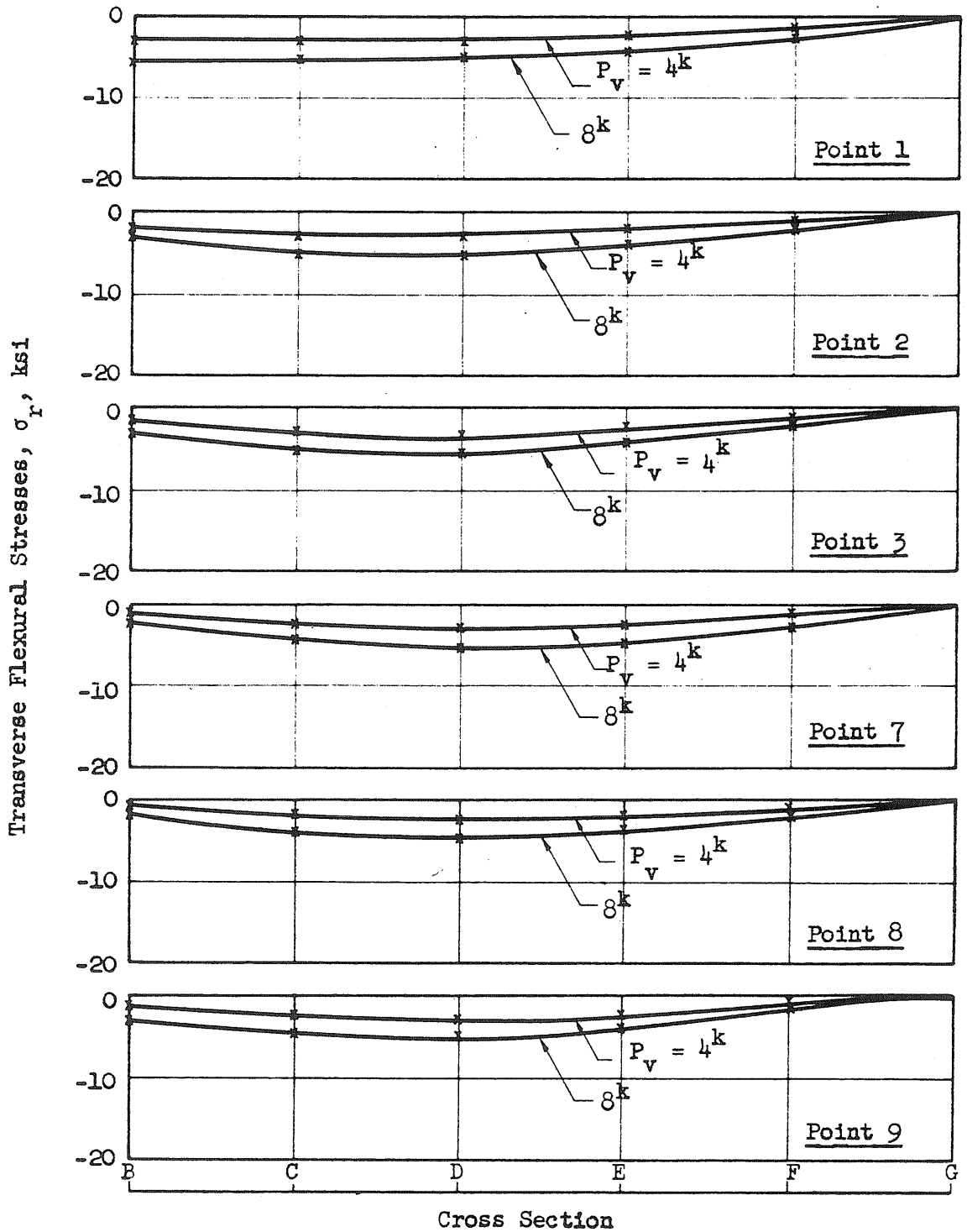

FIG. 41 EXPERIMENTAL VALUES OF TRANSVERSE FLEXURAL STRESSES AT POINTS 1, 2, 3, 7, 8, AND 9

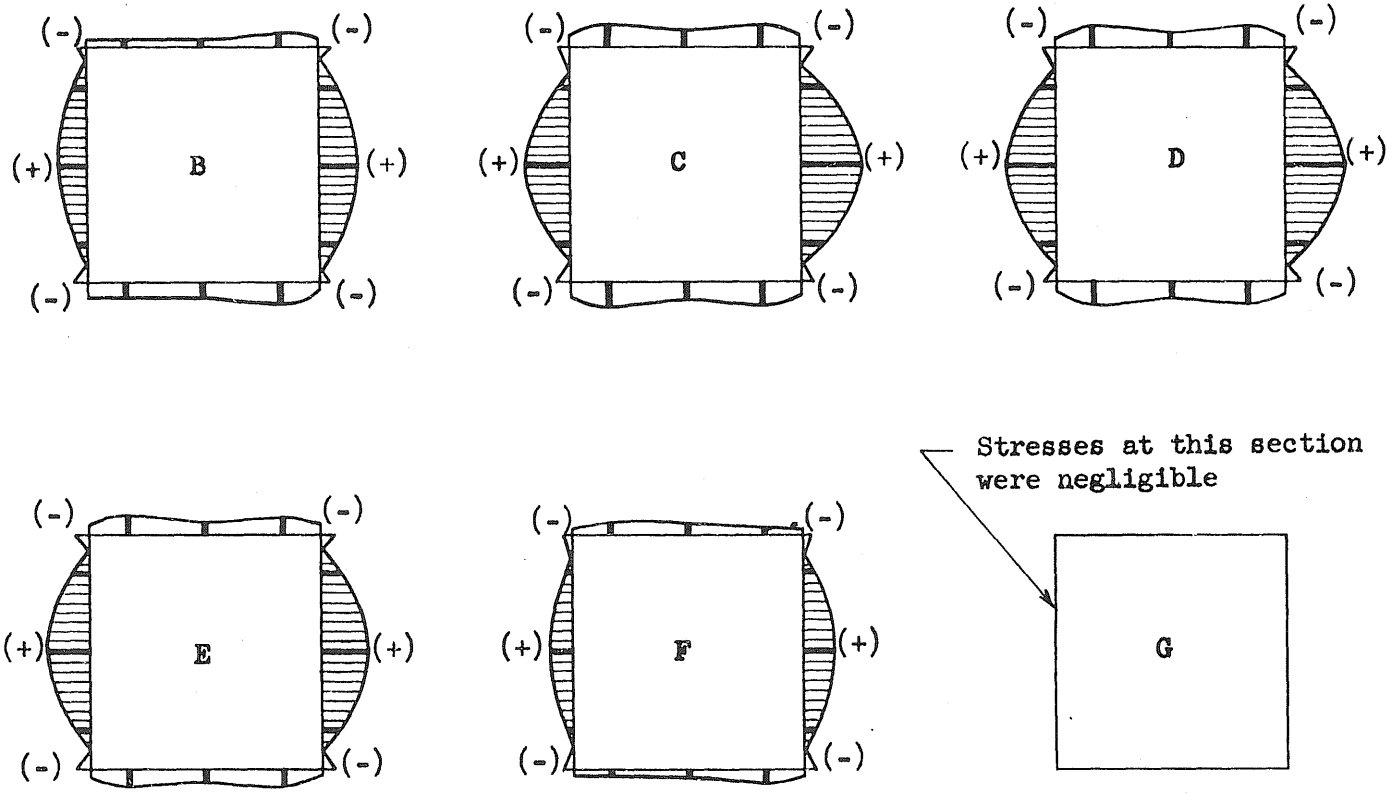

FIG. 42 EXPERIMENTAL VALUES OF TRANSVERSE FLEXURAL STRESSES AT VARIOUS SECTIONS OF TEST SPECIMEN FOR $P_v = 8^k$

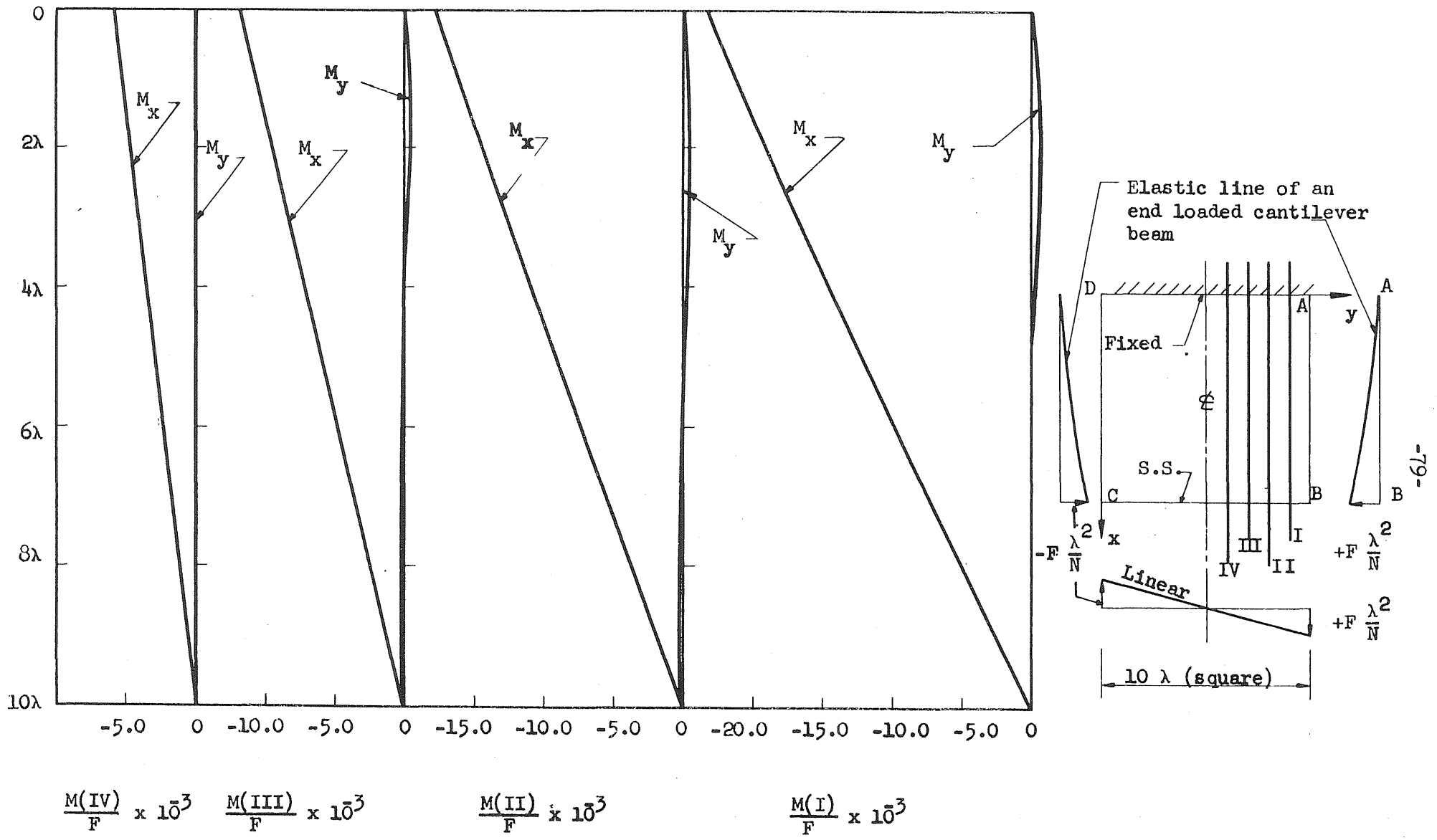

FIG. 43 CASE 1 VARIATION OF BENDING MOMENT IN x AND y DIRECTIONS

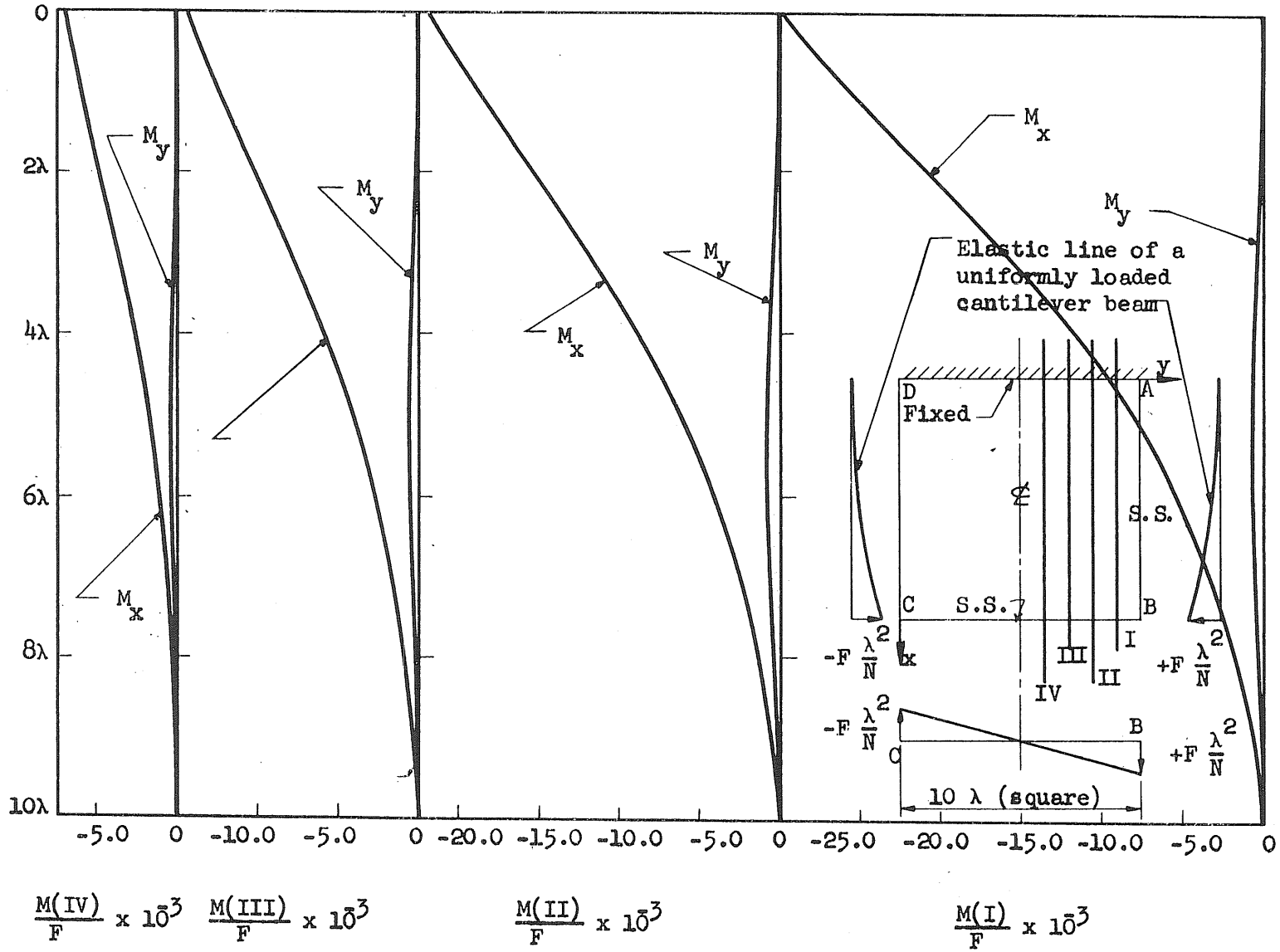

FIG. 44 CASE 2 VARIATION OF BENDING MOMENT IN x AND y DIRECTIONS

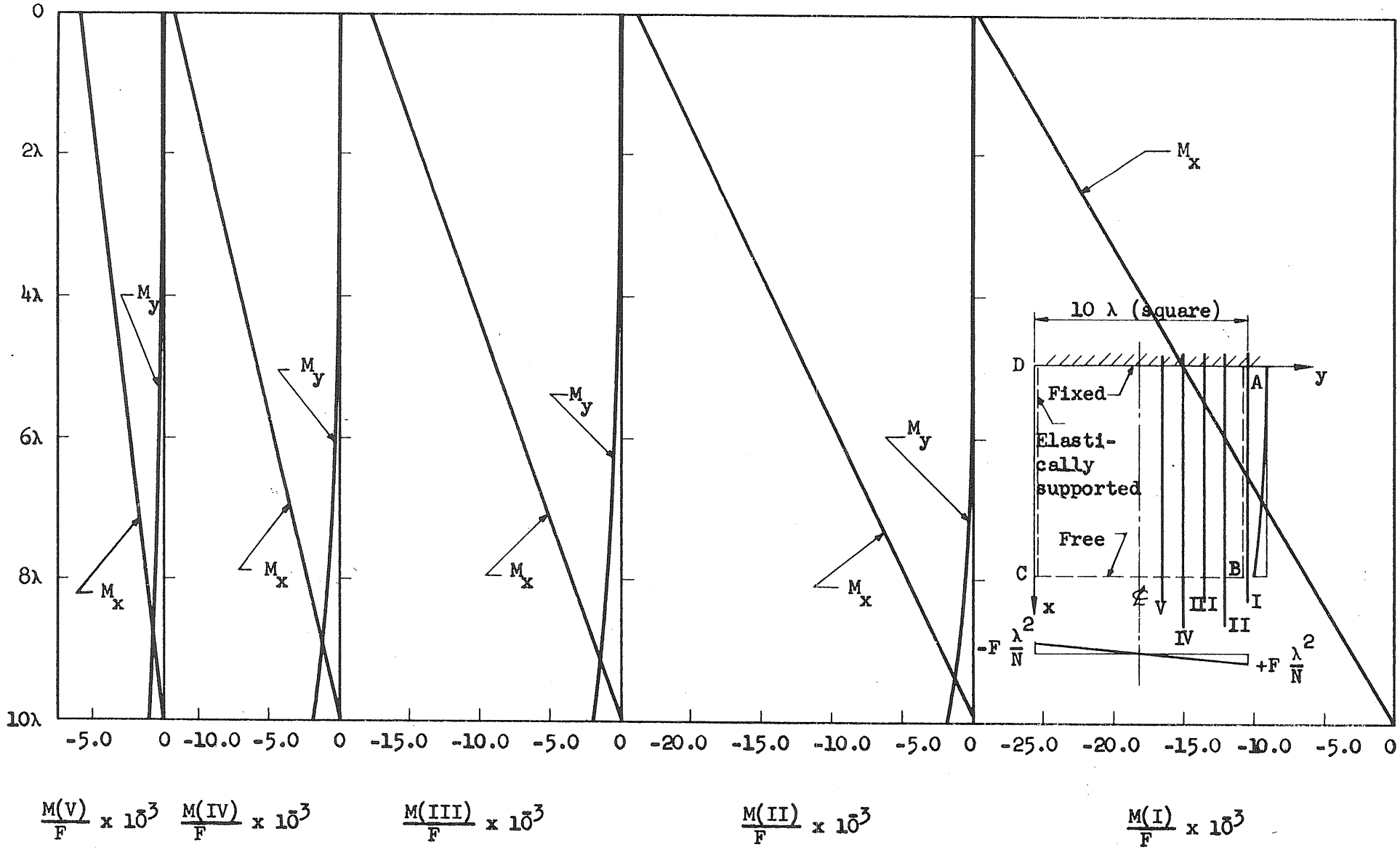

FIG. 45 CASE 3 VARIATION OF BENDING MOMENT IN x AND y DIRECTIONS

Appendix A

APPLICATION OF APPROXIMATE FORMULA FOR TRANSVERSE FLEXURAL STRESSES

In this Appendix, the approximate procedure of the Sect. 2.2.2 for the determination of transverse flexural stresses in a curved box member is applied to an idealized structure for illustrative purposes.

Example

For the structure and loading shown in Fig. (9a),

$P_h = 10^k$, $t = 1$ in.,

$c = 100$ in., $b = 12$ in.

$\bar{r} = 57.7$ in.

Determine:

a. The section where the maximum transverse flexural stresses occur in the member.

b. The value of maximum transverse flexural stress in section (a) above.

c. Transverse flexural stresses at the points indicated in Fig. (9b) for section (a) above.

d. The value of maximum transverse flexural stress at the section, $\alpha = 0$.

Solution

a. The maximum transverse flexural stress in the member occurs at the section where bending moment, M, is maximum. Referring to Fig. (9a),

$$M = P\ (c \cos \alpha + \bar{r} \sin \alpha).$$

Maximizing M with respect to α, that is,

$$\frac{dM}{d\alpha} = 0$$

results in,

$$\alpha = \tan^{-1} \frac{\bar{r}}{c} = \tan^{-1} \frac{57.7}{100} = \tan^{-1} 0.577 \quad \text{or} \quad \alpha = 30^{\circ}.$$

Therefore,

$$M_{max} = -10\ [(100)(0.866) + (57.7)(0.500)] = -1154 \text{ in. k}$$

b. Maximum flexural stress at any given section occurs at the inner corners. Using Eq. (11)

$$\sigma_{ri} = \frac{3}{4} \frac{1154}{(51.7)(1)^2} = 16.7 \text{ ksi}$$

The sign of this stress is to be determined from the distortion diagram shown in Fig. (9b).

c. To determine the stresses at other points, m_i and m_o should first be determined from Eqs. (8) and (9).

$$m_i = \frac{1154}{(8)(51.7)} = 2.80 \frac{\text{in.k}}{\text{in}}$$

$$m_o = \frac{1154}{(8)(63.7)} = 2.26 \frac{\text{in.k}}{\text{in}}$$

The transverse flexural moment per unit width at any point, m, is determined from these values of m_i and m_o and the assumption that the quantity (m.r) varies linearly from $+m_i r_i$ to $-m_o r_o$ across the top and bottom walls, and that m varies linearly across the inner and outer walls. The values of m for the points indicated in Fig. (9b) are given in Table (A.1). Also given in this table are the values of σ_r determined from Eq. (10). In Table (A.1) the flexural moments which produce tension in the outer fibers, and tensile stresses are considered positive.

TABLE A.1

Point	m (in.k/in)	σ_r (ksi)
1	+1.87	+11.2
2	-1.87	-11.2
3	-1.80	-10.8
4	+1.57	+ 9.4
5	+1.50	+ 9.0
6	-1.50	- 9.0
7	-1.57	- 9.4
8	+1.80	+10.8

d. The bending moment at section $\alpha = 0$, is

$$M = -(10)(100) = -1000 \text{ in.k}$$

Since the section $\alpha = 0$ is at the point of tangency of the member, the value of m_i or σ_{ri} computed at this section is to be divided by 2, or

$$\sigma_{ri} = (\tfrac{1}{2})(\tfrac{3}{4}) \frac{1000}{(51.7)(1)^2} = 7.3 \text{ ksi}$$

APPENDIX B

TABULATION OF RESULTS

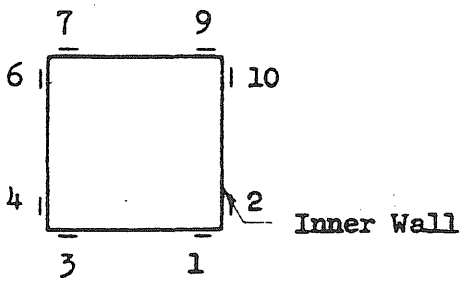

Cross Section

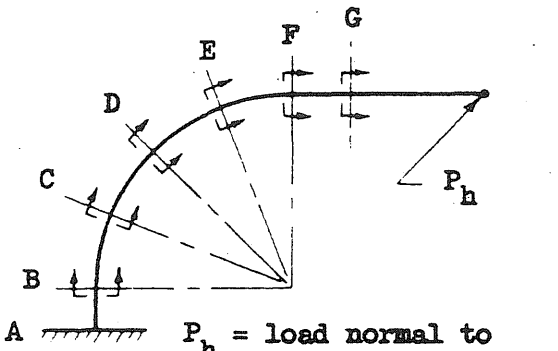

TABLE B.1 RATIO $\frac{\sigma_{rm}}{M/rt^2}$ FOR VARIOUS POINTS

Section	Point	$\sigma_{rm}/(M/rt^2)$			
		$P_h = 4^k$	$P_h = 8^k$	$P_h = 12^k$	$P_h = 16^k$
C	10	0.453	0.453	0.454	0.449
	12	0.445	0.445	0.445	0.442
	1	0.431	0.434	0.433	0.428
	9	0.383	0.389	0.390	0.388
	3	0.400	0.400	0.408	0.413
	7	0.386	0.393	0.396	0.386
	4	0.478	0.482	0.485	0.479
	6	0.386	0.393	0.390	0.389
Average		0.420	0.424	0.425	0.422
D	10	0.426	0.434	0.439	0.437
	12	0.468	0.472	0.474	0.468
	1	0.421	0.423	0.425	0.422
	9	0.391	0.397	0.401	0.400
	3	0.462	0.464	0.468	0.464
	7	0.429	0.429	0.429	0.424
	4	0.497	0.499	0.500	0.474
	6	0.412	0.420	0.421	0.419
Average		0.438	0.442	0.445	0.439
E	10	0.426	0.430	0.431	0.429
	12	0.381	0.387	0.388	0.383
	1	0.346	0.350	0.352	0.346

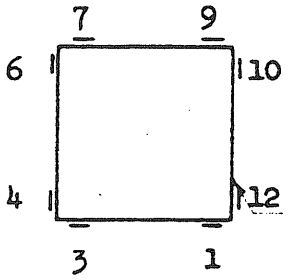

Cross Section

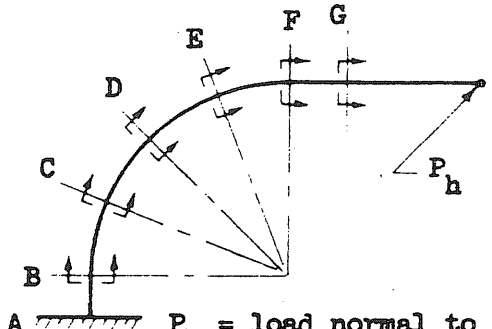

P_h = load normal to plane of curvature

TABLE B.1 (Cont'd.) RATIO $\frac{\sigma_{rm}}{M/rt^2}$ FOR VARIOUS POINTS

Section	Point	$\sigma_{rm}/(M/rt^2)$			
		$P_h = 4^k$	$P_h = 8^k$	$P_h = 12^k$	$P_h = 16^k$
E	9	0.377	0.375	0.376	0.372
	3	0.365	0.369	0.369	0.368
	7	0.370	0.374	0.374	0.371
	4	0.414	0.424	0.426	0.427
	6	0.414	0.424	0.426	0.427
Average		0.387	0.392	0.393	0.390
Grand Average		0.418			
Maximum		0.500			
Minimum		0.346			
Theoretical		0.533			

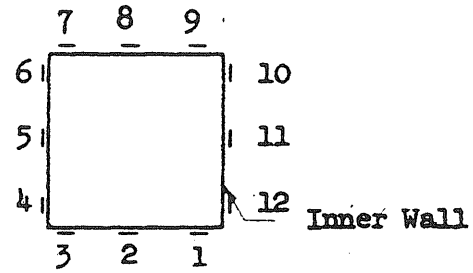

Cross Section

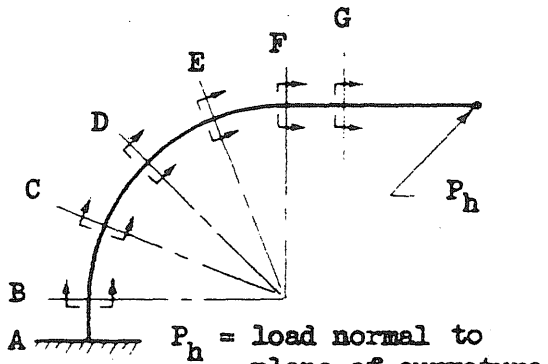

TABLE B.2 EXPERIMENTAL AND COMPUTED VALUES OF TRANSVERSE FLEXURAL STRESSES, σ_r, DUE TO P_h

Section	Point	σ_{rm} (ksi)				σ_{rc} (ksi)*
		$P_h = 4^k$	$P_h = 8^k$	$P_h = 12^k$	$P_h = 16^k$	$P_h = 16^k$
B	1	-3.2	- 6.4	- 9.4	-12.3	- 8.6
	2	-0.1	- 0.2	0	- 0.1	0
	3	+3.3	+ 6.7	+10.2	+13.2	+ 6.9
	4	+2.4	+ 4.7	+ 7.2	+ 9.3	+ 6.7
	5	-0.5	- 0.9	- 1.4	- 2.2	0
	6	-2.8	- 5.7	- 8.4	-11.1	- 6.7
	7	-2.3	- 4.5	- 7.1	- 9.1	- 6.9
	8	-0.3	- 0.2	- 0.4	- 0.4	0
	9	+2.7	+ 5.4	+ 8.2	+10.6	+ 8.6
	10	+2.8	+ 5.6	+ 8.4	+10.7	+ 9.0
	11	-0.5	- 1.2	- 1.9	- 2.9	0
	12	-3.6	- 7.2	-11.0	-14.2	- 9.0
C	1	-7.2	-14.5	-21.7	-28.6	-35.6
	2	-0.5	- 0.9	- 1.3	- 1.5	0
	3	+5.4	+10.8	+16.5	+22.8	+28.8
	4	+6.2	+12.5	+18.9	+24.9	+27.7
	5	+0.4	+ 0.7	+ 0.9	+ 1.0	0
	6	-5.0	-10.2	-15.2	-20.2	-27.7
	7	-5.2	-10.6	-16.0	-20.8	-28.8
	8	+0.4	+ 0.9	+ 1.3	+ 1.8	0
	9	+6.4	+13.0	+19.5	+25.9	+35.6

* σ_{rc} for other values of P_h can be obtained by proportions.

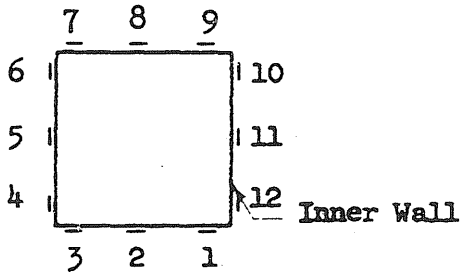

Cross Section

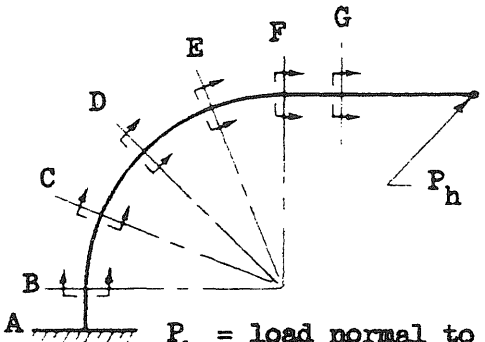

P_h = load normal to plane of curvature

TABLE B.2 (Cont'd.) EXPERIMENTAL AND COMPUTED VALUES OF TRANSVERSE FLEXURAL STRESSES, σ_r, DUE TO P_h

Section	Point	σ_{rm} (ksi)				σ_{rc} (ksi)*
		$P_h = 4^k$	$P_h = 8^k$	$P_h = 12^k$	$P_h = 16^k$	$P_h = 16^k$
C	10	+ 7.9	+15.9	+23.9	+31.5	+37.4
	11	+ 0.2	+ 0.4	+ 0.4	+ 0.4	0
	12	- 7.8	-15.6	-23.4	-31.0	-37.4
D	1	- 9.6	-19.3	-29.1	-38.5	-48.6
	2	- 0.5	- 1.1	- 1.8	- 2.3	0
	3	+ 8.5	+17.1	+25.9	+34.2	+39.3
	4	+ 8.8	+17.7	+26.6	+33.6	+37.8
	5	+ 0.2	+ 0.5	+ 0.9	+ 1.0	0
	6	- 7.3	-14.9	-22.4	-29.7	-37.8
	7	- 7.9	-15.8	-23.7	-31.2	-39.3
	8	+ 0.2	+ 0.2	+ 0.3	+ 0.5	0
	9	+ 8.9	+18.1	+27.4	+36.5	+48.6
	10	+10.2	+20.8	+31.6	+41.9	+51.1
	11	+ 0.5	+ 1.1	+ 1.6	+ 1.9	0
	12	-11.2	-22.6	-34.1	-44.9	-51.1
E	1	- 8.8	-17.8	-26.9	-35.2	-54.3
	2	- 0.2	- 0.5	- 0.8	- 1.2	0
	3	+ 7.5	+15.2	+22.8	+30.3	+43.9
	4	+ 8.2	+16.8	+25.3	+33.8	+42.2
	5	+ 0.4	+ 0.9	+ 1.3	+ 1.7	0
	6	- 6.4	-12.8	-19.4	-25.6	-42.2

* σ_{rc} for other values of P_h can be obtained by proportions.

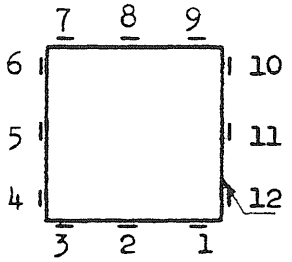

Cross Section

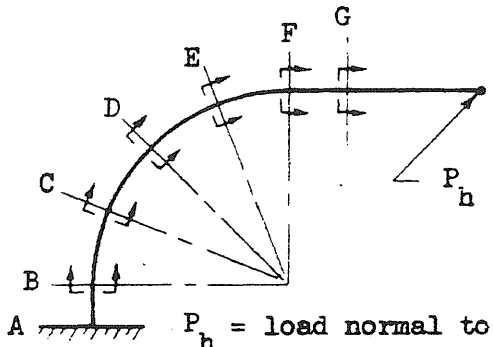

P_h = load normal to plane of curvature

TABLE B.2 (Cont'd) EXPERIMENTAL AND COMPUTED VALUES OF TRANSVERSE FLEXURAL STRESSES, σ_r, DUE TO P_h

Section	Point	σ_{rm} (ksi)				σ_{rc} (ksi)*
		$P_h = 4^k$	$P_h = 8^k$	$P_h = 12^k$	$P_h = 16^k$	$P_h = 16^k$
E	7	- 7.6	-15.4	-23.1	-30.5	-43.6
	8	0	- 0.1	- 0.2	- 0.4	0
	9	+ 9.6	+19.1	+28.7	+37.9	+54.3
	10	+11.4	+23.0	+34.6	+45.9	+57.0
	11	+ 0.4	+ 0.6	+ 1.0	+ 1.3	0
	12	-10.2	-20.7	-31.2	-41.0	-57.0
F	1	- 6.1	-12.1	-18.2	-24.0	-25.8
	2	- 0.2	- 0.4	- 0.4	- 0.5	0
	3	+ 5.4	+11.1	+16.9	+22.7	+20.9
	4	+ 6.4	+13.1	+19.6	+26.1	+20.1
	5	+ 0.3	+ 0.5	+ 0.8	+ 1.2	0
	6	- 6.0	+12.8	-18.1	-23.9	-20.1
	7	- 6.1	-11.9	-17.9	-23.8	-20.9
	8	+ 0.1	+ 0.1	+ 0.2	+ 0.4	0
	9	+ 6.3	+12.1	+17.9	+21.7	+25.8
	10	+ 6.7	+13.7	+20.7	+27.5	+27.2
	11	+ 0.4	+ 0.9	+ 1.7	+ 2.3	0
	12	- 6.8	-13.3	-19.9	-26.3	-27.2
G	1	- 2.6	- 5.3	- 8.0	-10.5	0
	2	- 0.3	- 0.4	- 0.7	- 0.8	0
	3	+ 1.9	+ 3.9	+ 5.8	+ 7.5	0

* σ_{rc} for other values of P_h can be obtained by proportions.

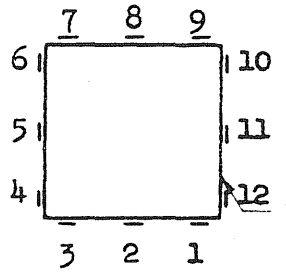

Cross Section

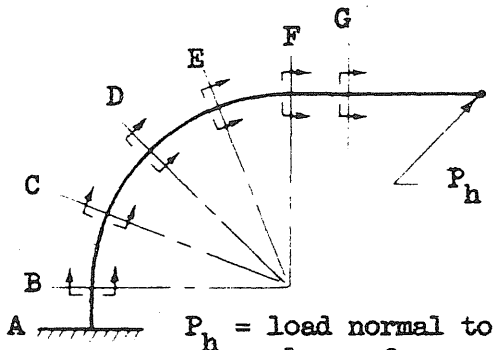

P_h = load normal to plane of curvature

TABLE B.2 (Cont'd.) EXPERIMENTAL AND COMPUTED VALUES OF TRANSVERSE FLEXURAL STRESS, σ_r, DUE TO P_h

Section	Point	σ_{rm} (ksi)				σ_{rc} (ksi)*
		$P_h = 4^k$	$P_h = 8^k$	$P_h = 12^k$	$P_h = 16^k$	$P_h = 16^k$
G	4	+2.4	+4.8	+7.1	+ 9.7	0
	5	0	+0.1	+0.1	+ 0.2	0
	6	-2.1	-4.3	-6.4	- 8.2	0
	7	-2.2	-4.3	-6.5	- 8.6	0
	8	+0.1	+0.3	+0.4	+ 0.6	0
	9	+2.8	+5.5	+8.2	+11.0	0
	10	+2.7	+5.6	+8.4	+11.1	0
	11	+0.1	+0.1	+0.3	+ 0.3	0
	12	-2.5	-5.3	-7.9	-10.3	0

* σ_{rc} for other values of P_h can be obtained by proportions.

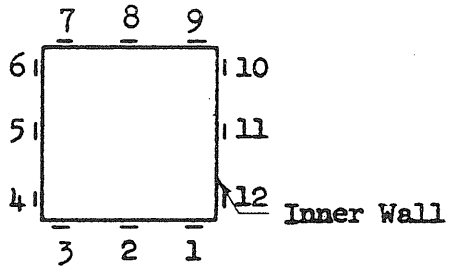

Cross Section

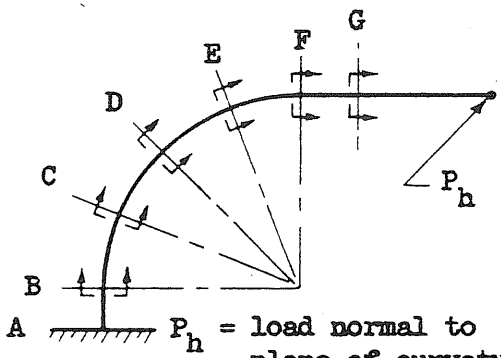

TABLE B.3 EXPERIMENTAL AND COMPUTED VALUES OF AXIAL FLEXURAL STRESSES, σ_θ DUE TO P_h

Section	Point	$\sigma_{\theta m}$ (ksi)				$\sigma_{\theta c}$ (ksi) x	
		$P_h = 4^k$	$P_h = 8^k$	$P_h = 12^k$	$P_h = 16^k$	$P_h = 16^k$ Eq. (13)*	$P_h = 16^k$ Eq. (15)**
B	1	-1.7	- 3.6	- 5.4	- 7.1		- 5.6
	2	-1.3	- 2.6	- 3.8	- 5.2		- 5.0
	3	-1.0	- 1.9	- 2.8	- 3.8		- 4.6
	4	-0.4	- 0.7	- 0.8	- 1.2		- 2.9
	5	-0.4	- 0.9	- 1.2	- 1.7	Not Applicable	0
	6	+0.2	+ 0.4	+ 0.9	+ 1.3		+ 2.9
	7	+1.2	+ 2.5	+ 3.8	+ 5.1		+ 4.6
	8	+2.1	+ 4.3	+ 6.5	+ 8.6		+ 5.0
	9	+2.3	+ 4.5	+ 6.8	+ 8.7		+ 5.6
	10	+1.8	+ 3.5	+ 5.2	+ 6.6		+ 4.0
	11	+0.6	+ 1.3	+ 1.8	+ 2.1		0
	12	-0.7	- 1.5	- 2.4	- 3.1		- 4.0
C	1	-7.0	+14.0	-21.2	-28.0	-24.8	-11.7
	2	-4.0	- 8.1	-12.1	-15.8	- 9.8	-10.5
	3	-0.4	- 0.7	- 1.0	- 1.0	+ 3.5	- 9.5
	4	+2.1	+ 4.1	+ 6.4	+ 8.5	+ 7.1	- 6.0
	5	+0.3	+ 0.5	+ 0.7	+ 0.8	0	0
	6	-1.7	- 3.5	- 5.2	- 6.8	- 7.1	+ 6.0
	7	-0.1	- 0.2	- 0.3	- 0.6	- 3.5	+ 9.5

x $\sigma_{\theta c}$ for other values of P_h can be obtained by proportions.

* Computed by semi-empirical formula, a = 8.625 in.

** Computed from "plane-section" assumption.

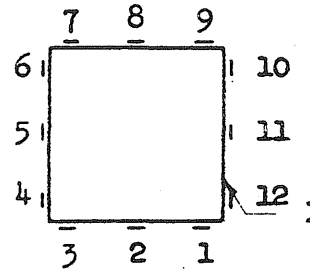

Cross Section

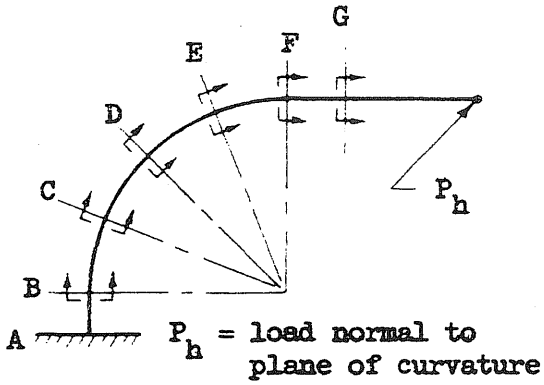

TABLE B.3 (Cont'd.) EXPERIMENTAL AND COMPUTED VALUES OF AXIAL FLEXURAL STRESSES, σ_θ, DUE TO P_h

Section	Point	$\sigma_{\theta m}$ (ksi)				$\sigma_{\theta c}$ (ksi) x	
		$P_h = 4^k$	$P_h = 8^k$	$P_h = 12^k$	$P_h = 16^k$	$P_h = 16^k$ Eq. (13)*	$P_h = 16^k$ Eq. (15)**
C	8	+ 3.9	+ 7.9	+11.8	+15.7	+ 9.8	+10.5
	9	+ 7.1	+14.3	+21.3	+28.2	+24.8	+11.7
	10	+ 4.7	+ 9.4	+14.1	+18.6	+21.3	+ 8.3
	11	0	0	- 0.1	- 0.3	0	0
	12	- 4.0	- 8.2	-12.3	-16.4	-21.3	- 8.3
D	1	- 9.9	-20.0	-30.2	-40.1	-33.9	-16.1
	2	- 4.7	- 9.8	-14.9	-19.5	-13.4	-14.4
	3	+ 0.6	+ 1.3	+ 1.9	+ 2.5	+ 4.8	-13.0
	4	+ 3.8	+ 7.6	+11.6	+14.9	+ 9.7	- 8.3
	5	+ 0.2	+ 0.5	+ 0.9	+ 1.2	0	0
	6	- 3.2	- 6.3	- 9.5	-12.4	- 9.7	+ 8.3
	7	- 0.3	- 0.4	- 0.6	- 0.6	- 4.8	+13.0
	8	+ 4.8	+ 9.6	+14.6	+19.3	+13.4	+14.4
	9	+10.2	+20.4	+30.8	+40.9	+33.9	+16.1
	10	+ 6.9	+13.8	+20.7	+27.4	+29.1	+11.4
	11	+ 0.1	+ 0.3	+ 0.3	+ 0.4	0	0
	12	- 6.4	-12.8	-19.5	-25.7	-29.1	-11.4
E	1	-10.0	-20.4	-30.6	-40.5	-37.9	-18.0
	2	- 5.1	-10.2	-15.4	-20.5	-14.9	-16.1

x $\sigma_{\theta c}$ for other values of P_h can be obtained by proportions.

* Computed by semi-empirical formula, a = 8.625 in.

** Computed from "plane-section" assumption.

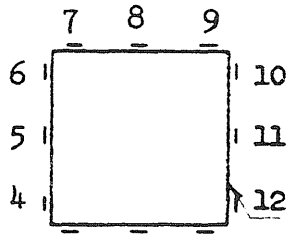

Cross Section

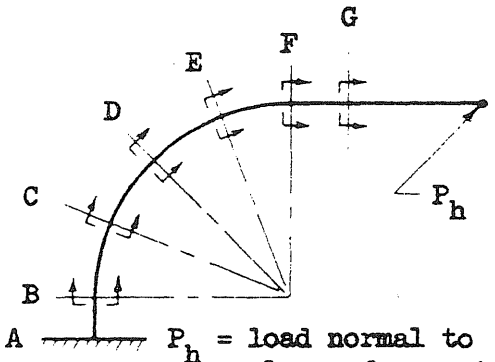

TABLE B.3 (Cont'd.) EXPERIMENTAL AND COMPUTED VALUES OF AXIAL FLEXURAL STRESSES, σ_θ, DUE TO P_h

Section	Point	$\sigma_{\theta m}$ (ksi)				$\sigma_{\theta c}$ (ksi) x	
		$P_h = 4^k$	$P_h = 8^k$	$P_h = 12^k$	$P_h = 16^k$	$P_h = 16^k$ Eq. (13) *	$P_h = 16^k$ Eq. (15) **
E	3	- 0.2	- 0.3	- 0.5	- 0.6	+ 5.4	-14.5
	4	+ 3.2	+ 6.5	+ 9.8	+13.1	+10.8	- 9.2
	5	+ 0.2	+ 0.4	+ 0.7	+ 1.0	0	0
	6	- 2.5	- 5.0	- 7.6	- 9.9	-10.8	+ 9.2
	7	+ 0.3	+ 0.6	+ 1.0	+ 1.3	- 5.4	+14.5
	8	+ 5.5	+10.9	+16.4	+21.7	+14.9	+16.1
	9	+11.1	+22.1	+33.2	+43.8	+37.9	+18.0
	10	+ 7.9	+15.8	+23.4	+31.0	+32.5	+12.7
	11	+ 0.4	+ 0.7	+ 1.0	+ 1.3	0	0
	12	- 6.3	-12.9	-19.4	-25.7	-32.5	-12.7
F	1	- 6.8	-13.6	-20.4	-27.2		-17.1
	2	- 4.6	- 9.2	-13.7	-17.9		-15.2
	3	- 1.7	- 3.3	- 5.0	- 6.5		-13.8
	4	+ 0.5	+ 1.3	+ 2.0	+ 2.7	Not Applicable	- 8.8
	5	- 0.1	- 0.1	- 0.2	- 0.1		0
	6	- 0.9	- 2.0	- 2.5	- 3.2		+ 8.8
	7	+ 1.3	+ 2.9	+ 4.8	+ 5.8		+13.8
	8	+ 4.3	+ 8.7	+13.1	+17.4		+15.2
	9	+ 7.2	+14.4	+21.5	--		+17.1

x $\sigma_{\theta c}$ for other values of P_h can be obtained by proportions.

* Computed by semi-empirical formula, a = 8.625 in.

** Computed from "plane-section" assumption.

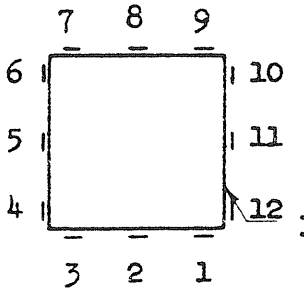

Cross Section

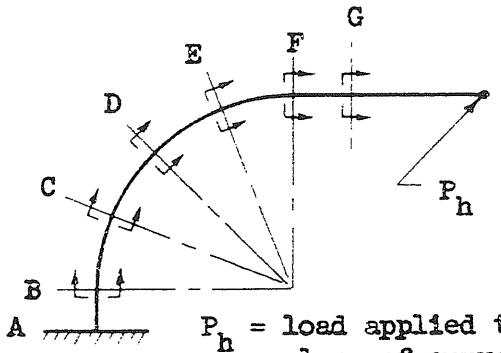

P_h = load applied to plane of curvature

TABLE B.3 (Cont'd.) EXPERIMENTAL AND COMPUTED VALUES OF AXIAL FLEXURAL STRESSES, σ_θ, DUE TO P_h

Section	Point	$\sigma_{\theta m}$ (ksi)				$\sigma_{\theta c}$ (ksi) x	
		$P_h = 4^k$	$P_h = 8^k$	$P_h = 12^k$	$P_h = 16^k$	$P_h = 16^k$ Eq. (13)*	$P_h = 16^k$ Eq. (15)**
F	10	+5.3	+10.1	+15.5	+20.7		+12.4
	11	+0.4	+ 0.6	+ 1.2	+ 1.0		0
	12	-4.5	- 9.1	-13.6	-17.9		-12.4
G	1	-3.3	- 6.6	-10.0	-13.2		-13.2
	2	-3.4	- 6.7	-10.0	-13.2		-13.2
	3	-3.4	- 6.8	-10.2	-13.4		-13.2
	4	-2.5	- 5.0	- 7.5	- 9.7		- 8.8
	5	-0.1	- 0.1	- 0.4	- 0.4		0
	6	+2.2	+ 4.4	+ 6.7	+ 9.1		+ 8.8
	7	+3.1	+ 6.6	+10.0	+13.3		+13.2
	8	+3.2	+ 6.6	+ 9.8	+13.1		+13.2
	9	+3.4	+ 6.8	+10.1	+13.5		+13.2
	10	+2.4	+ 4.8	+ 7.2	+ 9.5		+ 8.8
	11	+0.2	+ 0.3	+ 0.4	+ 0.5		0
	12	-2.0	- 4.2	- 6.5	- 8.5		- 8.8

Not Applicable

x $\sigma_{\theta c}$ for other values of P_h can be obtained by proportions.

* Computed by semi-empirical formula, a = 8.625 in.

** Computed by "plane-section" assumption.

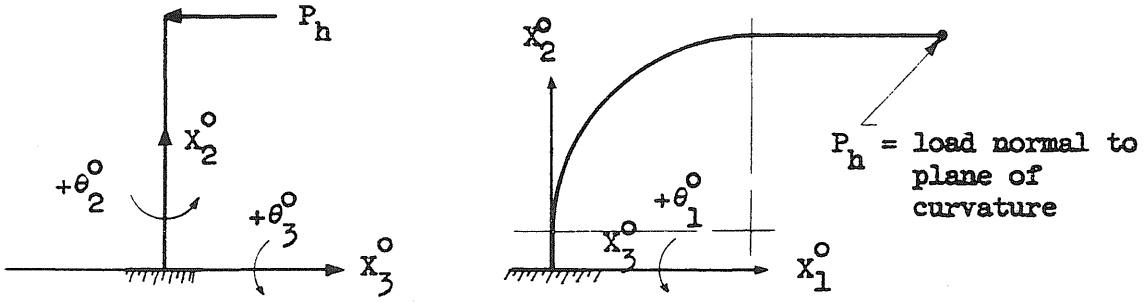

TABLE B.4 MEASURED VALUES OF BASE ROTATIONS, DUE TO P_h

	P_h	Test 1			Test 2		
		θ°_1 (10^{-3}) rad.	θ°_2 (10^{-3}) rad.	θ°_3 (10^{-3}) rad.	θ°_1 (10^{-3}) rad.	θ°_2 (10^{-3}) rad.	θ°_3 (10^{-3}) rad.
Loading	0	0	0	0	0	0	0
	4	+0.0766	+0.4362	-0.0769	+0.0383	+0.8000	-0.1730
	8	+0.2296	+1.6000	0	+0.0383	+3.0736	-0.2450
	12	+0.2296	+3.1580	+0.1923	-0.0383	+5.4736	-0.3654
	16	+0.2680	+4.7580	+0.5965	-0.1149	+7.1579	-0.4038
Unloading	12	+0.2680	+4.2527	+0.2885	-	-	-
	8	+0.1914	+3.4948	+0.1731	-0.0766	+5.9368	-0.5384
	4	+0.0766	+2.1895	+0.0385	-	-	-
	0	0	+0.1263	0	+0.5359	+0.5894	+0.7885

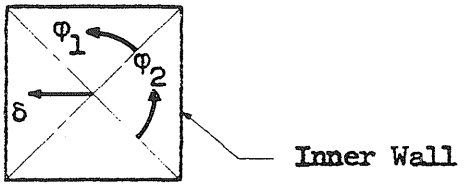

Cross Section

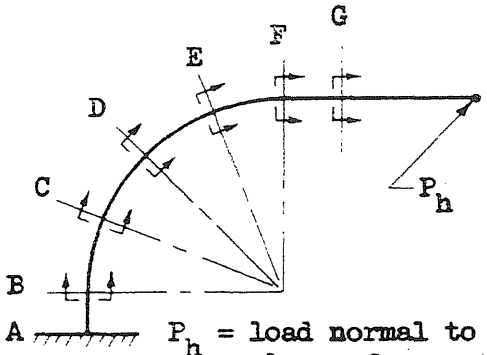

P_h = load normal to plane of curvature

TABLE B.5 MEASURED AND COMPUTED CENTER LINE DEFLECTIONS IN DIRECTION NORMAL TO PLANE OF CURVATURE, DUE TO P_h

Section	P_h kips	δ_m^* (in.)					δ_c (in.)
		Test 1		Test 2		Average	By simple theory **
		Loading	Unloading	Loading	Unloading		
D	4	0.06	0.09	0.09	-	0.08	0.04
	8	0.14	0.17	0.16	0.20	0.17	0.09
	12	0.24	0.24	0.24	-	0.24	0.13
	16	0.30	-	0.32	-	0.31	0.17
E	4	0.11	0.13	0.12	-	0.12	0.09
	8	0.23	0.26	0.26	0.29	0.26	0.18
	12	0.36	0.38	0.39	-	0.38	0.28
	16	0.49	-	0.50	-	0.50	0.37
F	4	0.17	0.19	0.11	-	0.15	0.15
	8	0.34	0.38	0.36	0.41	0.37	0.30
	12	0.52	0.55	0.57	-	0.55	0.45
	16	0.71	-	0.76	-	0.73	0.60

* δ_m = measured deflection reduced to fully fixed support condition.

** δ_c = computed from Eq. (15).

TABLE B.6 MEASURED ROTATIONS OF DIAGONAL OF AN 11.25 x 11.25 SQUARE SUBJECTED TO CORNER DEFLECTIONS OF TEST SPECIMEN FOR $P_h = 12^k$

Section	φ_1 (rad.)			φ_2 (rad.)			Average φ for Section
	Test 1	Test 2	Average	Test 1	Test 2	Average	
D	-	+0.0005	+0.0005	-	-0.0007	-0.0007	-0.0001
E	-0.0025	-0.0015	-0.0020	-0.0017	-0.0010	-0.0014	-0.0017
F	-0.0070	-0.0064	-0.0067	-0.0069	-0.0066	-0.0068	-0.0068

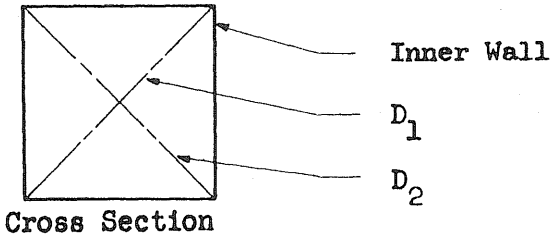

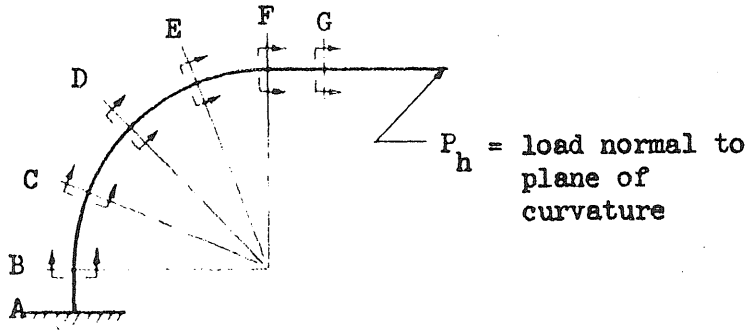

TABLE B.7 COMPUTED CHANGES IN DIAGONAL LENGTHS OF AN 11.25 x 11.25 SQUARE SUBJECTED TO CORNER DEFLECTIONS OF TEST SPECIMEN, DUE TO P_h

Section	P_h kips	D_1^* - D (in.)					D_1^* - D (in.)				
		Test 1		Test 2		Average	Test 1		Test 2		Average
		Loading	Unloading	Loading	Unloading		Loading	Unloading	Loading	Unloading	
D	4	-0.031	-0.034	-0.028	-	-0.031	+0.027	+0.032	+0.034	-	+0.031
	8	-0.064	-0.071	-0.063	-0.068	-0.066	+0.054	+0.059	+0.063	+0.061	+0.059
	12	-0.098	-0.102	-0.093	-	-0.098	+0.088	+0.088	+0.084	-	+0.087
	16	-0.131	-	-0.127	-	-0.129	+0.112	-	+0.110	-	+0.111
E	4	-0.023	-0.021	-0.030	-	-0.025	+0.025	+0.022	+0.020	-	+0.022
	8	-0.052	-0.078	-0.043	-0.050	-0.056	+0.043	+0.040	+0.047	+0.047	+0.044
	12	-0.090	-0.094	-0.084	-	-0.089	+0.062	+0.058	+0.047	-	+0.056
	16	-0.132	-	-0.127	-	-0.130	+0.079	-	+0.081	-	+0.080
F	4	-0.024	-0.018	-	-	-0.021	+0.011	+0.019	-	-	+0.015
	8	-0.056	-0.052	-	-	-0.054	+0.015	+0.013	-	-	+0.014
	12	-0.083	-0.088	-	-	-0.085	+0.019	+0.014	-	-	+0.016
	16	-0.129	-	-	-	-0.129	+0.008	-	-	-	+0.008

* Indicates changed length of the diagonal.

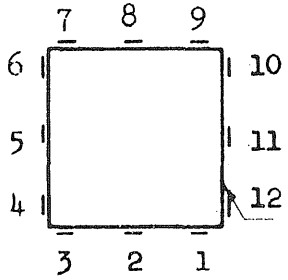

Inner Wall

Cross Section

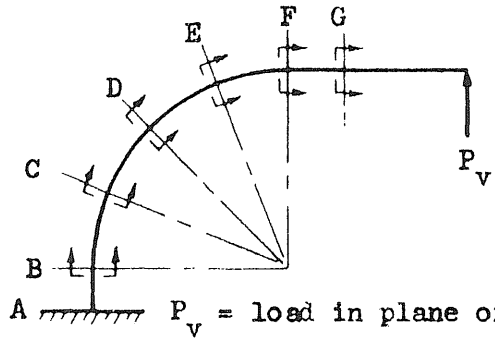

P_v = load in plane of curvature

TABLE B.8 EXPERIMENTAL AND COMPUTED VALUES OF AXIAL FLEXURAL STRESSES, σ_θ, DUE TO P_v

Section	Point	$\sigma_{\theta m}$ (ksi)		$\sigma_{\theta c}$ (ksi)*	Section	Point	$\sigma_{\theta m}$ (ksi)		$\sigma_{\theta c}$ (ksi)*	Section	Point	$\sigma_{\theta m}$ (ksi)		$\sigma_{\theta c}$ (ksi)*
		$P_v = 4^k$	$P_v = 8^k$	$P_v = 8^k$			$P_v = 4^k$	$P_v = 8^k$	$P_v = 8^k$			$P_v = 4^k$	$P_v = 8^k$	$P_v = 8^k$
B	1	+3.9	+ 7.6	+ 7.4	C	1	+4.7	+ 9.7	+ 7.3	D	1	+4.2	+ 8.7	+ 6.8
	2	-0.9	- 1.9	- 0.7		2	-1.4	- 2.5	- 0.7		2	-1.4	- 2.5	- 0.7
	3	-5.1	-10.2	- 7.3		3	-6.3	-12.2	- 7.4		3	-6.3	-12.2	- 6.8
	4	-4.5	- 9.1	-10.2		4	-4.9	- 9.7	-10.0		4	-4.5	- 9.2	- 9.4
	5	-2.2	- 4.3	-10.2		5	-0.6	- 1.2	-10.0		5	-0.6	- 1.2	- 9.4
	6	-4.6	- 8.7	-10.2		6	-5.5	-10.8	-10.0		6	-4.4	- 8.4	- 9.4
	7	-4.9	- 9.4	- 7.3		7	-6.2	-12.4	- 7.4		7	-5.7	-11.5	- 6.8
	8	-0.7	- 1.4	- 0.7		8	-1.1	- 2.4	- 0.7		8	-0.9	- 1.9	- 0.7
	9	+4.0	+ 7.5	+ 7.4		9	+5.1	+ 9.8	+ 7.3		9	+5.2	+10.2	+ 6.8
	10	+6.5	+12.6	+12.3		10	+7.3	+14.3	+12.0		10	+7.5	+14.6	+11.3
	11	+6.3	+12.6	+12.3		11	+5.1	+10.1	+12.0		11	+4.7	+ 9.4	+11.3
	12	+7.0	+14.4	+12.3		12	+7.1	+14.4	+12.0		12	+6.6	+13.5	+11.3

* $\sigma_{\theta c}$ for other values of P_v can be obtained by proportions.

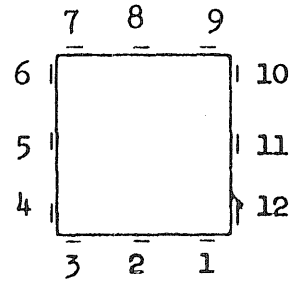

Cross Section

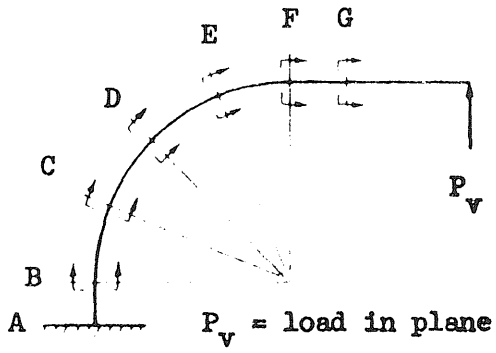

P_v = load in plane of curvature

TABLE B.8 (Cont'd.) EXPERIMENTAL AND COMPUTED VALUES OF AXIAL FLEXURAL STRESSES, σ_θ, DUE TO P_v

Section	Point	$\sigma_{\theta m}$ (ksi)		$\sigma_{\theta c}$ (ksi)*	Section	Point	$\sigma_{\theta m}$ (ksi)		$\sigma_{\theta c}$ (ksi)*	Section	Point	$\sigma_{\theta m}$ (ksi)		$\sigma_{\theta c}$ (ksi)*
		$P_v = 4^k$	$P_v = 8^k$	$P_v = 8^k$			$P_v = 4^k$	$P_v = 8^k$	$P_v = 8^k$			$P_v = 4^k$	$P_v = 8^k$	$P_v = 8^k$
E	1	+3.8	+ 8.3	+ 6.2	F	1	+2.7	+ 5.7	+5.4	G	1	+2.4	+4.8	+4.4
	2	-1.2	- 2.0	- 0.7		2	-0.8	- 1.4	-0.7		2	0	0	0
	3	-5.4	-10.7	- 6.3		3	-3.8	- 7.4	-5.6		3	-2.2	-4.5	-4.4
	4	-4.1	- 8.3	- 8.7		4	-4.0	- 7.8	-7.8		4	-3.7	-7.0	-6.6
	5	-0.7	- 1.4	- 8.7		5	-2.3	- 4.5	-7.8		5	-3.6	-7.3	-6.6
	6	-3.9	- 7.7	- 8.7		6	-3.9	- 7.7	-7.8		6	-3.6	-7.1	-6.6
	7	-5.6	-11.1	- 6.3		7	-3.8	- 7.6	-5.6		7	-2.3	-4.5	-4.4
	8	-1.0	- 2.0	- 0.7		8	-0.5	- 1.2	-0.7		8	+0.1	+1.0	0
	9	+4.2	+ 8.5	+ 6.2		9	+3.4	+ 6.5	+5.4		9	+2.5	+4.8	+4.4
	10	+6.5	+12.7	+10.3		10	+5.1	+10.1	+9.0		10	+3.6	+7.2	+6.6
	11	+4.0	+ 8.5	+10.3		11	+4.3	+ 8.7	+9.0		11	+3.4	+7.0	+6.6
	12	+6.0	+12.1	+10.3		12	+4.4	+ 9.0	+9.0		12	+3.4	+6.9	+6.6

* $\sigma_{\theta c}$ for other values of P_v can be obtained by proportions.

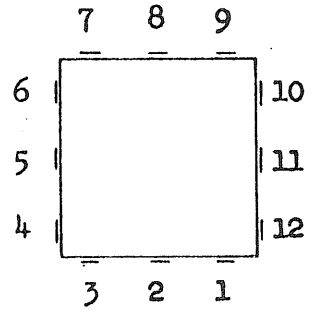

Cross Section

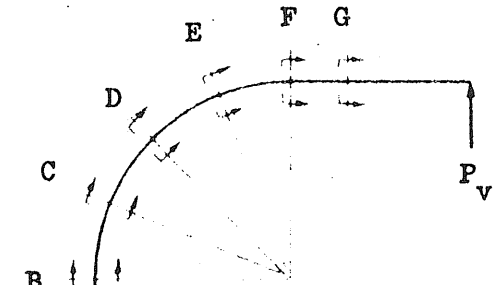

P_v = load in plane of curvature

TABLE B.9 *MEASURED VALUES OF TRANSVERSE FLEXURAL STRESSES, σ_r, DUE TO P_v

Section	Point	σ_{rm} (ksi)		Section	Point	σ_{rm} (ksi)		Section	Point	σ_{rm} (ksi)	
		$P_v = 4^k$	$P_v = 8^k$			$P_v = 4^k$	$P_v = 8^k$			$P_v = 4^k$	$P_v = 8^k$
B	1	-2.4	- 5.8	C	1	-2.9	- 5.1	D	1	-3.0	- 5.3
	2	-1.5	- 2.8		2	-2.5	- 4.7		2	-2.3	- 4.5
	3	-1.3	- 2.8		3	-2.6	- 5.3		3	-2.5	- 5.2
	4	+0.9	+ 1.5		4	+1.5	+ 2.8		4	+1.8	+ 3.2
	5	+3.5	+ 6.8		5	+6.1	+12.3		5	+5.9	+11.8
	6	+0.9	+ 2.4		6	-1.4	- 2.7		6	+1.7	+ 3.8
	7	-1.3	- 2.1		7	-2.7	- 5.1		7	-2.8	- 5.2
	8	-1.2	- 2.0		8	-2.1	- 4.2		8	-2.1	- 4.1
	9	-1.7	- 3.4		9	-2.3	- 5.0		9	-2.2	- 4.6
	10	+2.1	+ 3.7		10	+2.7	+ 5.0		10	+2.9	+ 5.6
	11	+6.5	+12.9		11	+7.6	+15.1		11	+7.4	+14.6
	12	+1.9	+ 4.2		12	+2.9	+ 6.2		12	+2.9	+ 6.4

* No simple procedure for computation of these stresses is available.

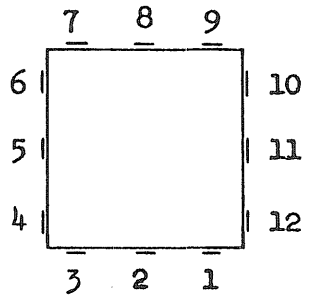

Cross Section

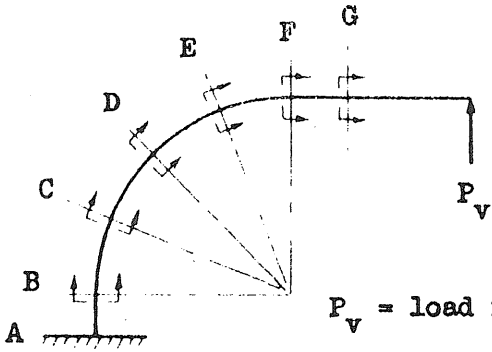

P_v = load in plane of curvature

TABLE B.9 (Cont'd.) * MEASURED VALUES OF TRANSVERSE FLEXURAL STRESSES, σ_r, DUE TO P_v

Section	Point	σ_{rm} (ksi)		Section	Point	σ_{rm} (ksi)		Section	Point	σ_{rm} (ksi)	
		$P_v = 4^k$	$P_v = 8^k$			$P_v = 4^k$	$P_v = 8^k$			$P_v = 4^k$	$P_v = 8^k$
E	1	-2.3	- 4.1	F	1	-1.5	-2.7	G	1	+0.1	+0.3
	2	-1.9	- 3.8		2	-1.1	-2.2		2	0	-0.1
	3	-2.1	- 4.3		3	-1.0	-2.1		3	+0.2	+0.3
	4	+1.5	+ 2.7		4	+0.4	+0.9		4	-0.1	-0.2
	5	+5.1	+10.3		5	+2.6	+5.1		5	-0.2	-0.4
	6	+1.6	+ 3.5		6	+0.3	+1.0		6	-0.3	-0.5
	7	-2.6	- 5.0		7	-1.6	-3.0		7	-0.2	-0.3
	8	-2.0	- 3.9		8	-1.2	-2.4		8	-0.1	-0.1
	9	-3.2	- 4.5		9	-0.9	-1.8		9	+0.2	+0.4
	10	+2.7	+ 5.0		10	+1.6	+2.9		10	+0.3	+0.5
	11	+5.7	+12.9		11	+4.0	+7.8		11	+0.1	+0.5
	12	+2.4	+ 5.1		12	+1.0	+2.4		12	0	+0.2

* No simple procedure for computation of these stresses is available.